Evolutionary and pulsational properties of white dwarf stars

Leandro G. Althaus · **Alejandro H. Córsico** · **Jordi Isern** · **Enrique García–Berro**

Abstract White dwarf stars are the final evolutionary stage of the vast majority of stars, including our Sun. Since the coolest white dwarfs are very old objects, the present population of white dwarfs contains a wealth of information on the evolution of stars from birth to death, and on the star formation rate throughout the history of our Galaxy. Thus, the study of white dwarfs has potential applications to different fields of astrophysics. In particular, white dwarfs can be used as independent reliable cosmic clocks, and can also provide valuable information about the fundamental parameters of a wide variety of stellar populations, like our Galaxy and open and globular clusters. In addition, the high densities and temperatures characterizing white dwarfs allow to use these stars as cosmic laboratories for studying physical processes under extreme conditions that cannot be achieved in terrestrial laboratories. Last but not least, since many white dwarf stars undergo pulsational instabilities, the study of their properties constitutes a powerful tool for applications beyond stellar astrophysics. In particular, white dwarfs can be used to constrain fundamental properties of elementary particles such as axions and neutrinos, and to study problems related to the variation of fundamental constants.

These potential applications of white dwarfs have led to a renewed interest in the calculation of very detailed evolutionary and pulsational models for these stars. In this work, we review the essentials of the physics of white dwarf stars. We enumerate the reasons that make these stars excellent chronometers and we describe why white dwarfs provide tools for

Leandro G. Althaus and Alejandro H. Córsico
Facultad de Ciencias Astronómicas y Geofísicas, Universidad Nacional de La Plata, Paseo del Bosque s/n, (1900) La Plata, Argentina
Instituto de Astrofísica La Plata, IALP, CONICET-UNLP
E-mail: althaus,acorsico@fcaglp.unlp.edu.ar

J. Isern
Institut de Ciències de l'Espai, CSIC, Campus de la UAB, Facultat de Ciències, Torre C-5, 08193 Bellaterra, Spain
Institut d'Estudis Espacials de Catalunya, c/Gran Capità 2–4, Edif. Nexus 104, 08034 Barcelona, Spain
E-mail: isern@ieec.fcr.es

E. García–Berro
Departament de Física Aplicada, Universitat Politècnica de Catalunya, c/Esteve Terrades 5, 08860 Castelldefels, Spain
Institut d'Estudis Espacials de Catalunya, c/Gran Capità 2–4, Edif. Nexus 104, 08034 Barcelona, Spain
E-mail: garcia@fa.upc.edu

a wide variety of applications. Special emphasis is placed on the physical processes that lead to the formation of white dwarfs as well as on the different energy sources and processes responsible for chemical abundance changes that occur along their evolution. Moreover, in the course of their lives, white dwarfs cross different pulsational instability strips. The existence of these instability strips provides astronomers with an unique opportunity to peer into their internal structure that would otherwise remain hidden from observers. We will show that this allows to measure with unprecedented precision the stellar masses and to infer their envelope thicknesses, to probe the core chemical stratification, and to detect rotation rates and magnetic fields. Consequently, in this work, we also review the pulsational properties of white dwarfs and the most recent applications of white dwarf asteroseismology.

Keywords stars: evolution · stars: white dwarfs · stars: interiors · stars: oscillations

1 Introduction

White dwarf stars are the final evolutionary stage of the vast majority of stars. Indeed, more than 97% of all stars, including our Sun, are expected to ultimately end their lives passively, getting rid of their outer layers and forming white dwarfs. For this reason, the present population of white dwarfs contains valuable information about the evolution of individual stars from birth to death and about the star formation rate throughout the history of our Galaxy. These stellar remnants are the cores of low- and intermediate-mass hydrogen burning stars, and have no appreciable sources of nuclear energy. Hence, as time passes by, white dwarfs will slowly cool and radiate the stored thermal energy, becoming dimmer and dimmer.

The interest in the study of white dwarf stars in recent years has been triggered in part by their importance relative to some open questions in other fields of astrophysics — see the recent reviews of Winget & Kepler (2008), Fontaine & Brassard (2008), and also the valuable early reviews on the physics and evolutionary properties of white dwarfs of Koester & Chanmugam (1990) and D'Antona & Mazzitelli (1990). The huge amount of high-quality observational data of these stars, obtained from both space-borne observatories and from ground-based telescopes, has made possible to use the white dwarf cooling sequence as independent age and distance indicators for a wide variety of stellar populations. As a matter of fact, an accurate knowledge of the rate at which white dwarfs cool constitutes a fundamental issue and provides an independent cosmic clock to constrain the age and previous history of the Galactic populations including the disk (Winget et al. 1987; García–Berro et al. 1988a,b; Hernanz et al. 1994; Torres et al. 2002) and globular and open clusters (Richer et al. 1997; Von Hippel & Gilmore 2000; Hansen et al. 2002; Von Hippel et al. 2006; Hansen et al. 2007; Winget et al. 2009; García–Berro et al. 2010). In addition, because white dwarf progenitors lose their outer layers — which are carbon-, nitrogen- and oxygen-rich — at the top of the asymptotic giant branch (AGB), they are significant contributors to the chemical evolution of the Galaxy. More than 10,000 spectroscopically identified white dwarfs with determined effective temperatures (T_{eff}) and gravities ($\log g$) have been currently detected (Kleinman et al. 2004; Kepler et al. 2007), giving us the opportunity to explore the white dwarf mass distribution, which ultimately provides insights into mass-loss processes during stellar evolution and the mass budget of the Galaxy.

White dwarfs usually play a key role in some types of interacting binaries, such as cataclysmic variables, where mass transfer from a companion star onto the white dwarf gives rise to very strong energetic events. In addition, white dwarfs in binary systems are the candidate progenitors of Type Ia supernovae, which are thought to be the result of the explosion of a

white dwarf exceeding the Chandrasekhar limit due to accretion from a mass-losing companion star. Understanding the evolutionary and structural properties of white dwarfs helps improving our konwledge of supernova events, with the important underlying implications for cosmology. Also, the presence of white dwarfs in binary systems with millisecond pulsar companions allows to constrain the age of millisecond pulsars and thereby the timescale for magnetic field decay (van Kerkwijk et al. 2005).

Surveys carried out by the MACHO team (Alcock et al. 1995; Alcock et al. 1997; Alcock et al. 2000) suggest that a substantial fraction of the halo dark matter could be in the form of very cool white dwarfs. Since then, the EROS (Lasserre et al. 2000; Goldman et al. 2002; Tisserand et al. 2006), OGLE (Udalski et al. 1994), MOA (Muraki et al. 1999) and SuperMACHO (Becker et al. 2005) teams have monitored millions of stars during several years in both the Large Magellanic Cloud (LMC) and the Small Magellanic Cloud (SMC) to search for microlensing events. Most of them have challenged the results of the MACHO experiment — see, for instance, Yoo et al. (2004) and references therein. In addition, there have been claims that white dwarfs could be the stellar objects reported in the Hubble Deep Field (Ibata et al. 1999; Méndez & Minniti 2000). However, these claims remain inconclusive for lack of spectroscopic identifications. The Hubble Deep Field South has provided another opportunity to test the contribution of white dwarfs to the Galactic dark matter. In particular, three white dwarf candidates among several faint blue objects which exhibit significant proper motion have been recently found (Kilic et al. 2005). They are assumed to belong to the thick-disk or halo populations. If these are spectroscopically confirmed it would imply that white dwarfs account for $\lesssim 10\%$ of the Galactic dark matter, which would fit comfortably within the results of the EROS team. All in all, the study of the white dwarf population has important ramifications for our understanding of the structure and evolution of the Milky Way (Díaz–Pinto et al. 1994; Isern et al. 1998; Torres et al. 1998; García–Berro et al. 1999; Torres et al. 2001; Torres et al. 2002; García–Berro et al. 2004; Camacho et al. 2007; Torres et al. 2008).

Besides the implications of the white dwarf cooling theory for the study of stellar populations, white dwarfs constitute also extremely interesting objects in their own right. Typically, the mass of white dwarfs is about half that of the Sun, and their size resembles that of a planet. Their compact nature translates into large average densities, large surface gravities and low luminosities. At the extremely high densities of white dwarfs, electrons become degenerate and quantum mechanics — the Pauli principle — determines their equation of state, their structure, and the existence of a limiting mass above which no stable white dwarf can exist (Chandrasekhar 1939). These properties turn white dwarfs into extremely attractive objects as cosmic laboratories to study numerous physical processes under extreme conditions that cannot be achieved in terrestrial laboratories. Just to indicate a few ones, we mention the equation of state, crystallization and physical separation processes at very high density (García-Berro et al. 1988a; García-Berro et al. 1988b; Isern et al. 1991; Segretain et al. 1994; Isern et al. 1997; Winget et al 2009; García-Berro et al. 2010), the physics of neutrino emission (Winget et al. 2004), the existence of axions (Isern et al. 2008) and the variation of fundamental constants (García–Berro et al. 1995). The study of the structure and evolution of white dwarfs thus allows us to test our current understanding of the behavior of matter at extreme densities and pressures.

In the course of their evolution, white dwarfs cross several pulsational instability phases. The pulsational pattern of variable white dwarfs has become a powerful tool for probing their inner regions that would otherwise remain unaccessible to direct observations (Fontaine & Brassard 2008; Winget & Kepler 2008). The recent development of white dwarf asteroseismological techniques, combined with the improvements in the evolutionary models for

these stars have allowed to face some key problems in astrophysics, such as the core chemical composition of low-mass stars and the implications for thermonuclear reaction rates, and the theory of crystallization at high densities. In addition, pulsating white dwarfs are powerful tools which have applications beyond stellar astrophysics. In particular, pulsating white dwarfs can be used to constrain the properties of elementary particles, such as axions and neutrinos (Isern et al. 1992; Córsico et al. 2001b; Isern et al. 2010).

All these potential applications of white dwarfs have led to a renewed interest in the calculation of full evolutionary models for these stars. In this work we discuss the essentials of the physics of white dwarf evolution in order to understand the reasons that make these stars excellent chronometers and potential tools with a wide variety of applications. In Sect. 2, we will describe a simple model for white dwarf evolution, making use of the fact that these stars are strongly degenerate stellar configurations, and thus taking advantage of the fact that the mechanical and thermal structures can be treated separately. This simple model will allow us to understand the evolution of white dwarf as a simple cooling process. In Sect. 4, we will describe the predictions obtained from the full theory of stellar evolution, based on our present understanding of the physical processes occurring in the interior of these stars. In Sect. 5, special emphasis will be placed on the formation and evolution of H-deficient white dwarfs. We will discuss the pulsational properties and asteroseismological tools in Sects. 6 to 8. Furthermore, we will discuss as well the most recent asteroseismological results for the different classes of pulsating white dwarfs. This is done in Sect. 9. The observational aspects of white dwarfs are briefly touched upon. The interested reader is referred to the review articles of Koester (2002), Hansen & Liebert (2003) — for general overviews of the field — Barstow (2006) — for hot white dwarfs — and Winget & Kepler (2008) and Fontaine & Brassard (2008) — for recent accounts of the observational aspects and applications of pulsating white dwarfs. However, we will discuss in some detail the statistical properties of the white dwarf population, and in particular, the white dwarf luminosity function.

2 The essentials of white dwarfs

2.1 A historical perspective

White dwarf stars have captured the attention of astronomers since their early discovery in 1914, when H. Russell (Russell 1914) noticed that the star now known as 40 Eridani B, was located well below the main sequence on the Hertzsprung-Russell diagram, see Fig. 1. He rapidly realized that this star was characterized by a very small radius (hence the "dwarf" in the name), comparable to the size of the Earth. But a major puzzle was posed by the discovery that the companion star to Sirius, Sirus B, was also a white dwarf. The determination of the spectral type (Adams 1915) and luminosity of Sirius B provided the first estimate of its radius. Because the mass of this star was known to be about $1 M_{\odot}$, it was possible to infer the mean density of a white dwarf for the first time: 5×10^4 gr/cm^3. The measurement of the gravitational redshift by Adams (1925) resulting from the strong gravity of Sirius B provided an independent test of the high density of this white dwarf, and at the same time a confirmation of general relativity. It is nonetheless interesting to note that nowadays the accepted value of the effective temperature of the star is much larger than the originally estimated, thus implying a much larger average density of about 10^6 gr/cm^3.

It was clear for astronomers that these stars were indeed a new class of star quite different from ordinary stars. But the extraordinary value of the density derived for Sirius B was difficult to explain at that time, and the answer had to wait until the advent of quantum
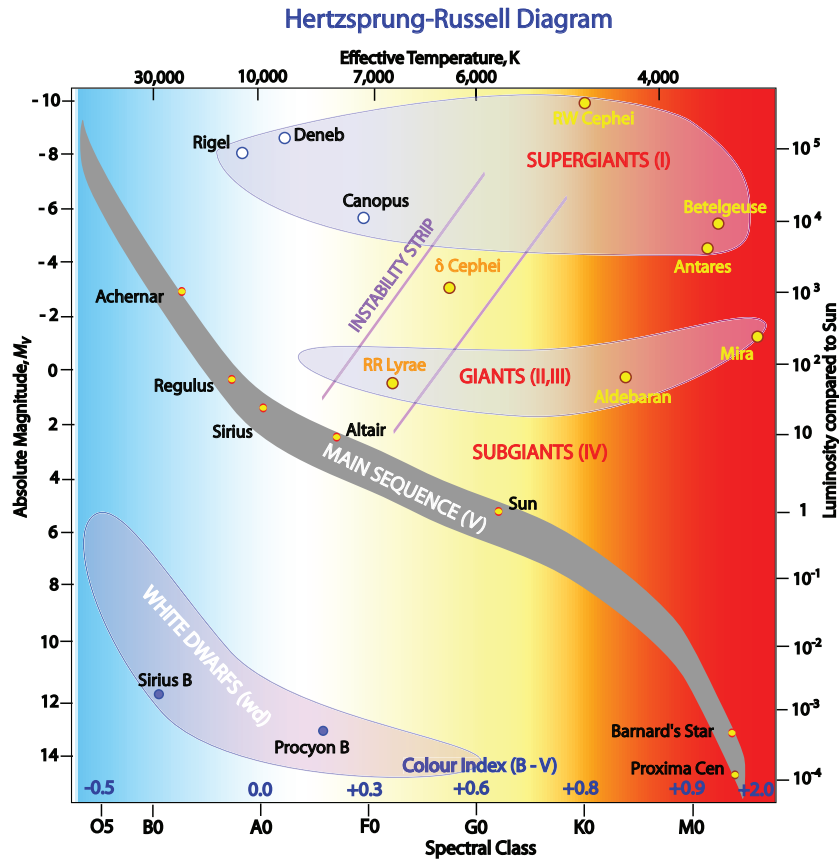
Hertzsprung-Russell Diagram

Fig. 1 Hertzsprung-Russell diagram. The location of white dwarfs is clearly seen below the main sequence. From R. Hollow, CSIRO.

mechanics. As a matter of fact, the existence of white dwarfs provided one of the first tests of the quantum theory of matter and a demonstration of the Pauli exclusion principle for electrons. The realization that completely degenerate electrons should be the source of internal pressure in the interiors of white dwarf (Fowler 1926) led to the conclusion that white dwarfs should be stable objects, and established the study of the zero-temperature configurations. Subsequent investigations by Anderson (1929), Stoner (1930) and Chandrasekhar (1931), demonstrated the fundamental conceptual coupling of relativity and quantum statistical mechanics, which yielded another key breakthrough, the existence of a limiting mass, where gravitational forces overwhelm degenerate electron pressure, and above which no stable white dwarf can exist. This limiting mass, also known as the Chandrasekhar limiting mass, constitutes one of the most important concepts in stellar astrophysics, and it is responsible for the differences in the evolutionary properties of low and and high mass stars an in their final outcomes.
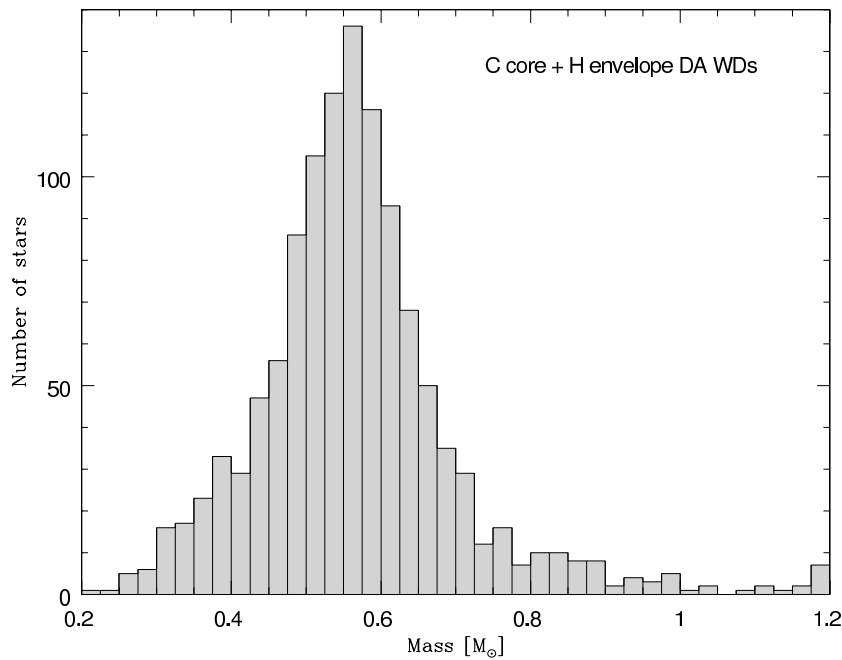
Fig. 2 Mass distribution of H-rich white dwarfs with $T_{eff} > 12,000$ K. The peak mass is located at $M = 0.562 M_{\odot}$. From Madej et al. (2004). Reproduced by permision of ESO.

2.2 Mass distribution

The number of known white dwarfs has increased significantly from one in 1914 in the first Herztsprung-Russell diagram to about 1,000 in the 1970s as a result of targeted searches for high proper motion stars. More recently, imaging surveys provided by the Sloan Digital Sky Survey (SDSS) have largely expanded the number of spectroscopically identified white dwarfs to about 10,000 (Eisenstein et al. 2006), including the detection of ultracool white dwarfs, pulsating H-rich white dwarfs and H-deficient white dwarfs. This increase in the number of detected white dwarfs has extraordinarily improved our knowledge of the white dwarf luminosity and mass functions. In addition, spectroscopy of this much enlarged sample led to the discovery of new and interesting species of degenerate stars (Eisenstein et al. 2006; Koester et al. 2009).

It is now accepted that white dwarfs constitute the end-product of all stars with initial masses up to $\sim 11 M_{\odot}$ (Siess 2007). Most of the mass of a typical white dwarf is contained in its core, which is made of the products of He burning, mostly carbon and oxygen. Small amounts of H and He are left over after the mass-loss phases have ended. Taking into account the previous thermonuclear history and the efficiency of gravitational settling, it is expected that the structure of a typical white dwarf corresponds to that of a compositionally stratified object with a mass of about $0.6 M_{\odot}$ consisting of a carbon-oxygen core surrounded by a thin, He-rich envelope — of at most $0.01 M_{\odot}$ — surrounded itself by a thinner H-rich layer of $\sim 10^{-4} M_{\odot}$. Although very thin, the outer layers are extremely opaque to radiation and regulate the energy outflow of the star, thus playing, as we saw, a crucial role in the evolution of a white dwarf.

An important property of the white dwarf population is their mass distribution, which conveys information about the evolution of our Galaxy. From the mass distribution of white dwarfs it is possible to constrain the late stages of stellar evolution since it reveals the amount of mass lost during the lifetime of the star from the main sequence (Liebert et al. 2005). The surface gravities and effective temperatures of white dwarfs are usually determined from model atmosphere fits to spectral lines. On average, it turns out that white dwarfs are characterized by surface gravities $\log g \simeq 8$. Coupled with theoretical mass-radius relations, this yields average masses of $M \approx 0.6 M_\odot$. In passing, we note that for cool white dwarfs, H and He spectral lines are not visible and the stellar radius (and mass) have to be inferred from accurate trigonometric parallaxes and mass-radius relations. Typical white dwarf mass distributions (see Fig. 2) show that the values of the masses of most white dwarfs cluster around this value (Kepler et al. 2007), with a tail extending towards high stellar masses. The rather narrow mass distribution of white dwarfs is a remarkable characteristic of these stars. Massive white dwarfs have spectroscopically determined masses within 1.0 and $1.3 M_\odot$ and are believed to harbor cores composed mainly of oxygen and neon — at least for non-rotating stars (Domínguez et al. 1996; Ritossa et al. 1996) — in contrast to average-mass white dwarfs, for which carbon-oxygen cores are expected. The existence of such massive white dwarfs has been suggested to be the result of the merger of two averaged-mass white dwarfs in close binaries (Guerrero et al. 2004; Lorén-Aguilar et al. 2009) or of the evolution of heavy-weight intermediate-mass single stars that have experienced repeated carbon-burning shell flashes (Ritossa et al. 1999). Finally, the white dwarf mass distribution comprises a population of low-mass remnants. Because low-mass progenitors would need exceedingly large ages to reach the white dwarf stage, these low-mass white dwarfs are mostly produced in binary systems, where the stellar evolution has been truncated by mass transfer (Sarna et. al 1999).

2.3 The white dwarf luminosity function

Fifty years ago (Schmidt 1959) it was first recognized that the coolest and faintest white dwarfs are the remnants of the earliest stars formed in the Solar neighborhood, and that the cooling theory which we will review below could be very useful to estimate the time elapsed since star formation started in the Galactic disk. The fundamental tool for studying the properties of the white dwarf population is the white dwarf luminosity function, which is defined as the number of white dwarfs per cubic parsec and unit bolometric magnitude (or luminosity) as a function of the bolometric magnitude (or luminosity). The white dwarf luminosity function not only can provide valuable information about the age, structure and evolution of our Galaxy but it also provides an independent test of the theory of dense plasmas (Isern et al. 1997; Isern et al. 1998). Also, it directly constrains the current death rate of low- and intermediate-mass stars in the local neighborhood which, in turn, provides an important tool to evaluate pre-white dwarf stellar evolutionary sequences. Furthermore, the relative simplicity of the structure and evolution of white dwarfs makes them extremely useful as astroparticle physics laboratories (Raffelt 1996; Córsico et al. 2001b). However, in order to use the white dwarf luminosity function to attack these astrophysical problems, it is necessary to have good observational data, good evolutionary models and good input physics. Three decades later, the white dwarf luminosity function has helped in dealing with all these problems and many more. The observational white dwarf luminosity function, its uses and inherent limitations have been discussed over the years in a number of excellent
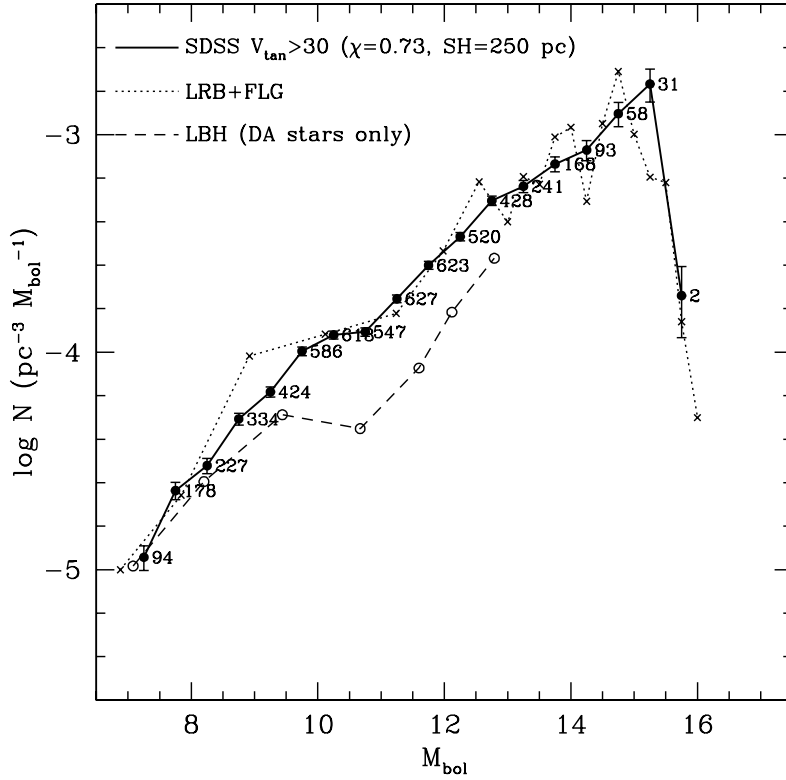
Fig. 3 Luminosity function of disk white dwarfs derived from the SDSS, from Harris et al. (2006). Reproduced by permission of the AAS.

papers (Weidemann 2000; Méndez & Ruiz 2001; Bergeron et al. 2001; Hansen & Liebert 2003).

At the present time, the most promising source of large numbers of new white dwarfs in both the disk and halo is the SDSS (York et al. 2000). Thus far, about 10,000 white dwarfs have been identified in the SDSS (Harris et al. 2006; Eisenstein et al. 2006; DeGennaro et al. 2008) using the reduced proper motion diagram first described in Luyten (1922). For this sample, the disk white dwarf luminosity function was constructed using improved proper motions based on comparison of positions between the SDSS and USNO surveys, high quality *ugriz* photometry, and improved atmospheric models. The resulting white dwarf luminosity function is surprisingly smooth and drops off abruptly at $M_{bol} = 15.3$ — see Fig. 3.

2.4 Spectroscopic classification

Traditionally, white dwarfs have been classified into two distinct families according to the main constituent of their surface. Spectroscopic observations reveal that the surface composition of most white dwarfs consists almost entirely of H with at most traces of other ele-
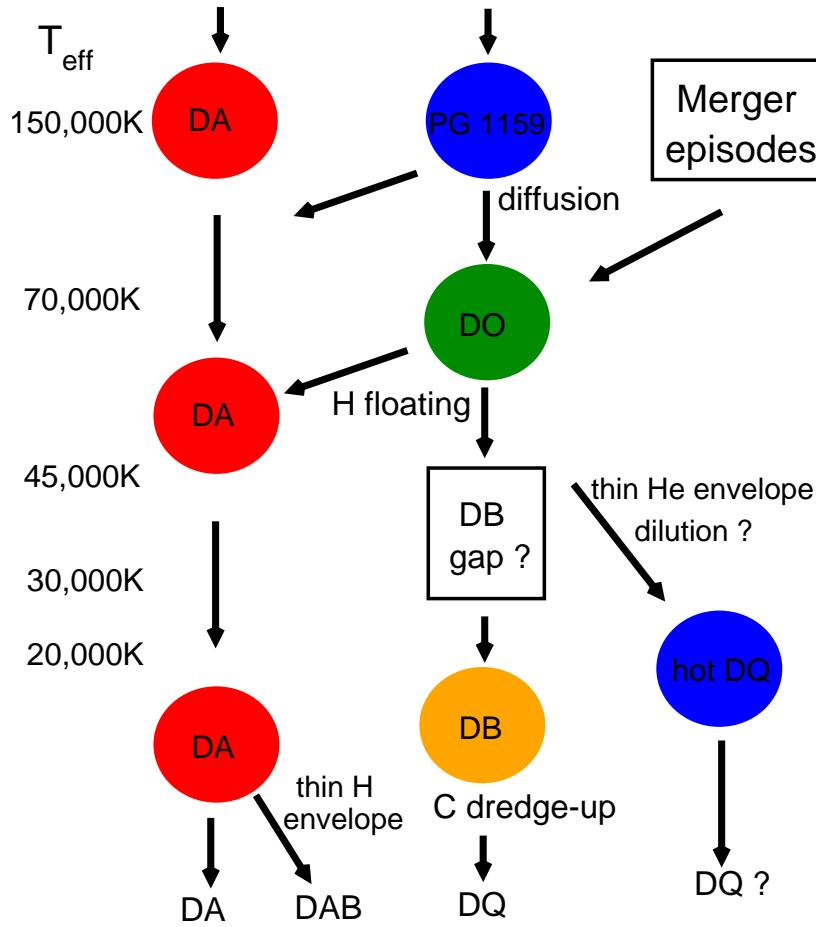
Fig. 4 A scheme of the several evolutionary paths that hot white dwarfs may follow as they evolve. The left column gives the effective temperature. Most white dwarfs are formed with H-rich envelopes (DA spectral type), and remain as such throughout their entire evolution (second column). H-deficient white dwarfs like DOs may follow different paths, either from the hot and He-, carbon-, and oxygen-rich PG 1159 stars or from post-merger events. Traces of H in PG 1159s and DOs may lead to other white dwarf varieties. PG 1159 stars are also believed to be the predecesors of the recently discovered new class of white dwarfs: the hot DQs, with carbon-rich atmospheres. Accretion of metals by cool He-rich white dwarfs from interstellar medium or from circumstellar matter may lead to DZ white dwarfs.

ments. These are the so-called DA white dwarfs and they comprise about 85% of all white dwarfs — see Eisenstein et al. (2006) and references therein. To the other family belong the H-deficient white dwarfs with He-rich atmospheres, usually known as non-DA white dwarfs, which make up to almost 15% of the total population. H-deficient white dwarfs are thought to be the result of late thermal flashes experienced by post-AGB progenitors or of merger episodes. The non-DA white dwarfs are usually divided into several different subclasses: the DO spectral type (with effective temperatures $45\,000\ \mathrm{K} \leq T_{\mathrm{eff}} \leq 200\,000\ \mathrm{K}$) that shows relatively strong lines of singly ionized He (HeII), the DB type ($11\,000\ \mathrm{K} \leq T_{\mathrm{eff}} \leq 30\,000$ K), with strong neutral He (HeI) lines, and the DC, DQ, and DZ types ($T_{\mathrm{eff}} < 11\,000$ K) showing traces of carbon and metals in their spectra. As a DO white dwarf evolves, the

HeII recombines to form HeI, ultimately transforming into a DB white dwarf. The transition from DO to the cooler DB stage is interrupted by the non-DA gap (that occurs at $30\,000$ K $< T_{\mathrm{eff}} < 45\,000$ K) where few objects with H-deficient atmospheres have been observed (Eisenstein et al. 2006). To this list, we have to add those white dwarfs with hybrid atmospheres or peculiar abundances, and the recent discovery of a new white dwarf spectral type with carbon-dominated atmospheres, the "hot DQ" white dwarfs, with $T_{\mathrm{eff}} \sim 20\,000$ K (Dufour et al. 2007, 2008a). Hot DQ white dwarfs are thought to be the cooler descendants of some PG 1159 stars, and the result of convective mixing at smaller effective temperatures (Dufour et al. 2008a; Althaus et al. 2009b).

Although this classification is in line with our understanding that most giant stars will evolve into white dwarfs with either H-rich atmospheres or H-deficient composition, the existence of some of these white dwarfs poses a real challenge to the theory of stellar evolution, which cannot adequately explain their origin. Finally, there is ample observational evidence that individual white dwarfs undergo spectral evolution, i.e., the surface composition of a given white dwarf may change as it evolves as a result of competing processes such as convection, mass-loss episodes, accretion, radiative levitation and gravitational settling. The interplay between these processes may help to understand the different evolutionary paths that white dwarfs may follow as the surface temperature decreases, see Fig. 4. For instance, the empirical evidence that the ratio of DA to non-DA white dwarfs changes with effective temperature and the existence of the non-DA gap are interpreted as the result of changes in the surface composition from He-dominated to H-dominated and vice versa as evolution proceeds. Also, the presence of traces of H in the outer layers of the hot H-deficient white dwarfs like PG 1159s or DOs can turn the spectral type of these white dwarfs into that of a DA type as a result of gravitational settling.

White dwarfs span a wide range of both effective temperatures and luminosities. Values of T_{eff} range from about $150\,000$ K for the hottest members to $4\,000$ K for the coolest degenerate dwarfs. The stellar luminosity ranges from roughly 10^3 to about 10^{-5} $L_{\odot}$ for the faintest observed white dwarfs. The majority of known white dwarfs have temperatures higher than the Sun and hence the "white" in their name. Because the intrinsic faintness of most white dwarfs, quantitative studies of these stars, traditionally based on photometric and spectroscopic observations, are restricted to nearby objects. Hence, the vast majority of observed white dwarfs are representative of the solar neighborhood. Other observational techniques and the advent of large-scale ground-based surveys and deep Hubble Space Telescope exposures, have revealed the presence of white dwarf populations located well beyond our own neighborhood, such as in distant open and globular clusters and, most probably, in the Galactic halo, thus enabling us to extract information and to constrain the properties of such populations.

2.5 Simple treatment of white dwarf structure and evolution

As previously mentioned, white dwarfs have numerous applications in different fields of astrophysics. In particular, the use of white dwarfs as accurate cosmic clocks has led over the years to the development of detailed evolutionary models of these stars, including sophisticated constitutive microphysics. Before describing such models, we will discuss a simple treatment of white dwarf evolution. At the high densities of white dwarf interiors, matter is completely pressure-ionized and the chemical potential of the electron gas is much larger than the thermal energy. This means that the Fermi-Dirac distribution that characterizes electrons reduces to a step-like function. In particular, all the energy states up to the Fermi energy

(ε_F) are occupied. Thus, to a very good approximation, electrons are almost completely degenerate, and those electrons with energies close to ε_F will make the largest contribution to the pressure. Hence, to a first approximation, the mechanical structure of white dwarfs can be described in terms of a Fermi gas at zero temperature.

A key feature to understand the evolution of white dwarfs is that in degenerate configurations, the mechanical and thermal structures are, to a good approximation, decoupled from each other and, thus, can be treated separately. This basic property of degenerate structures will allow us to derive a simple picture of how white dwarfs evolve with time and to discuss the role played by the different physical processes in the evolution of these stars. Indeed, the remaining thermal reservoir (which implies $T \neq 0$) is responsible for radiation and, thus, for the evolution of white dwarfs. Instead, for the mechanical structure, the limit $T = 0$ is usually assumed. Accordingly, in what follows, we will treat the mechanical and thermal structures separately. We begin by describing the structure of white dwarfs, as given by the zero-temperature approximation. Then in Sect. 2.5.2 we will describe a simple model to understand the basic thermal properties of white dwarfs responsible for their evolution. We will show that evolution can be described essentially as a rather simple cooling process, where the source of star luminosity is approximately provided by the change in the internal energy stored in the ions.

2.5.1 Zero-temperature approximation: Chandrasekhar's theory

In this approximation, the structure of a white dwarf is determined by the pressure of non-interacting completely degenerate electrons. In the limit of complete degeneracy, the electron pressure can be easily derived by considering only the energy states up to ε_F. The pressure and mass density have the well-known form:

$$
\begin{aligned}
P &= \frac{8\pi}{3h^3} \int_0^{p_F} \frac{(p^4/m_e)dp}{\sqrt{1+(p/m_ec)^2}} \\
&= A\,[x(x^2+1)^{1/2}(2x^2-3) + 3\sinh^{-1}(x)] \\
\rho &= C\,x^3,
\end{aligned}
\tag{1}
$$

where the dimensionless Fermi momentum is given by $x = p_F/m_ec$, $A = \pi m_e^4 c^5/3\,h^3$ and $C = 8\pi m_e^3 c^3 \mu_e M_u/3\,h^3$, and the rest of the symbols have their usual meaning. Note that this expression is valid for any relativistic degree.

For a spherically symmetric white dwarf at zero temperature, the equilibrium structure is specified by the equations of hydrostatic equilibrium and mass conservation

$$
\begin{aligned}
\frac{dP}{dr} &= -\frac{Gm\rho}{r^2} \\
\frac{dm}{dr} &= 4\pi r^2 \rho \;,
\end{aligned}
\tag{2}
$$

together with the equation of state given in Eq. (1) and the usual boundary conditions. Here, r is the radial coordinate and m the mass inside a sphere of radius r.

Chandrasekhar (1939) showed that the problem can be reformulated into a second order differential equation for a dimensionless function with essentially two parameters that have

to be specified: the chemical composition via the molecular weight per electron (μ_e) and the central density. To see this, note first that Eqs. (2) can be casted in the form

$$\frac{d}{dr}\left(\frac{r^2}{\rho}\frac{dP}{dr}\right) = -4\pi G r^2 \rho \ . \tag{3}$$

Introducing the variables $\eta = r/\alpha$, $y = \sqrt{1+x^2}$, and $\Phi = y/y_0$, it is straightforwardly found

$$\frac{1}{\eta^2}\frac{d}{d\eta}\left(\eta^2\frac{d\Phi}{d\eta}\right) = -\left(\Phi^2 - \frac{1}{y_0^2}\right)^{3/2}, \tag{4}$$

where $y_0^2 = x_0^2 + 1$ is related to the central density, ρ_0, via Eq. (1), that is, $\rho_0 = C(y_0{}^2 - 1)^{3/2}$ and α is given by

$$\alpha = \left(\frac{2A}{\pi G}\right)^{1/2}\frac{1}{Cy_0}\ . \tag{5}$$

Eq. (4) describes the structure of completely degenerate configurations based on the equation of state of a degenerate electron gas. It takes into account the gradual change from non-relativistic to relativistic electrons, with increasing density. Eq. (4) is solved numerically with the boundary conditions: $\Phi(0) = 1$ and $\Phi(\eta_I) = 1/y_0$, where η_I defines the radius of the stellar configuration, $R = \alpha\,\eta_I$. For a fixed value of μ_e, i.e., a given chemical composition, a one-parameter family of models is thus obtained integrating Eq. (4) for different values of the central density, thus defining implicitly a relation between mass and radius such that the more massive the star, the smaller its size. This is the famous mass-radius relation for white dwarf stars. In the limit $\rho \to \infty$, the relativistic "softening" of the equation of state (for relativistic electrons, $P \sim \rho^{4/3}$) causes the radius R to become zero, while the mass approaches a limiting value $5.826/\mu_e^2\,M_\odot$, the Chandrasekhar limiting mass. According to our present understanding of stellar evolution, a core made of carbon and oxygen is expected for most white dwarfs. In this case, $\mu_e \approx 2$, and the Chandrasekhar mass becomes $1.45\,M_\odot$. For larger masses, gravitational forces overwhelm the electron pressure support, and no stable white dwarf can exist.

The theoretical mass-radius relation for white dwarfs, which can be improved by including corrections to the equation of state and finite-temperature effects, is an accepted underlying assumption in nearly all studies of white dwarfs properties, including the white dwarf mass distribution and the luminosity function, which in turn convey important information about Galactic evolution and about the late stages of stellar evolution. Because of this, it is essential to provide observational support for this theoretical relation. This means that it is necessary to obtain independent measures of the mass and radius of individual white dwarfs. The best way to do this is for white dwarfs in visual binaries, where the stellar mass can be inferred from Kepler's law and the radius can be obtained from a fit to the spectrum of the white dwarf atmosphere, once the distance to the binary system is known. Independent determinations of radius and mass can also be obtained from white dwarfs with measured gravitational redshifts in binary systems. Although independent mass and radius determinations are available only for a few white dwarfs, they strongly support the theoretical mass-radius relation and the existence of a limiting mass. Another remarkable consequence of these observational determinations is that they discard the existence

of white dwarfs with H-rich cores. Note that for white dwarfs with H-rich cores ($\mu_e \simeq 1$), the mass of the equilibrium configuration is much larger for a given stellar radius than that resulting from a carbon-oxygen composition. This is in agreement with the results of the stellar evolution theory, which predicts that H is burnt into heavier elements in evolutionary stages previous to the white dwarf formation.

The Chandrasekhar limiting mass is one of the most important concepts in astrophysics. The existence of a limiting mass has strong implications not only for the theory of white dwarfs itself, but also for stellar evolution in general. This is particularly true regarding the occurrence of mass-loss episodes: low-mass stars must lose a large fraction of their mass at some point of their evolution to end-up as white dwarfs with masses smaller than $1.4 M_\odot$. Finally, the concept of the Chandrasekhar limiting mass is intimately connected with the most energetic events known in the Universe: supernovae. Those supernovae which do not show H in their spectra — known as type I supernova (SNIa), or thermonuclear supernovae — are thought to be the result of a instability of a white dwarf with a mass close to the Chandrasekhar mass. One of the two proposed mechanisms to explain the properties of SNIa involves a massive white dwarf progenitor in a binary system accreting from a non-degenerate companion — see Branch et al. (1995) and Kotak (2008) for a recent review. The second mechanism involves the merger of two white dwarfs with sufficiently large stellar masses due to the secular radiation of gravitational waves in a close binary system — see Lorén–Aguilar et al. (2009) and references therein for recent three-dimensional calculations of this phenomenon. In the first scenario, mass transfer from an accretion disk onto the massive white dwarf may cause the white dwarf to exceed the Chandrasekhar mass, thus leading to a thermonuclear runaway and a explosion that completely disrupts the white dwarf. In the second scenario, the coalescence process may lead to high enough temperatures to ignite the degenerate merger remnant, leading again to the same final output. On the other hand, core collapse supernovae arise from stars with degenerate cores with masses larger than the Chandraskhar limiting mass.

2.5.2 Mestel's model of white dwarf evolution

The zero-temperature model we have described in the previous section provides an appropriate description of the mechanical structure of white dwarfs. However, white dwarfs are not zero temperature stars. In fact, they are observed to have high surface temperatures and to lose energy, which implies the existence of temperature gradients, and consequently of higher interior temperatures. Thus, white dwarfs are not static objects and are expected to experience some kind of evolution. As we already mentioned, the advantage of dealing with degenerate configurations is that the mechanical and thermal properties are effectively decoupled from each other. This allows us to capture the main features of white dwarf evolution by means of a very simple model, which is often referred to as the Mestel's model (Mestel 1952). Here, the problem of the evolution of white dwarfs reduces essentially to two main aspects. The first of these consists in the determination of the total energy content, E, of the star, whilst the second one is the determination of the rate at which this energy is radiated away.

The first problem involves a detailed knowledge of the thermodynamics of the degenerate core of the white dwarf, which contains more than 99% of the mass, and the structure of which is specified, as we saw, by completely degenerate electrons ($T = 0$). An important property of the core, which simplifies the evaluation of E, is that it is characterized by an almost constant temperature, T_c. This is because degenerate electrons are very efficient at transporting energy, and thus a very small temperature gradient is required to transport

the energy flux in the core. Although the assumption of an isothermal core is not valid in young and hot white dwarfs, where neutrinos constitute a main energy sink, it is completely justified in evolved and cool white dwarfs. The second problem involves the solution of the equation of energy transfer through the non-degenerate envelope above the core. In the envelope, energy is transferred by radiation and/or convection, which are less efficient mechanisms than electron conduction. In fact, the extremely large temperature drop between the core and the surface occurs mainly in the opaque envelope. Because of this, the envelopes of white dwarfs play a key role in white dwarf evolution, since they control the rate at which energy is transferred from the core into space.

In what follows, a simple approach to solve the problem of energy transfer in the outer layers of a white dwarf will be explained. By making reasonable simplifications, simple power law relations between the surface luminosity, the stellar mass and the central temperature of the white dwarf will be derived. The first of these simplifications concerns the way in which energy is transported throughout the envelope. We will assume that energy is transferred only by radiation, which is true except for cool white dwarfs, where convection is the dominant mechanism of transport in the outer layers. In this case, the structure of the envelope is specified by the equation of hydrostatic equilibrium, Eq. (2), and the equation of radiative transfer, as given by the photon diffusion equation (Kippenhahn & Weigert 1990)

$$\frac{dT}{dr} = -\frac{3}{4ac} \frac{\kappa\rho}{T^3} \frac{L_r}{4\pi r^2} \,,$$
(6)

where L_r is the luminosity or the net flux of energy transported through the sphere of radius r (erg /s), and κ is the radiative opacity. A common approximation for the radiative opacity is to adopt Kramers's law for bound-free and free-free processes: $\kappa = \kappa_0 \, \rho \, T^{-3.5}$, where κ_0 depends on the chemical composition of the envelope. We will also assume that the envelope is thin enough that $m \approx M$ (low density), and that any source or sink of energy can be neglected in the envelope, so that $L_r \approx L$, where L means the surface luminosity. Under these assumptions, the equation for the thermal structure of the envelope can be derived by dividing the hydrostatic equilibrium equation by Eq. (6):

$$\frac{dP}{dT} = \frac{16\pi ac}{3\kappa_0} \frac{GMT^{6.5}}{\rho L} \,.$$
(7)

To integrate this equation the equation of state for the envelope must be specified. Because white dwarfs are observed to have high effective temperatures, and considering the smaller densities characterizing the very outer layers, we expect the envelope to be non-degenerate. Thus, we will assume that the equation of state is that of a non-degenerate, ideal gas (ions and electrons), which is given by

$$P = \frac{\Re}{\mu}\rho T \qquad \text{with} \quad \mu^{-1} = \sum_i (1+Z_i)\frac{X_i}{A_i} \,.$$
(8)

Here $\Re$ is the gas constant, μ is the mean molecular weight, A_i the atomic weight, Z_i the charge number, and X_i the abundance by mass fraction of the chemical species i. Thus, Eq. (7) becomes now

$$P\,dP = \frac{16\pi ac}{3\kappa_0}\,\frac{\Re GM}{L\mu}\,T^{7.5}\,dT\,. \tag{9}$$

We integrate this equation from the surface, where we assume $P = 0$ and $T = 0$, to the base of the envelope as defined by the transition layer. This layer is an idealized representation of the abrupt transition that separates the inner degenerate core from the thin, non-degenerate envelope. The integration yields

$$\rho_{\mathrm{tr}} = \left(\frac{32\pi ac}{8.5\,3\kappa_0}\,\frac{\mu}{\Re}\,\frac{GM}{L}\right)^{1/2}\,T_{\mathrm{tr}}^{3.25}\,, \tag{10}$$

which provides a relation between the density and temperature at the transition layer (ρ_{tr} and T_{tr}, respectively) for a white dwarf characterized by stellar mass M and surface luminosity L. At the transition layer, the pressure of degenerate electrons is equal to the pressure of an ideal gas (pressure is continuous across the transition layer). This gives us another relation between density and temperature at the transition layer. Note that we consider non-relativistic electrons. In the non-relativistic limit, $x \to 0$ and Eqs. (1) reduce to $P \sim (\rho/\mu_e)^{5/3}$. Thus, we have

$$10^{13}\left(\frac{\rho_{\mathrm{tr}}}{\mu_e}\right)^{5/3} = \frac{\Re}{\mu_e}\rho_{\mathrm{tr}}T_{\mathrm{tr}} \quad\Longrightarrow\quad \rho_{\mathrm{tr}} = 2.4\times 10^{-8}\mu_e\,T_{\mathrm{tr}}^{3/2}\,. \tag{11}$$

Because we have assumed that the entire core is isothermal, we can replace T_{tr} by the core temperature, T_{c}. Finally, from the last two equations we arrive at a simple power law relation between the surface luminosity, the stellar mass and the central temperature of the white dwarf:

$$L = 5.7\times 10^5\,\frac{\mu}{\mu_e^2}\,\frac{1}{Z(1+X)}\,\frac{M}{M_\odot}\,T_{\mathrm{c}}^{3.5} \quad \mathrm{erg}\,/\mathrm{s}\,, \tag{12}$$

where Z and X are, respectively, the metallicity of the envelope and the H abundance by mass.

Although some of the assumptions made in the treatment of the envelope are not usually verified in white dwarfs, the simple relation given by Eq. (12) enables us to infer some important features of these stars. Specifically, for typical compositions and a stellar mass of $M = 1\,M_\odot$, we find that for $L = 10\,L_\odot$ and $L = 10^{-4}\,L_\odot$, the central temperatures are of the order of $T_{\mathrm{c}} \approx 10^8$ K and $T_{\mathrm{c}} \approx 4\times 10^6$ K, respectively. The high central temperatures expected for high-luminosity white dwarfs discard the presence of H in the degenerate core. In fact, simple stability arguments show that at the high densities of the core, stable nuclear burning is not possible, because the white dwarf would be destroyed by a thermal runaway (Mestel 1952). The fact that no nuclear sources can be present in the core of white dwarfs at their birth, constrains their origin and suggests that white dwarfs must be the result of complete H exhaustion occurred at some point in the evolution of their progenitors.

Before proceeding forward, we can make a simple estimate of the radial extent of the envelope of a typical white dwarf. To this end, we use Eqs. (6) and (10), and Kramers' law to obtain

$$dT = -\frac{1}{4.25}\,\frac{GM\mu}{\Re}\,\frac{1}{r^2}\,dr. \tag{13}$$

We integrate this equation over the radial extent of the envelope

$$\int_0^{T_{\mathrm{tr}}} dT = -\frac{1}{4.25}\,\frac{GM\mu}{\Re}\int_R^{R_{\mathrm{tr}}} \frac{1}{r^2}\,dr, \tag{14}$$

to obtain

$$T_{\mathrm{tr}} = \frac{1}{4.25}\,\frac{G\mu}{\Re}\,\frac{M}{R}\left(\frac{R}{r_{\mathrm{tr}}} - 1\right) \tag{15}$$

For a low-luminosity white dwarf with $M = 1\,M_\odot$, $R = 0.01\,R_\odot$ and $T_c = 4 \times 10^6$ K, we get $R - r_{\mathrm{tr}} \approx 30$ km. Thus, a very thin envelope isolates the degenerate core from the outer space. Through this thin envelope, the temperature drops appreciably from the central to surface values. Although the envelope controls the rate at which energy is transferred from the core to the space, it has nevertheless little influence on the structure of the white dwarf. In fact, the radius of a white dwarf is well approximated by the calculations that assume complete degeneracy throughout.

The absence of nuclear energy sources in the white dwarf interiors brings us to our first point, namely the total energy content, E, of a white dwarf. The precise question to be answered is the following one. If there is no stable nuclear burning, which energy sources are involved when a normal white dwarf radiates energy? It is clear that some energy source or reservoir must be present, since if this was not the case it may not shine. We will focus on this issue in what follows. The first point to be noted is that although white dwarfs cannot contract appreciably, because of electron degeneracy — under the conditions of strong degeneracy, pressure is almost independent of temperature — the residual contraction resulting from the gradually decreasing ion pressure plays an important role in the energy budget of the star. This is because white dwarfs are compact objects, and hence a small change of the radius releases an important amount of gravitational energy. For instance, for a white dwarf with $M = 1\,M_\odot$, a change of 1% in the radius produces a change in the gravitational energy

$$|\Delta E_{\mathrm{grav}}| \propto \frac{GM^2}{R}\,\frac{\Delta R}{R} \sim 10^{48}\text{ erg}. \tag{16}$$

At a typical luminosity of $L = 0.1\,L_\odot$, this energy would be lost in about 10^8 yr. Thus, the energy released by contraction is by no means negligible. It can be shown from the virial theorem for degenerate configurations that the gravitational energy released during contraction is of the same order of magnitude of the stellar luminosity L.

If we neglect neutrino losses, the total energy content of the white dwarf results from contributions of ions, electrons and gravitational energy, i.e., $E = E_{\mathrm{ion}} + E_{\mathrm{elec}} + E_{\mathrm{grav}}$. The luminosity is given by the temporal decrease of the total energy E:

$$L = -\frac{dE}{dt} = -\frac{d}{dt}(E_{\mathrm{ion}} + E_{\mathrm{elec}} + E_{\mathrm{grav}}). \tag{17}$$

According to the virial theorem for degenerate configurations, the release of gravitational energy is used to increase the Fermi energy of the electrons, ε_F — specifically the density-dependent contribution of the energy of electrons (Koester 1978). This behavior is different from that of a non-degenerate gas, where the released gravitational energy is used to increase the internal energy of both ions and electrons. This gives rise to an important simplification of the treatment, since in order to compute the temporal change of E, only the changes in the *thermal* contribution to E need to be considered. Indeed, if we assume that the core is isothermal, the luminosity of the star can be written in terms of the decrease of the central temperature as

$$L = -\frac{\partial}{\partial T_c}(E_{\text{ion}}^T + E_{\text{elec}}^T)\frac{dT_c}{dt}. \tag{18}$$

where E_{ion}^T and E_{elec}^T are the total ion and electron thermal energies. Thus, in terms of the specific heat of ions and electrons, the luminosity equation becomes

$$L = -\langle C_V \rangle M \frac{dT_c}{dt}, \tag{19}$$

where $\langle C_V \rangle = C_V^{\text{elec}} + C_V^{\text{ion}}$ and M is the white dwarf mass. Thus, we have a simple relation between the luminosity and the rate of change of the central temperature. Clearly, the source of luminosity of a white dwarf is essentially the decrease in the thermal energy of ions and electrons. Because of this, white dwarf evolution is described as a cooling process. However, at low temperatures, $C_V^{\text{elec}} \ll C_V^{\text{ion}}$, since strongly degenerate electrons barely contribute to the specific heat. In fact, for strongly degenerate electrons, we have

$$C_V^{\text{elec}} \propto \frac{k_B T}{\varepsilon_F} \to 0. \tag{20}$$

Thus, we arrive at the core feature of white dwarf evolution: the source of luminosity of a cool white dwarf is basically the change of the internal energy stored in the ions.

Using the relation between luminosity and central temperature given by Eq. (12), which reads $L = CMT_c^{3.5}$, where C is a constant, we get

$$CMT_c^{3.5} = -\langle C_V^{\text{ion}}\rangle M \frac{dT_c}{dt}. \tag{21}$$

We now assume an ideal gas for a single ion. That is, we adopt $C_V^{\text{ion}} = 3\Re/2A$, where A is the atomic weight, and integrate Eq. (21) from an initial time t_0 to the present time t. We define the *cooling time* as $t_{\text{cool}} = t - t_0$, and the following cooling law is obtained

$$t_{\text{cool}} \approx \frac{10^8}{A}\left(\frac{M/M_\odot}{L/L_\odot}\right)^{5/7} \text{years}, \tag{22}$$

where it has been assumed that the central temperature at the beginning of white dwarf formation is much larger than the present central temperature of the white dwarf. This is the Mestel's model of white dwarf evolution (Mestel 1952), and it provides a simple power law relation between the cooling time of a white dwarf, and its stellar mass, surface luminosity,
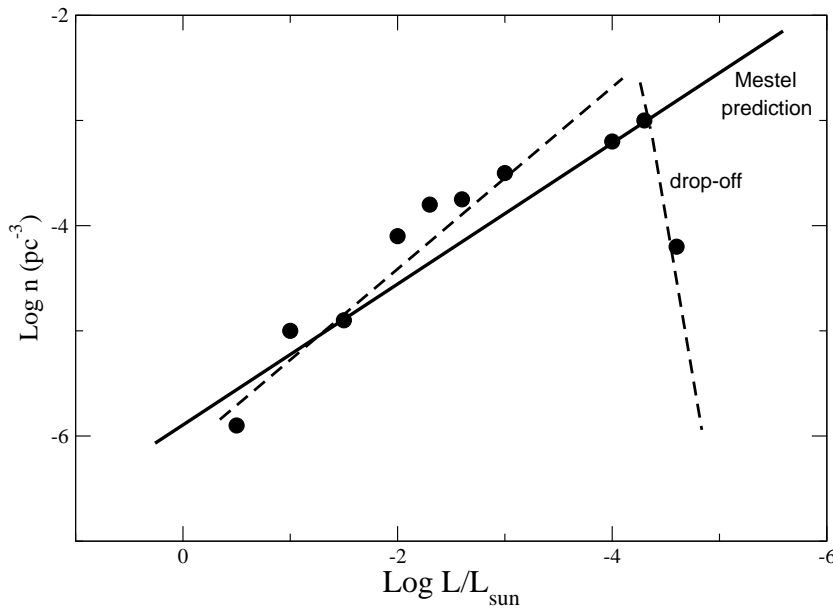
Fig. 5 A schematic view of the observed white dwarf luminosity function, as a function of the luminosity (dots). The prediction of the Mestel law is shown as solid line. Note the sharp cutoff at low luminosities.

and core chemical composition. For $A = 12$ (a pure carbon core), typical cooling ages for the faintest observed white dwarfs ($L \sim 10^{-4.5} L_{\odot}$) of 10^{10} yr are derived. These evolutionary timescales are sufficiently long that white dwarfs remain visible for a long time. Thus, the white dwarf phase constitutes a major phase in stellar life. Cool white dwarfs are very old objects, and considering the relative simplicity of the physical processes responsible for their evolution, these stars turn out to be robust tools to date stellar populations.

Although Mestel's model is the simplest picture of how white dwarfs evolve, it captures the essentials of the physics of white dwarf evolution. It shows that the cooling time of a white dwarf is related essentially to its core chemical composition, its mass and its luminosity. The following major features emerge:

1. The cooling times depend on the core chemical composition (A) of the white dwarf: oxygen white dwarfs are expected to cool faster than carbon white dwarfs because the specific heat per gram of oxygen is smaller than that of carbon — there are more ions in a gram of carbon than in a gram of oxygen.
2. Because of their larger thermal content, in principle, massive white dwarfs are characterized by longer cooling times. Moreover, it has to be taken into account as well that these white dwarfs also have much smaller radii and, thus, they have smaller luminosities.
3. The cooling times increase as the luminosity decreases.

2.5.3 Improvements to Mestel's model

As previously mentioned, the white dwarf luminosity function gives the number of white dwarfs per unit volume and interval of magnitude, as a function of the magnitude. To a first approximation, this number is proportional to the characteristic cooling time, $\tau_{cool} =$

$dt_{cool}/d\log(L/L_\odot)$. According to Mestel's law, more and more white dwarfs should be observed at fainter luminosities, as it is indeed the case, see Fig. 3. Nonetheless, as clearly shown in Fig. 3, the white dwarf luminosity function presents an abrupt drop-off at very low luminosities ($L \sim 10^{-4.5} L_\odot$). This steep cutoff cannot be explained within the frame of Mestel's theory. Fig. 5 depicts a schematic view of the observed white dwarf luminosity function together with the prediction given by the Mestel cooling law. Clearly, the theoretical model predicts that the number of white dwarfs should increase monotonically with decreasing luminosity. This discrepancy between theory and observation motivated the exploration of physical effects that might be responsible for shortening the cooling times at very low luminosities. However, nowadays we know that this shortage of white dwarfs at very low luminosities is a consequence of the finite age of the Galactic disk. Namely, we know that the origin of the cutoff is due entirely to the fact that the coolest white dwarfs have not had time enough to cool down to luminosities lower than that of the observed drop-off.

However, let us go step by step. The Mestel model is a reasonable description of the behavior of real white dwarfs only at intermediate luminosities, where the assumptions of ideal gas, isothermal core, and non-degenerate radiative envelope are more or less valid. Nevertheless, it requires major improvements if we want to use cool white dwarfs as reliable cosmic clocks. In what follows, we will comment on the main basic improvements to be considered in the physics of white dwarfs and on the expected impact on the cooling times.

2.5.4 Coulomb interactions and Debye cooling

At the high densities characteristic of white dwarf interiors, matter is completely pressure-ionized. As early recognized (Kirshnitz 1960; Abrikosov 1960; Salpeter 1961), Coulomb interactions modify the thermodynamical properties of the ion gas, in particular the specific heat. This, in turn, modifies the cooling times of white dwarfs, see Eq. (21). The strength of Coulomb interactions — relative to the thermal kinetic energy — is determined by the Coulomb coupling parameter $\Gamma = (Ze)^2/ak_BT = 2.26 \times 10^5 Z^{5/3}\rho^{1/3}/T$, where a is the inter-ionic separation and k_B is the Boltzmann constant. For small values of Γ, Coulomb forces are of minor importance (relative to thermal motions) and the ions behave like an ideal non-interacting gas. But, once Γ becomes of order unity, ions begin to undergo short-range correlations, eventually behaving like a liquid. For large enough Γ (~ 180) they form a lattice structure, experiencing a first order phase transition with the corresponding release of latent heat. This results in a new source of energy, which introduces an extra delay in the cooling of white dwarfs. In the case of Coulomb plasmas, the latent heat is small, of the order of k_BT_s per ion, where T_s is the temperature of solidification. Its contribution to the total luminosity is small, $\sim 5\%$, but not negligible (Shaviv & Kovetz 1976). In addition, there is an increase in the specific heat of ions in the crystallized region (according to the Dulong-Petit law) due to the extra degree of freedom associated with lattice vibration. But most importantly, as the white dwarf cools further, fewer modes of the lattice are excited, and the heat capacity drops according to the Debye law. This reduced heat capacity starts to manifest once the temperature drops below the Debye temperature ($\theta_D = 4 \times 10^3 \rho^{1/2}$), resulting in a fast cooling phase ($C_V \propto T^3$) once $\theta_D/T > 15$. As a result, the thermal content of the white dwarf gets smaller. This fast cooling is expected to take place in very cool white dwarfs, that is, those characterized by very low surface luminosities.

We can estimate the importance of the Debye cooling for white dwarfs as follows. From Eq. (21), and approximating the specific heat of ions in the Debye regime by $C_V^{ion} \sim 3.2\pi^4(T_c/\theta_D)^3\Re/A$, to a first approximation we obtain:

Table 1 Onset of Debye cooling.

M ($M_\odot$)	θ_D (K)	L ($L_\odot$)
0.6	7.0×10^6	10^{-7}
1.0	2.2×10^7	$10^{-5.1}$
1.2	4.0×10^7	$10^{-4.1}$

$$C \int_{t_0}^{t} dt' = -\frac{16\pi^4}{5} \frac{\Re}{A} \frac{1}{\theta_D^3} \int_{T_0}^{T} T_c^{-1/2} \, dT_c, \tag{23}$$

where T_0 is the initial temperature from which Debye cooling begins ($T_0 < \theta_D$) and $T < T_0$. The integration yields the cooling time during the Debye phase

$$t_D \sim \frac{32\pi^4}{5} \left(\frac{T}{\theta_D}\right)^3 \left[\left(\frac{T_0}{T}\right)^{1/2} - 1\right] \frac{TM}{L} \frac{\Re}{A}. \tag{24}$$

Note that the cooling time during the Debye phase is shorter than the result obtained from Mestels law (given by the last factor) when T is smaller than about $0.1\theta_D$. For instance, if $T = 0.05\theta_D$ then t_D is a factor of 4 smaller than that obtained using Mestel's law. It was hoped that this reduction in the cooling times would explain the deficit of observed white dwarfs below $\sim 10^{-4.5} L_\odot$. However, it is difficult to attribute to the onset of Debye cooling the deficiency of white dwarfs observed at low luminosities. This can be easily shown computing, for a given white dwarf mass, the luminosity at which Debye cooling becomes relevant using again the relation between the luminosity and the central temperature ($L = CMT_c^{3.5}$), and adopting the central temperature corresponding to the onset of rapid Debye cooling (of about $0.1\theta_D$, as we have just shown). We use the Chandrasekhar's model to estime the central density to compute θ_D. Table 1 lists, for a given stellar mass, the Debye temperature, θ_D, and the luminosity at the onset of the rapid Debye cooling phase. Note that, for a typical white dwarf, fast Debye cooling occurs at extremely low luminosities, and thus no observable consequences are expected in this case. Debye cooling is relevant at observable luminosities only for very massive white dwarfs, which are much less abundant, see Fig. 2.

¿From these simple estimates it can be concluded that the shortage of dim white dwarfs is difficult to explain in terms of a rapid cooling. The absence of very low luminosity white dwarfs suggests instead that the Galaxy is not sufficiently old to contain cooler (and thus older) white dwarfs. This means that the cutoff of the white dwarf luminosity function is the result of the finite age of the Galaxy — see, for instance, Winget et al. (1987), García-Berro et al. (1988b), and references therein, for a discussion. This feature has been extensively and quantitatively explored by numerous investigations to construct detailed white dwarf luminosity functions on the basis of sophisticated evolutionary models in order to constrain the age of the disk of our Galaxy and to understand crucial aspects of the history of the Galactic disk, like the past star formation rate.

2.5.5 Physical separation processes

As already mentioned, when the Coulomb coupling parameter reaches the critical value $\Gamma \simeq 180$, crystallization at the center of the white dwarf sets in. Coulomb interactions lead

quite naturally to crystallization, and the subsequent release of latent heat affects the evolution of white dwarfs, as shown in the pioneering works of Van Horn (1968) and Lamb & Van Horn (1975). The typical luminosities at which this occurs are $\log(L/L_\odot) \lesssim -3$. Later, Stevenson (1980) and Mochkovitch (1983) examined the release of gravitational energy associated with changes in the chemical composition induced by crystallization in carbon-oxygen mixtures. Because of the spindle shape of the phase diagram of carbon-oxygen mixtures, the solid formed upon cyrstallization is richer in oxygen than the liquid. As the solid (oxygen-rich) core grows at the center of the white dwarf, the lighter carbon-rich liquid left behind is efficiently redistributed by Rayleigh-Taylor instabilities (Isern et al. 1997). In addition, the effects of sedimentation during the liquid phase of minor species such as ^{22}Ne, the most abundant impurity present in the central regions of a white dwarf, and of ^{56}Fe, the second most important impurity, have also been studied — see Isern et al. (1991) and Xu & Van Horn (1992) respectively, and also Deloye & Bildsten (2002) and García–Berro et al. (2008) for the impact of ^{22}Ne sedimentation on the cooling times of white dwarfs. All these works show that a change in the composition of the cores of white dwarfs, either by phase separation upon crystallization or by sedimentation during the liquid phase, introduces an additional source of energy: the release of gravitational energy due to chemical differentiation.

Strong empirical evidence for the occurrence of these physical separation processes in the cores of white dwarfs has been recently presented in García–Berro et al. (2010). These authors have convincingly shown that these processes constitute an important piece of physics that has to be considered to date stellar populations using white dwarf cooling times. In particular, the contribution of phase separation of carbon-oxygen mixtures upon crystallization on the white dwarf cooling times can be assessed as follows. The local energy budget of the white dwarf can be written as:

$$\frac{dL_r}{dm} = -\varepsilon_\nu - P\frac{dV}{dt} - \frac{dE}{dt}, \tag{25}$$

where L_r is the local luminosity, ε_ν corresponds to the energy per unit mass per second due to neutrino losses, $V = 1/\rho$, and E is the internal energy per unit mass. If the white dwarf is made of two chemical species with atomic numbers Z_0 and Z_1, mass numbers A_0 and A_1, and abundances by mass X_0 and X_1, respectively ($X_0 + X_1 = 1$), where the suffix 0 refers to the heavier component, this equation can be written as:

$$-\left(\frac{dL_r}{dm} + \varepsilon_\nu\right) = C_v\frac{dT}{dt} + T\left(\frac{\partial P}{\partial T}\right)\frac{dV}{dt} - l_s\frac{dM_s}{dt}\delta(m - M_s) + \left(\frac{\partial E}{\partial X_0}\right)\frac{dX_0}{dt}, \tag{26}$$

where l_s is the latent heat and $\dot{M}_s$ is the rate at which the solid core grows. The delta function indicates that the latent heat is released at the solidification front (Isern et al. 1997; Isern et al. 2000). Chemical differentiation contributes to the luminosity not only through compressional work, which is negligible, but also via the change in the chemical abundances, which leads to the last term of this equation. We mention that, to a first order, the largest contribution to L_r from the change in E cancels the $P\,dV$ work for any evolutionary change (with or without a compositional change). This is, of course, a well known result that can be related to the release of gravitational energy. Integrating over the whole star, the next expression is obtained:

$$L + L_v = -\int_0^M C_v \frac{dT}{dt}\, dm - \int_0^M T \left(\frac{\partial P}{\partial T}\right) \frac{dV}{dt}\, dm$$
$$+ \; l_s \frac{dM_s}{dt} - \int_0^M \left(\frac{\partial E}{\partial X_0}\right) \frac{dX_0}{dt}\, dm \tag{27}$$

The first term of the equation is the well known contribution of the heat capacity of the star to the total luminosity. The second term represents the contribution to the luminosity due to the change of volume. It is in general small since only the thermal part of the electronic pressure, the ideal part of the ions, and the Coulomb terms contribute. However, when the white dwarf enters into the Debye regime this term provides about the 80% of the total luminosity, preventing the sudden disappearence of the star (D'Antona & Mazzitelli 1990). The third term represents the contribution of the latent heat to the total luminosity at freezing, Since the latent heat of a Coulomb plasma is small, its contribution to the total luminosity is modest although not negligible. The last term is the energy released by the chemical readjustment of the white dwarf, that is the release of the energy stored in the form of chemical potentials. In normal stars the last term is usually negligible, since it is much smaller than the energy released by nuclear reactions, but it must be taken into account when all other energy sources are small. It can be further expanded and related to the difference between the chemical abundance of the liquid and the solid as (Isern et al. 1997):

$$\int_0^M \left(\frac{\partial E}{\partial X_0}\right) \frac{dX_0}{dt}\, dm = (X_0^{\mathrm{sol}} - X_0^{\mathrm{liq}}) \left[\left(\frac{\partial E}{\partial X_0}\right)_{M_s} - \left\langle \frac{\partial E}{\partial X_0} \right\rangle\right] \frac{dM_s}{dt} \tag{28}$$

where $(\partial E/\partial X_0)_{M_s}$ is evaluated at the boundary of the solid core, and

$$\left\langle \frac{\partial E}{\partial X_0} \right\rangle = \frac{1}{\Delta M} \int_{\Delta M} \left(\frac{\partial E}{\partial X_0}\right) dm \tag{29}$$

The first term in the square bracket in Eq. (28) represents the energy released in the crystallizing layer — as a result of the increasing concentration of oxygen — and the second term is the energy absorbed on average in the convective region (ΔM) driven by the Rayleigh-Taylor instability above the cyrstallization front, as a result of the decreasing concentration of oxygen. Because $(\partial E/\partial X_0)$ is negative — since it is dominated by the ionic contributions, which are negative — and essentially depends on the density, the square bracket is negative, and thus the process of phase separation results in a net release of energy. It is clear that the energy released by this process will be dependent on the initial oxygen profile at the beginning of the white dwarf phase, resulting in a smaller contribution in the case of initially higher oxygen abundances. Note that a change in the initial chemical profile may also affect the degree of mixing in the liquid layers and thus the energy absorbed there, hence altering the net energy released by the process.

Furthermore, it is possible to define the total energy released per gram of crystallized matter due to the change in chemical composition as:

$$\varepsilon_g = -(X_0^{\mathrm{sol}} - X_0^{\mathrm{liq}}) \left[\left(\frac{\partial E}{\partial X_0}\right)_{M_s} - \left\langle \frac{\partial E}{\partial X_0} \right\rangle\right] \tag{30}$$

¿From this, the decrease in the cooling rate introduced by chemical differentiation upon solidification can be easily estimated to a good approximation if it is assumed that the luminosity of the white dwarf only depends on the temperature of the nearly isothermal core. In this case:

$$\Delta t = \int_0^M \frac{\varepsilon_{\mathrm{g}}(T_{\mathrm{c}})}{L(T_{\mathrm{c}})}\,dm \tag{31}$$

where ε_{g} is is the energy released per unit of crystallized mass and T_{c} is the temperature of the core when the crystallization front is located at m. For the case of an otherwise typical $0.6M_\odot$ white dwarf, the total energy released by chemical differentiation amounts to $\Delta E \sim 2 \times 10^{46}$ erg and the corresponding time delay at $L = 10^{-4.5}\,L_\odot$ is $\Delta t \sim 1.8$ Gyr. Of course, the total increase in the cooling times depends on the initial chemical profile and on the transparency of the envelope as well. The importance of the envelope is crucial for two reasons. Clearly, more transparent envelopes result in faster energy losses and shorter cooling times. The second reason is more subtle and has been largely overlooked until recently (Fontaine et al. 2001). At approximately the same evolutionary stage at which crystallization sets in, the external convection zone penetrates the region where thermal conduction by degenerate electrons is very efficient. Such an occurrence (known as convective coupling), initially produces a further decrease in the cooling rate, but this will be the subject of our next section.

2.5.6 Convection

In the envelope of cool white dwarfs, energy is transferred not only by radiation, but also by convection, which is a consequence of the recombination of the main atmospheric constituents. With decreasing temperature, the base of the convection zone gradually moves deeper into the star, following the region of partial ionization. As long as convection does not reach the degenerate core, the convergence of the envelope temperature profile to the radiative temperature gradient causes the central temperature to be independent of the outer boundary conditions, namely the chemical stratification of the envelope or the detailed treatment of convection. When this is the case the heat flow depends basically on the opacity at the edge of the degenerate core, as it is assumed in the Mestel approximation. However, at low luminosities convection reaches the degenerate core and the radiative gradient convergence is lost. The thermal profile of an old white dwarf becomes thus strongly constrained, with the consequence that changes in the atmospheric parameters are reflected in changes in the core temperature. In fact, the degenerate core is isothermal, and convection — which extends from the atmosphere to the outer edge of the core — is essentially adiabatic. This so-called convective coupling modifies the relationship between the luminosity of the white dwarf and its core temperature, and, thus, the rate of cooling of cool white dwarfs (D'Antona & Mazzitelli 1989; Fontaine et al. 2001). In particular, the core temperature becomes smaller — convection is much more efficient than radiation at transporting energy — as compared with the predictions of purely radiative envelopes. Due to the lower central temperature, the star has initially an excess of thermal energy that has to get rid of. This causes a decrease in the cooling rate at low luminosities. Depending on the chemical stratification of the outer layer, convective coupling occurs at different times in the lifes of white dwarfs (D'Antona & Mazzitelli 1989). This is critical to understand the different cooling speeds of cool white dwarfs with different envelope compositions. Finally, convection, and the corresponding mixing episodes, plays a key role in the interpretation of spectral evolution (the observed
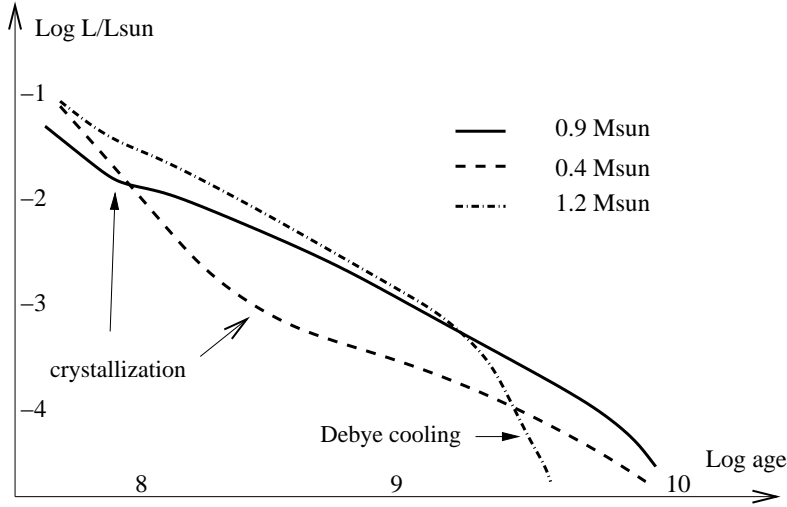
Fig. 6 Surface luminosity as a function of the cooling time for white dwarfs with a carbon core and different stellar masses. The onset of crystallization and Debye cooling are indicated. These cooling curves are based on reliable relationships between the luminosity and the central temperature, and better input physics than those assumed in the Mestel's model. See text for details.

change in surface composition of a white dwarf as it evolves) of these stars. This is particularly true if the white dwarf is formed with a thin H envelope, and convection penetrates beyond the surface H layers (Fontaine et al. 2001).

2.5.7 Specific heat of electrons

The Mestel model assumes that electrons are completely degenerate and so $C_V^{\rm elec} \ll C_V^{\rm ion}$. This is true for low-luminosity (low $T_{\rm c}$) white dwarfs, where the specific heat of strongly degenerate electrons is $C_V^{\rm elec} \propto k_{\rm B} T / \varepsilon_F \to 0$. But at high luminosities and particularly for low-mass white dwarfs, the energy of electrons is not completely independent of temperature. Hence, the specific heat of electrons must be considered in the calculation of the thermal energy content of the white dwarf. For instance, for a $0.5 M_\odot$ carbon-rich white dwarf at $T_{\rm c} \sim 10^7$ K ($L \sim 10^{-3} L_\odot$), $C_V^{\rm elec} \sim 0.25 C_V^{\rm ion}$.

2.5.8 Changes in the Mestel's cooling law

All the previously described physical processes alter the cooling times of white dwarfs given by the simple Mestel's cooling law. Improved cooling times can be obtained by considering $L - T_{\rm c}$ relations that take into account energy transfer by convection in the envelope of cool white dwarfs, and a better treatment of the opacity and of the equation of state in the envelope than that assumed in the Mestel model. These improved $L - T_{\rm c}$ relations together with a more realistic treatment of the thermal energy content that considers the effects of Coulomb interactions (plus the release of latent heat on crystallization) and Debye cooling, as well as the specific heat of electrons can be used to calculate improved cooling times. The

results of these calculations are depicted in Fig. 6 — see, for instance, Koester (1972). The main conclusions are:

1. The dependence of cooling times on the stellar mass is different from that predicted by the Mestel model ($\tau \propto M^{5/7}$). This is especially true at high luminosities where the contribution of electrons to the specific heat increases the cooling times of low-mass white dwarfs — because of their smaller electron degeneracy — and at low luminosities where massive white dwarfs cool faster as a result of Debye cooling.

2. The impact of crystallization on the cooling times is strongly dependent on the stellar mass and core composition. In particular, massive white dwarfs crystallize at very high luminosities because of their larger densities. Thus, the corresponding delay introduced by the release of latent heat has a smaller effect on the cooling times.

3. The cooling times strongly depend on core chemical composition, as predicted by the Mestel's model ($\tau \propto 1/A$).

4. At observable luminosities, Debye cooling is relevant only for $M > 1 M_\odot$.

3 The progenitors of white dwarfs

3.1 Which stars become white dwarfs?

It is generally accepted that the immediate progenitors of the vast majority of white dwarfs are nuclei of planetary nebulae, which are the products of intermediate- and low-mass main sequence star evolution. Stars that begin their lives with masses less than about $10 \pm 2 M_\odot$ are expected to become white dwarfs (Ritossa et al. 1999; Siess 2007). Comparing this limit with the mass distribution on the main sequence at birth, this means that certainly more than 95% of all stars will become white dwarfs. Typically, a $8 M_\odot$ progenitor seems to lead to a remnant of $\sim 1 M_\odot$ and a $1 M_\odot$ star to one of about $0.5 M_\odot$. Because the exceedingly large time required for a low-mass main sequence star (less than $0.8 M_\odot$) to become a white dwarf, most white dwarfs with stellar masses smaller than $0.4 M_\odot$ are expected not to be the result of single stellar evolution, but instead, the result of mass transfer in binary systems.

The fact that the maximum mass of a white dwarf is about $1.4 M_\odot$ — the Chandrasekhar limiting mass — hints at the occurrence of strong mass loss during the progenitor star evolution, particularly during the AGB stage, in agreement with the existing observations for this evolutionary phase. For instance, in the famous Hyades cluster, stars with about $2 M_\odot$, the turn-off point, are still on the main sequence, but the cluster contains several white dwarfs. These white dwarfs have typical masses of $0.6 M_\odot$, but on the main sequence their progenitors must have been more massive than the turn-off point, or they would not have evolved — see, for instance, Weidemann (2000) and references therein. The difference between the turn-off age of the cluster and the cooling age of white dwarfs determines the time that the progenitor of the white dwarf spent on the main sequence and on the giant phase and, thus, determines the original progenitor mass. In this way a relation between initial and final masses can be constructed — see, Catalán et al. (2008), Casewell et al. (2009) and Salaris et al. (2009) for recent determinations of the initial and final masses as inferred from white dwarfs in stellar clusters.
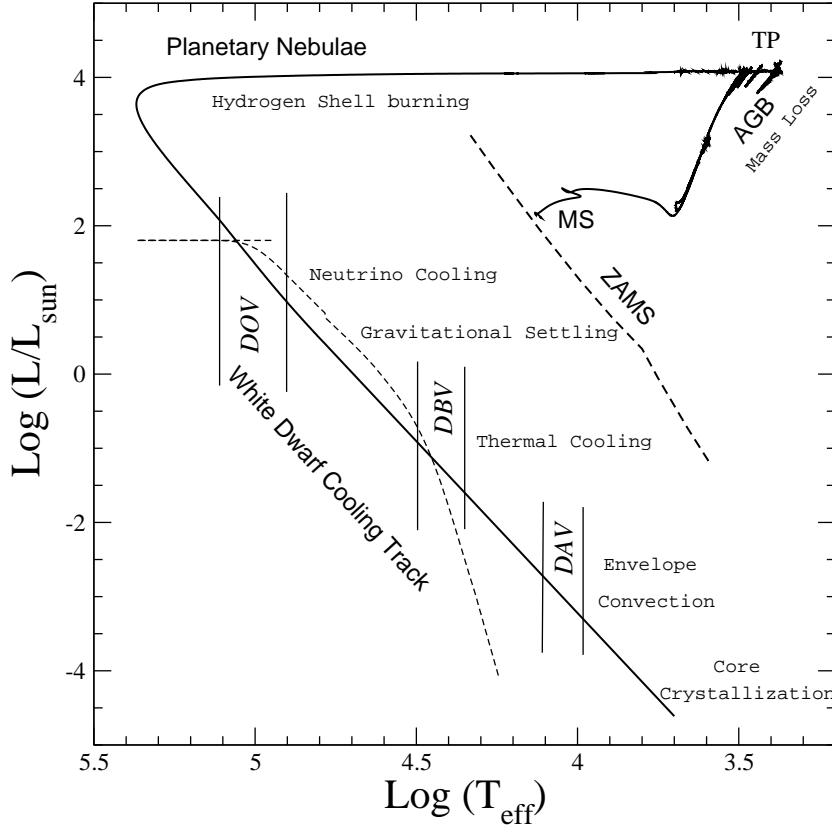
Fig. 7 Hertzsprung-Russell diagram for the full evolution of a $3.5\,M_\odot$ star from the ZAMS to the white dwarf domain. Mass-loss episodes at the thermally pulsing AGB reduce the stellar mass to $0.66\,M_\odot$. The various physical processes which occur as white dwarfs cool as well as the domain of the pulsating instability strips for the DOV, DBV and DAV are indicated. Thin dashed line displays the neutrino luminosity.

3.2 Prehistory of a typical white dwarf

The main phases in the life of a typical white dwarf progenitor are visualized in the Hertz-sprung-Russell diagram of Fig. 7. After the long-lived stage of central H burning during the main sequence phase, the progenitor star evolves to the red giant region to burn He in its core. Here, the carbon-oxygen core composition that will characterize the emerging white dwarf remnant is built up. After the end of core He burning, evolution proceeds to the AGB. There, the He burning shell becomes unstable and the star undergoes recurrent thermal instabilities commonly referred to as *thermal pulses*. As evolution proceeds along the AGB, the mass of the carbon-oxygen core increases considerably by virtue of the outward-moving He burning shell. Also, during this stage most of the remaining H-rich envelope is ejected through very strong mass-loss episodes. When the mass fraction of the remaining envelope is reduced to $\sim 10^{-3}\,M_\odot$ the remnant star moves rapidly to the left in the Hertzsprung-Russell diagram to the domain of the planetary nebulae. If the departure from the AGB takes place at an advanced stage in the He shell flash cycle, the post-AGB remnant may experience a last He thermal pulse on its early cooling branch, and eventually totally exhausts its residual H

content, thus giving rise to a H-deficient white dwarf (see below). When the remaining H envelope is reduced to $\sim 10^{-4} M_\odot$, nuclear energy generation becomes virtually extinct. The surface luminosity decreases rapidly, and the star enters the terminal phase of its life as a white dwarf.

The newly formed white dwarf is left mostly with only gravitational and thermal energy sources available. In fact, during most of its final evolution, the gravothermal (gravitational plus thermal energy) contribution drives the evolution, see Sect. 4. Since electrons are already degenerate in the interior, the stellar radius is not far from the equilibrium radius of the zero-temperature model, and the remaining contraction is small, but not entirely negligible. Hence, the star evolves almost at constant radius along a diagonal straight line in the white dwarf region of the Hertzsprung-Russell diagram.

3.3 The formation of white dwarfs with low H content

An important fraction of white dwarf stars is characterized by a H-deficient composition. In agreement with their DA counterparts, the mass distribution of these stars exhibits a sharp peak near $0.6 M_\odot$, but it lacks almost entirely the low- and high-mass components — see Sect. 5. The accepted mechanism for the formation of most H-deficient white dwarfs is the born-again scenario, that is the occurrence of a very late thermal pulse (VLTP) during the early stages of white dwarf evolution when H burning has almost ceased (Fujimoto 1977; Schönberner 1979; Iben et al. 1983; Herwig et al. 1999; Althaus et al. 2005a). During the VLTP, an outward-growing convection zone powered by the He burning shell develops and reaches the H-rich envelope of the star, with the consequence that most of the H content of the remnant is violently burned in the He flash-driven convection zone (Herwig et al. 1999; Miller Bertolami et al. 2006). The resulting H-burning luminosity, due mainly to proton captures by ^{12}C, may reach about $10^{11} L_\odot$ in a matter of a few hours. The star is then forced to evolve rapidly back to the AGB and finally into the domain of the He-, carbon-, and oxygen-rich PG 1159 stars (Werner & Herwig 2006) at high T_{eff}. Afterwards, the remnant evolves to the white dwarf domain, as a H-deficient star. We postpone the discussion of the evolutionary properties of H-deficient white dwarfs to Sect. 5.

Late thermal pulses (LTP) may also lead to the formation of white dwarfs with small H-rich envelopes. In contrast to a VLTP, a LTP occurs before the remnant star reaches the white dwarf stage, while the H burning shell is still active. This has the consequence that H will not be completely and violently burnt. Specifically, in a LTP the low H content results from the dilution of the residual H-rich envelope as a result of a dredge-up episode — when the remnant returns to the giant phase — and following stable proton burning at high effective temperatures. After a LTP episode, a large fraction of the residual H envelope is burnt. This is an important point since there is mounting evidence that some DA white dwarfs appear to be characterized by H-rich envelopes many orders of magnitude smaller than those predicted by the standard theory of stellar evolution. The hypothesis that LTPs may be responsible for the existence of such white dwarfs has been quantitatively explored by Althaus et al. (2005b), who have shown that a large fraction of the original H-rich material of a post-AGB remnant is indeed burned during the post-LTP evolution, with the result that, on the white dwarf cooling track the remaining H envelope becomes $10^{-6} M_\odot$, in agreement with asteroseismological inferences for some ZZ Ceti stars — see section 9.1 in this review and also Winget & Kepler (2008) and Castanheira & Kepler (2009).

This evolutionary scenario is illustrated in Fig. 8. Shortly after the occurrence of the LTP (A), the stellar remnant returns to the region of giant stars, where H is diluted by surface
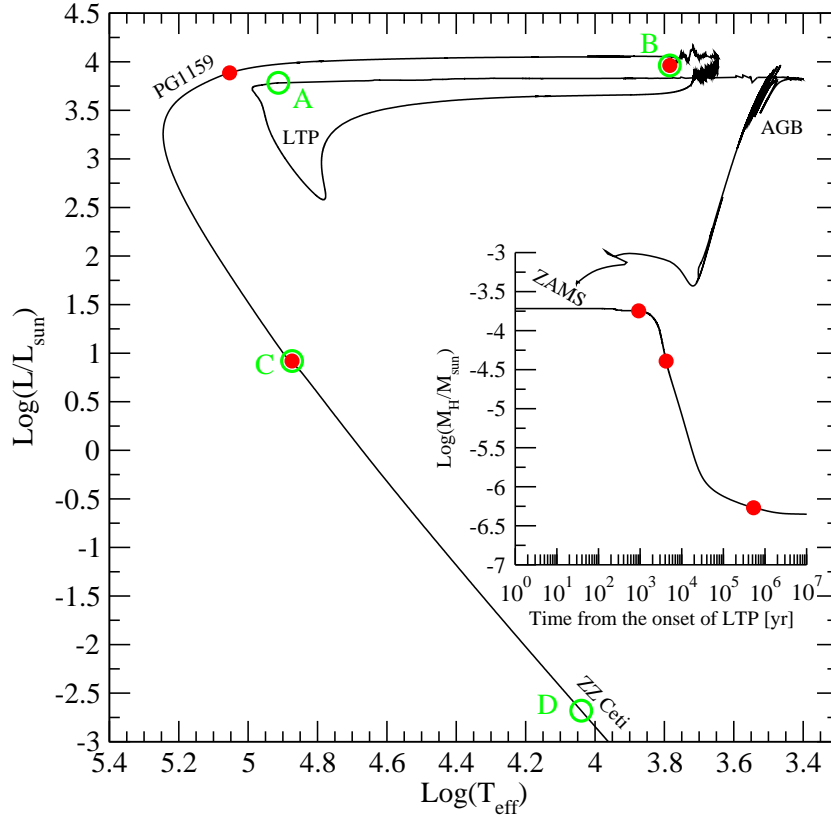
Fig. 8 Evolutionary scenario for the formation of a DA white dwarf with a thin H envelope. It is shown the Hertzsprung-Russell diagram for the complete evolution of the initially $2.7\,M_\odot$ stellar model from the ZAMS to the ZZ Ceti domain. The star undergoes a LTP after leaving the AGB at $\log T_{\text{eff}} = 4.9$ (A). As a result, the remnant evolves back to the red-giant domain where the H envelope is diluted by surface convection (B). Inset: temporal evolution of the H mass in solar units. Filled dots correspond to those stages indicated along the evolutionary track. Most of H is processed by nuclear burning during the PG 1159 stage. From Miller Bertolami et al. (2005).

convection and mixed inwards with the underlying intershell region formerly enriched in He, carbon and oxygen (B). Afterwards, evolution proceeds into the domain of the central stars of planetary nebulae at high T_{eff} to become a hybrid PG 1159 star. In the meantime, H is reignited and, after the point of maximum effective temperature is reached on the early white dwarf cooling track (C), the H content is reduced to $8 \times 10^{-7}\,M_\odot$, that is, about two orders of magnitude smaller than the amount of H predicted by the standard theory of stellar evolution. This value is the amount of H with which the star enters the white dwarf domain. The temporal evolution of the H content is illustrated in the inset of Fig. 8. Most of the residual H material is burnt over a period of roughly 100,000 yr during the PG 1159 stage. On the cooling track, H diffuses outwards, turning the white dwarf into one of the DA type with a thin pure H envelope of a few $10^{-7}\,M_*$.

3.4 The formation of low-mass white dwarfs

About 10% of the white dwarf population is characterized by stellar masses below $0.4\,M_\odot$ (Liebert et al. 2005). A handful of such white dwarfs have masses below $0.2\,M_\odot$ (Kawka & Vennes 2009). These low-mass white dwarfs constitute a separate sequence of white dwarfs with He cores (because the core mass is below that required for He ignition), necessarily resulting from binary star evolution. Indeed, the Galaxy is not old enough for these objects to have formed via single-star evolution. Instead, a companion has stripped the envelope from the now-visible white dwarf before it completed its red giant evolution. The binary nature has been confirmed by the numerous discoveries of periodic radial velocity variations of the Hα lines of low-mass DA white dwarfs (Marsh et al. 1995). Low-mass white dwarfs are usually found as the companions to millisecond pulsars (van Kerkwijk et al. 2005). This offers the possibility of constraining the ages and initial spin periods of the millisecond pulsars (Driebe et al. 1998; Hansen & Phinney 1998; Althaus et al. 2001; Benvenuto & De Vito 2005). In fact, millisecond pulsars are thought to be recycled during the mass transfer stage. When mass transfer ends, the pulsar begins to spin down, and from then on, the ages of the white dwarf and the pulsar component as inferred from its rate of period variation (spin down age) should be the same. Finally, the existence of some low-mass white dwarfs ($\sim 0.3\,M_\odot$) with carbon-oxygen cores resulting from single-star evolution is not discarded (Prada Moroni & Straniero 2009).

4 Detailed models of white dwarf evolution

Mestel's model with the improvements we have previously described provides a reasonable description of white dwarf evolution. However, if we want to use white dwarfs as reliable cosmic clocks to infer the age of stellar populations, we need to consider more elaborated treatments that include all the potential energy sources and the way energy is transported within the star. The main points to be considered are:

1. The thermal and hydrostatic evolution have to be treated simultaneously. In fact, the structure of a white dwarf changes with time in response to the energy radiated. This means that pressure is a function of density *and temperature.*
2. The thermal energy is not the only source of white dwarf luminosity. There are additional energy sources and sinks: residual contraction of the outer layers, nuclear burning, neutrino losses, and the gravitational energy released from physical separation processes in the core like carbon-oxygen phase separation upon crystallization and diffusion of minor species in the liquid phase.
3. The core of a white dwarf is never strictly isothermal, particularly in hot white dwarfs.
4. Changes in chemical composition during white dwarf evolution due to convective mixing, diffusion processes, nuclear reactions and accretion are expected to influence the cooling of white dwarfs.

A proper treatment of these issues requires a detailed knowledge of the previous history of the white dwarf. This is particularly true regarding the calculation of the early phases of white dwarf evolution at high luminosities where contraction is not negligible. In addition, the mass and chemical composition of the core and outer layers — which, as we saw, have a marked influence on the white dwarf evolution — are specified by the evolutionary history of the progenitor star. Thus, an accurate treatment of white dwarf evolution requires the use of complete stellar evolutionary codes to calculate the evolutionary history of the progenitor
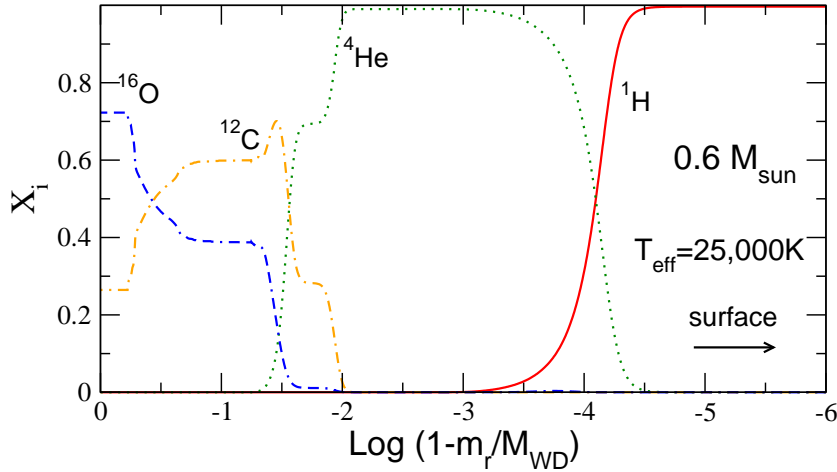
Fig. 9 ^{1}H, ^{4}He, ^{12}C, and ^{16}O distribution within a typical DA white dwarf in terms of the outer mass fraction $q = 1 - m/M$.

stars all the way from the main sequence, to the mass-loss and planetary nebulae phases. In what follows, we will comment on the main aspects to be considered in a detailed treatment of white dwarf evolution.

4.1 Chemical abundance distribution

The chemical composition of a white dwarf is determined by the nuclear history of the white dwarf progenitor. The chemical composition expected in a typical DA white dwarf is displayed in Fig. 9 in terms of the outer mass fraction q. The election of this coordinate strongly emphasizes the outer layers of the model. Three different regions can be distinguished: the carbon-oxygen core (95% of the mass), which is the result of convective He core burning and the subsequent steady He burning shell of prior evolutionary stages. Because of the larger temperatures in the helium burning shell, the oxygen abundance decreases in the outer regions of the carbon-oxygen core. Possible extra-mixing episodes during core He burning — like overshooting and semiconvection (Straniero et al. 2003) — and the existing uncertainties in the ^{12}C$(\alpha, \gamma)^{16}$O reaction rate turn the carbon-oxygen composition of the core into one of the main sources of uncertainty weighting upon the determination of white dwarf cooling times. The core chemical composition depends also on the initial stellar mass of the progenitor star. Lower oxygen abundances are generally expected in more massive white dwarf progenitors. In the case of massive white dwarfs — that is, those with $M \gtrsim 1.05 M_\odot$ — oxygen-neon cores are expected (Ritossa et al. 1996), while very low mass white dwarfs, are characterized by He cores. On top of the carbon-oxygen core is the He- and C- rich intershell, which is built up by mixing and burning episodes during the last thermal pulse on the AGB. The abundance of carbon in the intershell region, which stems from the short-lived convective mixing that has driven the carbon-rich zone upward during the peak of the last helium pulse on the AGB, depends on the occurrence of overshooting in the He-flash convection zone and on the number of previous thermal pulses. Except for the less massive white dwarfs, this intershell region is eroded by diffusion by the time evolution has reached the domain of the pulsating ZZ Ceti stars by $T_{\mathrm{eff}} \approx 12{,}000$K (Althaus et al. 2010a). Above

the intershell and below the H envelope, the He-rich buffer which results from prior H burning can be found. During the AGB, the mass of this buffer goes from almost zero — at the pulse peak when the He-flash convection zone is driven close to the base of the H layer — to $0.01\,M_\odot$.

The theory of stellar evolution provides upper limits for the mass of the various intershells. For a typical white dwarf of $0.6\,M_\odot$, the maximum H envelope mass that survives the hot pre-white dwarf stages is about $10^{-4}\,M_\odot$ and the total mass of the He buffer and the He-intershell amounts to $\sim 0.02\,M_\odot$. These values strongly depend on the stellar mass of the white dwarf (Renedo et al. 2010), and on the occurrence of LTP episodes, which may reduce the mass of the remnant H and He buffer considerably, see Sect. 3.3. Asteroseismological inferences on individual pulsating white dwarfs provide in some cases constraints to the thickness of the H and He envelopes and the core composition of white dwarfs (Winget & Kepler 2008). For instance, asteroseismological studies of DAVs carried out by Castanheira & Kepler (2008, 2009) indicate that the mass of the H envelope is in the range $10^{-4} \gtrsim M_{\mathrm{H}}/M_* \gtrsim 10^{-10}$, with a mean value of $M_{\mathrm{H}}/M_* = 5 \times 10^{-7}$, thus suggesting that an important fraction of DAs characterized by envelopes substantially thinner than those predicted by standard evolution could exist. We emphasize that the initial chemical stratification of white dwarfs is not known with sufficient detail from the stellar evolution theory or from observations. This, in turn, leads to some uncertainties in the evaluation of the cooling times.

4.2 Changes in the chemical abundance distribution

There are numerous physical processes that alter the chemical abundance distribution with which a white dwarf is formed. The effects of these changes on the evolutionary properties of white dwarfs may be important depending on the cooling stage or luminosity at which they occur. The most important of these processes is element diffusion. In particular, gravitational settling and chemical diffusion strongly influence the abundances produced by prior evolution. Gravitational settling is responsible for the purity of the outer layers that characterize most white dwarfs. In fact, because of the extremely large surface gravity of white dwarfs, gravitational settling rapidly leads to the formation of a pure H envelope, the thickness of which gradually increases as evolution proceeds. In some cases, the occurrence of accretion processes may lead to the existence of cool white dwarf with traces of heavy elements in their outer layers. At the chemical interfaces, characterized by large chemical gradients, chemical diffusion strongly smears the chemical profile, see Fig. 9. Here, the diffusion time scale is comparable to the white dwarf evolutionary time scale, so equations describing diffusion have to be solved simultaneously with the equations describing white dwarf evolution (Iben & Macdonald 1985; Althaus et al. 2003, 2005a).

Under certain circumstances, diffusion processes may trigger the occurrence of thermonuclear flashes in white dwarfs. In particular, note from Fig. 9 that inside the He buffer, chemical diffusion has led to a tail of H extending from the top layers and a tail of carbon from the bottom layers. If the white dwarf is formed with a thin enough He-rich buffer, a diffusion-induced H shell flash may be initiated, thus leading to the formation of a self-induced nova, during which the white dwarf increases its luminosity by many orders of magnitude in a very short time (Iben & MacDonald 1986). During this process, the mass of the H envelope is believed to be strongly reduced. Another physical process that may alter the chemical composition of a white dwarf is convection. Specifically, for cool white dwarfs with H envelopes thin enough ($< 10^{-6}\,M_\odot$), convective mixing will lead to dilution of H

with the underlying He layer, thus leading to the formation of He-rich outer layers. In addition, changes in the outer layer chemical composition are expected during the hot stages of white dwarf evolution as a result of residual nuclear burning. Finally, an efficient redistribution of carbon and oxygen upon crystallization, and sedimentation of minor species such as ^{22}Ne are expected to occur in the white dwarf core, with important energetics consequences, see sections 2.5.5 and 4.3.4.

4.3 Energy sources of white dwarfs

As we saw in Sect. 2.5.2, white dwarf evolution can be described essentially as a cooling process where the source of star luminosity is approximately provided by the change in the internal energy stored in the ions. However, there are additional energy sources and sinks that may considerably impact the cooling times, and hence they must be taken into account in detailed calculations:

4.3.1 Gravitational energy

Although white dwarfs evolve at almost constant radius, the role of contraction is by no means negligible. The radius at the beginning of the white dwarf phase can be up to twice the zero-temperature degenerate radius, and thus the contribution of compression to the energy output of the star can be important in very hot white dwarfs. In addition, changes in the internal density distribution owing to the increase in the core mass from H burning via the CNO cycle lead to an important release of gravitational potential energy from the core of pre-white dwarfs (or very young white dwarfs). Gravitational contraction is also relevant in the final evolutionary phases when Debye cooling has already depleted the thermal energy content of the core. Here, the residual contraction of the thin subatmospheric layers may provide up to 30% of the star luminosity. But, as mentioned in 2.5.2, for most of white dwarf evolution compression barely contributes to the surface luminosity. This stems from the fact that the compression work released in the core is almost completely employed by degenerate electrons to increase their Fermi energy.

4.3.2 Nuclear energy

Stable H shell burning via the CNO cycle and He shell burning are the main source of luminosity during the evolutionary stages preceding white dwarf formation. As a result of CNO burning, the H-rich envelope is consumed. Thus, below $\sim 100 L_\odot$ nuclear burning becomes a minor contribution to surface luminosity — the density and temperature at the base of the H-rich envelope become too low once $M_H \sim 10^{-4} M_\odot$. Thus, in a typical white dwarf, the role of nuclear burning as a main energy source ceases as soon as the hot white dwarf cooling branch is reached. But it never stops completely, and depending on the stellar mass and the exact amount of H left by prior evolution, it may become a non-negligible energy source for old DA white dwarfs. Detailed evolutionary calculations show that, for white dwarfs having low-metallicity progenitors, stable H burning via the proton-proton chains may contribute by more than 50% to the surface luminosity by the time cooling has proceeded down to luminosities ranging from $L \sim 10^{-2} L_\odot$ to $10^{-3} L_\odot$ (Iben & MacDonald 1985). More recent full calculations show that this H burning contribution at such low luminosities reaches 30% in the case of white dwarfs resulting from progenitors stars with metallicity $Z = 0.001$ (Renedo et al. 2010). However, predictions of the exact value of M_H and hence of the role

of residual H burning are tied to the precise mass loss history along the previous AGB and post-AGB phases, and particularly to the occurrence of late thermal pulses. In this sense it is worth mentioning that a small reduction in the H envelope by a factor of about 2 with respect to the upper theoretical limit is sufficient to strongly inhibit H burning, a fact that explains the different role of H burning obtained by different authors. Hence, a correct assessment of nuclear burning during the white dwarf stage requires the computation of the pre-white dwarf evolution, something that has not been possible until recently.

During the early stages of white dwarf evolution, unstable nuclear burning may also be relevant. As we mentioned in 3.3, a late He thermonuclear flash may take place after H burning is almost completely extinguished, thus eventually leading to a born-again episode and to the consumption of most of the H content. Also, a diffusion-induced H shell flash may occur at intermediate luminosities on the white dwarf cooling track, resulting in the formation of a self-induced nova (see Sect. 4.2). Again, a proper assessment of these nuclear burning episodes and their impact on the subsequent white dwarf evolution requires a detailed knowledge of the history of the progenitor star.

Finally, stable H burning may be dominant in low-mass white dwarfs, delaying their cooling for significant periods of time (Driebe et al. 1998; Althaus et al. 2001). These stars are the result of binary evolution and are characterized by thick H envelopes. In these low-mass white dwarfs, H burning can also become unstable, thus giving rise to thermonuclear flashes at early stages of white dwarf evolution. This bears important consequences for the interpretation of low-mass white dwarf companions to millisecond pulsars.

4.3.3 Neutrino losses

Energy is lost from white dwarfs not only in the form of photons, but also through the emission of neutrinos. Neutrinos are created in the very deep interior of white dwarfs and provide a main energy sink for hot white dwarfs. Because of their extremely small cross-sections for interaction with matter — at a central density of 10^6 gr/cm^3, typical of white dwarfs, the mean free path of neutrinos is $l_\nu \approx 3,000 R_\odot$ — once created, neutrinos leave the white dwarf core without interactions, carrying away their energy. In young white dwarfs, neutrinos increase the cooling rate and produce a temperature inversion. Neutrinos result from pure leptonic processes as a consequence of the electro-weak interaction. Under the conditions prevailing in hot white dwarfs the plasma-neutrino process is usually dominant, but for massive white dwarfs neutrino bremsstrahlung must also be taken into account (Itoh et al. 1996).

4.3.4 Additional energy sources

As discussed in Sect. 2.5.5, the energy balance during crystallization of the white dwarf core must take into account additional energy sources that have to be considered in a detailed treatment of white dwarf evolution. This comprises the release of latent heat and the release of gravitational energy associated with changes in the carbon-oxygen profile induced by crystallization (Salaris et al. 1997). As previously explained in that section, partial separation of carbon and oxygen, and hence changes of the initial distribution of these elements, is expected to occur after crystallization. The resulting release of gravitational potential energy depends on the initial fractions of carbon and oxygen and their distribution in the interior. The impact of these two energy sources on the white dwarf cooling times depends on the stellar mass of the white dwarf, resulting less relevant for the case of more massive white dwarfs, due to their larger luminosities at cyrstallization.

Finally, the gravitational settling of minor species in the core also make a contribution to the white dwarf luminosity. In particular, the slow diffusion of ^{22}Ne in the liquid white dwarf core releases enough gravitational potential energy as to impact the cooling times of massive white dwarfs (Deloye & Bildsten 2002; García–Berro et al. 2008; Althaus et al. 2010b). In fact, ^{22}Ne, which is the product of He burning on ^{14}N during prior evolution, has two extra neutrons (relative to $A = 2Z$). This results in an imbalance between the gravitational and electric fields, and leads to a slow gravitational settling of ^{22}Ne towards the center. As predicted by Deloye & Bildsten (2002), the possible impact of ^{22}Ne sedimentation on white dwarf cooling could be better seen in old, metal-rich clusters, such as NGC 6791, where the ^{22}Ne abundance expected in the cores of its white dwarfs could be as high as $\sim 4\%$ by mass. As a matter of fact, the occurrence of these physical separation processes — carbon-oxygen phase separation upon crystallization and ^{22}Ne sedimentation — in the core of cool white dwarfs and the associated slow down of the cooling rate has recently been demonstrated by García–Berro et al. (2010) to be a fundamental aspect to reconcile the longstanding age discrepancy in NGC 6791 (Bedin et al. 2008).

4.4 Energy transport in the outer layers

Although very thin, the non-degenerate outer layers control the rate at which energy flows from the interior into space. Because of this, a detailed knowledge of the processes responsible for energy transport in the outer layers constitutes a crucial aspect for an appropriate assessment of the cooling times (D'Antona & Mazzitelli 1990). The treatment is difficult because it involves energy transfer by radiation and/or convection in a partially degenerate, partially ionized and highly non-ideal gas. This difficulty becomes particularly relevant in cool white dwarfs, where convection has reached the degenerate core. In this case, the central temperature, and thus the cooling of white dwarfs, will be influenced by the thermal and pressure profiles of the subatmospheric layers, which have to be provided by non-gray model atmospheres. Over the years, detailed model atmospheres that include non-ideal effects in the gas equation of state and chemical equilibrium, and a complete treatment of energy absorption processes such as collision-induced opacity, have been developed (Bergeron et al. 1991; Saumon & Jacobson 1999; Rohrmann et al. 2002). In particular, the use of non-gray model atmospheres to derive outer boundary conditions gives rise to shallower outer convection zones, as compared with the standard gray treatment of the atmosphere. Finally, as a result of collision-induced absorption by molecular collisions at low effective temperatures, the emergent spectrum departs significantly from the blackbody emission and becomes blue as the effective temperature is lowered (Saumon et al. 1994; Hansen 1998; Rohrmann 2001), a prediction corroborated by deep Hubble Space Telescope exposures in globular clusters (Richer et al. 2006).

4.5 Results from detailed calculations

The time dependence of the luminosity contributions due to H burning (L_{nuc}) via proton proton and CNO nuclear reactions, He burning (L_{He}), neutrino losses (L_{neu}), gravothermal energy (L_{gravo}) — the release of thermal plus gravitational potential energy — and photon emission (surface luminosity, L_{sur}) for a typical white dwarf is shown in Fig. 10. The evolution from the planetary nebulae stage to the domain of the very cool white dwarfs is shown.
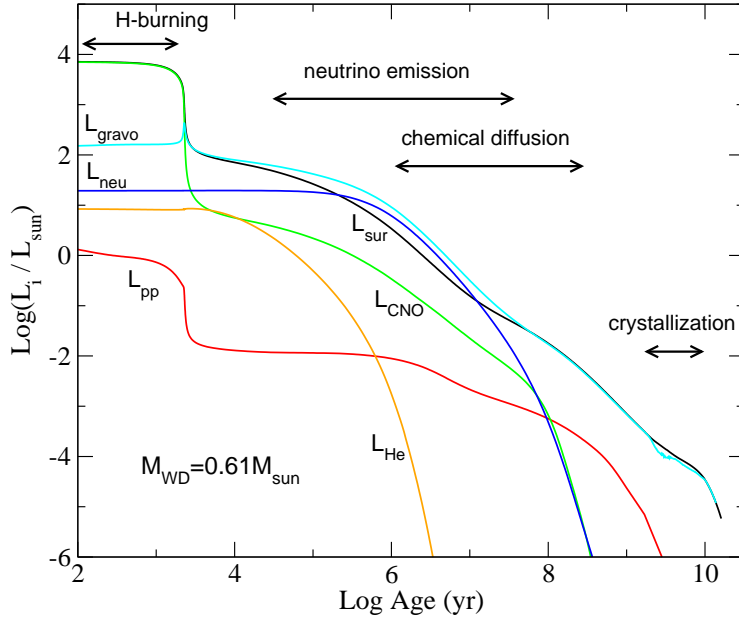
Fig. 10 Time dependence of the different luminosity contributions for a $0.61 M_{\odot}$ white dwarf: photon luminosity, L_{sur}, luminosity due to nuclear reactions (proton-proton, L_{pp}, CNO bicycle, L_{CNO}, He burning, L_{He}), neutrino losses, L_{neu}, and rate of gravothermal (compressional plus thermal) energy release L_{gravo}. The white dwarf progenitor corresponds to an initially $2 M_{\odot}$ star with metallicity $Z = 0.01$. Calculations include element diffusion, the release of latent heat upon cyrstallization, and outer boundary conditions as given by non-gray model atmospheres. The different physical processes of revelance during white dwarf evolution are indicated.

Luminosities are in solar units and the age is expressed in years from the moment at which the remnant reaches $\log T_{eff} = 4.87$ at high luminosity.

At early times, that is, for young white dwarfs, nuclear burning via CNO is the first contributor to the surface luminosity of the star. Here, there is a near balance between L_{nuc} and L_{sur} and between L_{gravo} and L_{neu} (like in an AGB star). During this stage, L_{gravo} results from the release of gravitational potential energy owing to the change in the internal density caused by the increase in the core mass from CNO H burning. This a short-lived phase (a few thousand years) and, thus, given the long-lived cooling times of white dwarfs, it is totally negligible in terms of age. Nevertheless, this phase is important as it configures the final thickness of the hydrogen-rich envelope of the white dwarf. After $\sim 10^4$ yr of evolution, nuclear reactions abruptly cease and the star begins to descend to the white dwarf domain and the surface luminosity of the star begins to decline steeply. Thereafter, the evolution is dictated by neutrino losses and the release of gravothermal energy — now essentially the release of internal energy from the core. Nuclear burning (via CNO) is a minor contribution. Note that during this stage, neutrino losses are the dominant energy sink ($L_{gravo} \approx L_{\nu}$). In fact, $L_{\nu} \approx 5 L_{sur}$ and as a result the white dwarf cooling is strongly accelerated. To this stage belong the pulsating DOV and DBV white dwarfs, so an eventual measurement of the rate of period change in some of these stars would allow to constrain the plasma-neutrino production rates (Winget et al. 2004). The time scale for CNO burning is larger than the evolutionary time scale. Burning occurs in the tail of H distribution and as a result the mass of the H envelope is not reduced by burning during this stage.
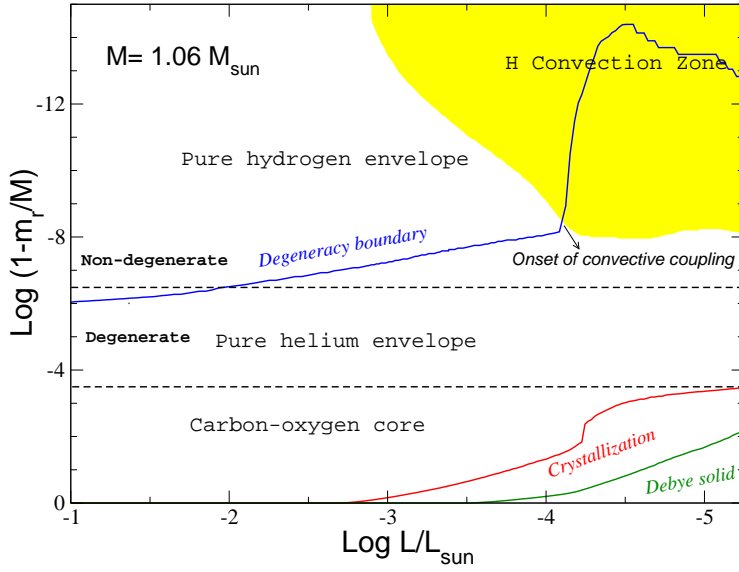
Fig. 11 The logarithm of the outer mass fraction of an evolving massive white dwarf as a function of the surface luminosity. The location of the different chemical regions and the domain of the physical processes relevant for the white dwarf evolution are indicated.

When $t_{\mathrm{cool}} \sim 10^7$ yr, the white dwarf is cool enough that neutrino is no longer relevant. $L_{\mathrm{gravo}} \approx L_{\mathrm{sur}}$ and the white dwarf verifies the Mestel approximations. This is the best understood stage in the life of a white dwarf. During it the star is characterized by a core still in the weakly-coupled Coulomb regime and a radiative envelope. There is no convection, nor neutrinos or nuclear burning or crystallization, and the ion thermal energy is the main source of energy. Below $\log(L/L_\odot) \sim -3$, the picture changes appreciably, as exemplified in Fig. 11 for the case of a massive white dwarf. At this luminosity, envelope convection becomes relevant and core crystallization sets in. As already mentioned, crystallization leads to the release of both latent heat and gravitational energy from phase separation, and convection eventually leads to the onset of convective coupling, with the consequent release of excess thermal energy, and the resulting slow down in the cooling rate. In intermediate-mass white dwarfs, convective coupling and crystallization take place more or less simultaneously, thus markedly changing the slope of the cooling curve. However, in massive white dwarfs, convective coupling occurs after most of the white dwarf has crystallized, as can be seen in Fig. 11 (Renedo et al. (2010). In this case, both energy contributions influence the cooling rate at different evolutionary stages. In addition, during these stages, appreciable energy release from ^{22}Ne sedimentation in the white dwarf core takes place in the case of white dwarfs stemming from metal-rich progenitors (see 4.3.4), notably impacting the rate of cooling (Althaus et al. 2010b).

The proton-proton burning shell may still make a contribution to surface luminosity at advanced stages, thus reducing the cooling rate of the white dwarf. As already discussed, this is relevant in the case of white dwarfs with low-metallicity progenitors, which are left with larger H envelopes on the cooling track. For a typical white dwarf resulting from a solar-metallicity progenitor, as shown in Fig. 10, residual proton-proton burning is a minor contribution. Eventually, H burning becomes virtually extinct at the lowest luminosities, and the surface luminosity is given by the release of internal energy from the core. During these

stages the contraction of the very outer layers may contribute to the surface luminosity. Finally, in the case of massive white dwarfs, the onset of Debye cooling with the consequent rapid decrease in the thermal energy content of the white dwarf core, is expected to occur at observable luminosities, as shown in Fig. 11.

5 H-deficient white dwarfs

5.1 PG 1159 stars and DO white dwarfs

White dwarf stars with H-deficient and He-rich atmospheres constitute about 15% of the white dwarf population, and are usually known as non-DA white dwarfs, see Sect. 2.4. Most of these white dwarfs are thought to be the progeny of PG 1159 stars (Dreizler & Werner 1996; Unglaub & Bues 2000; Althaus et al. 2005a), hot and luminous stars with H-deficient and He-, carbon- and oxygen-rich surface layers that constitute a transition stage between post-AGB stars and most of the H-deficient white dwarfs (Werner & Herwig 2006). Typical mass abundances observed in PG 1159 stars are $X_{He} \simeq 0.33$, $X_C \simeq 0.5$ and $X_O \simeq 0.17$, though notable variations are found from star to star (Dreizler & Heber 1998; Werner 2001). A large fraction of PG 1159 stars is believed to be the result of a born-again episode — a VLTP, see Sect. 3.3 —- which causes a hot white dwarf star to return to the AGB and then to the domain of the central stars of a planetary nebula as a hot H-deficient object and with a surface composition resembling that of the intershell region chemistry of AGB stars. Eventually, gravitational settling acting during the early stages of white dwarf evolution causes He to float and heavier elements to sink, giving rise to a He-dominated surface, and turning the PG 1159 star into a DO white dwarf (Unglaub & Bues 2000). During this stage, the evolution of the star is dictated essentially by neutrino losses and the release of gravothermal energy (O'Brien & Kawaler 2000; Althaus et al. 2005a). Because these white dwarfs are the hottest ones, the evolution during the DO stage proceeds very fast, with typical evolutionary time scales ∼1 Myr.

Several works have been devoted to the identification and spectral analysis of H-deficient objects like PG 1159 and DO white dwarfs — see Dreizler & Werner (1996), Dreizler et al. (1997) and references therein for earlier studies of spectroscopically confirmed DO white dwarfs. With the advent of large surveys, like the SDSS, the number of spectroscopically-identified H-deficient stars has increased considerably — see Hügelmeyer et al. (2006) and Kepler et al. (2007) for DO and DB white dwarfs, respectively. The determination of basic parameters of H-deficient white dwarfs, such as their mass and age, requires detailed evolutionary calculations appropriate for these stars. Such evolutionary calculations need to consider the evolutionary history that leads to the formation of H-deficient stars. Moreover, if consistent mass determinations of DO white dwarfs and PG 1159 stars are to be done, such calculations need to cover the entire evolutionary stage from the domain of luminous PG 1159 to the hot white dwarf stage (Dreizler & Werner 1996). Evolutionary tracks and mass-radius relations appropriate for both non-DA white dwarfs and PG 1159 stars have recently been computed by Althaus et al. (2009a). These sequences have been derived from models which cover the complete evolutionary history of progenitor stars with different initial masses evolved through the born-again episode and an up-to-date constitutive physics. The evolution of these white dwarf sequences in the $\log T_{eff} - \log g$ plane is shown in Fig. 12 together with the effective temperature and gravity of all known DO white dwarfs, and the approximate location of PG 1159 stars in this plane. The departure of the white dwarf cooling tracks from the zero-temperature predictions is noticeable during the early evolutionary
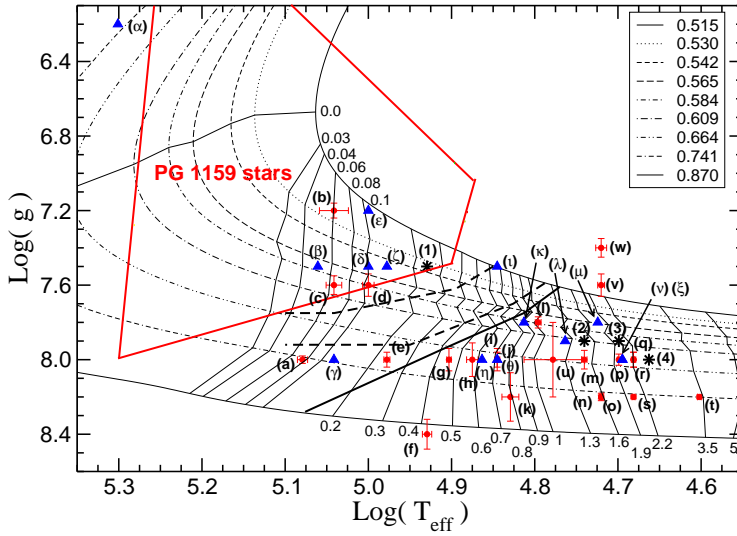
Fig. 12 Surface gravity, g (in cm/s^2), as a function of T_{eff} for the H-deficient white dwarf sequences of Althaus et al. (2009a). From bottom to top, curves correspond to sequences with stellar masses from 0.870 to 0.515 $M_\odot$. Also plotted are isochrones ranging from 0.03 to 5 Myr measured from the highest effective temperature point. The observed DO white dwarfs with spectroscopically-determined effective temperature and gravity as analyzed by Hügelmeyer et al. (2006), Dreizler & Werner (1996), and Dreizler et al. (1997) are also shown (filled circles and triangles, and star symbols, respectively). The thick solid line corresponds to the wind limit for PG 1159 stars taken from Unglaub & Bues (2000), and the two thick dashed lines to the wind limits for PG 1159 stars with H/He= 0.1 and 0.01 (upper and lower line, respectively). The region occupied by PG 1159 stars is also shown. From Althaus et al. (2009a).

stages at high effective temperatures, particularly in the case of low-mass sequences. Note that the bulk of observed DO white dwarfs have ages between 0.6 and 2.5 Myr, though the hottest members of the sample are indeed very young, with ages less than 0.10 Myr.

The mass distribution for DO white dwarfs and PG 1159 stars resulting from the evolutionary tracks shown in Fig. 12, is illustrated in Fig. 13, shaded region and solid line, respectively. The size of the bins in both distributions is 0.1 $M_\odot$. Note that massive DOs outnumber massive PG 1159 stars. A mean DO mass of 0.644 $M_\odot$ is obtained, considerably higher (by 0.071 $M_\odot$) than the mean mass of PG 1159 stars, 0.573 $M_\odot$. A possible explanation for this difference is simply that evolution through the PG 1159 stage proceeds considerably faster for massive stars (Miller Bertolami & Althaus 2006), thus decreasing the possibility of detection. However, analyzing the PG 1159+DO group as a whole, it can be seen that the difference in the mass distribution reflects the existence of some other important evolutionary channels operating within PG 1159 and DO stars (Althaus et al. 2009a). For instance, it is possible that not all PG 1159 stars evolve to DOs. In particular, those PG 1159 stars resulting from a LTP — low-mass remnants are more prone to experience a LTP episode — are expected to evolve into DA white dwarfs (near the winds limits shown in Fig. 12 with solid dashed lines), thus avoiding the DO stage, as shown by Unglaub & Bues (2000). This is so because, in contrast to a VLTP event, in a LTP, H is not burned, but instead diluted to low surface abundances (Miller Bertolami & Althaus 2006). Alternatively, some DO white dwarfs could result from evolutionary channels that do not involve only PG 1159 stars. For instance, they could be the result of post-merger evolution involving the giant, H-deficient RCrB stars, via the evolutionary link RCrB $\rightarrow$ EHe (extreme He stars)
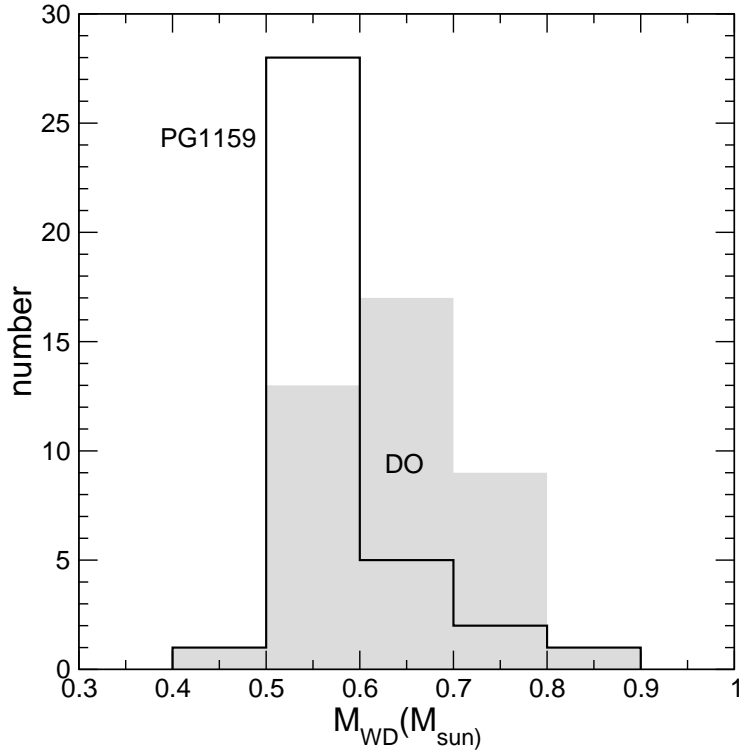
Fig. 13 The solid line and the shaded histogram show, respectively, the mass distribution for the PG 1159 and DO stars as inferred from the evolutionary calculations for these stars by Althaus et al. (2009a). Clearly, massive DO white dwarfs outnumber massive PG 1159 stars. From Althaus et al. (2009a).

$\rightarrow$ He-SdO$^+$ $\rightarrow$O(He) $\rightarrow$ DO — see Rauch et al. (2006) for a connection between O(He) stars and RCrB stars. This is reinforced by the recent study by Werner et al. (2008a,b) of the star KPD0005+5106, the hottest known DO white dwarf. These authors present evidence that KPD0005+5106 is not a descendant of PG 1159 stars, but more probably related to the O(He) stars and RCrB stars.

The group of young and hot DO white dwarfs is particularly relevant. Note that they are located considerably above the wind limit for PG 1159 stars (see Fig. 12). In fact, above this line, mass loss is large enough to prevent gravitational settling. Hence, the transformation of a PG 1159 star into a DO white dwarf should be expected approximately below this line. Although the estimated mass-loss rates could be overestimated by more than a factor of ten — in which case the transition from PG 1159 to DO would be near a line with $\log g \approx 7.5$ (Unglaub & Bues 2000) — it could be possible that the less massive and young DOs are not the descendants of PG 1159 stars. Also relevant is the fact that for ages less than about 0.3–0.4 Myr, the DO white dwarf population is markedly less massive than at greater ages. Indeed the number of detected old, less massive DOs is smaller than the number of young, less massive DOs, despite the evolutionary timescales being a factor about 5 for the former. This could indicate that some of the less massive DOs experience a tranformation in their spectral type after $\approx 0.3 - 0.4$ Myr of evolution. In particular, traces of H could turn the white dwarf spectral type from DO to DA as a result of gravitational settling. An
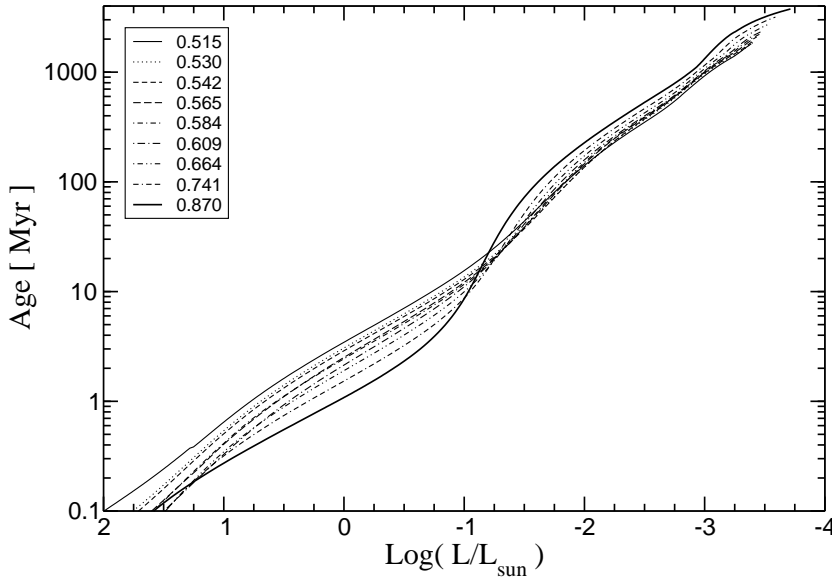
Fig. 14 Age (in Myr) versus luminosity (in solar units) for the H-deficient white dwarf sequences from Althaus et al (2009a).

approximate location where this transformation should occur is provided by the thick dashed lines shown in Fig. 12, which provides the wind limits for PG 1159 stars with different initial H abundances (Unglaub & Bues 2000). It is possible that the origin of low-mass, hot DOs can be connected with the merger of two low-mass, He-core white dwarfs (Guerrero et al. 2004; Lorén-Aguilar et al. 2009), which will evolve to become a low-gravity extreme He star and then a hot subdwarf (Saio & Jeffery 2000). The presence of H expected in this case, could lead to a transformation of the DO white dwarfs into DA ones.

Finally, in Fig. 14 it is shown the age (in Myr) as a function of the luminosity (in solar units) for the H-deficient sequences of Althaus et al. (2009a). At very high luminosities, residual He shell-burning constitutes an appreciable fraction of the surface luminosity. Except for these very high luminosity stages, evolution during the early stages is driven by neutrino emission and the release of gravothermal energy. In particular, neutrino losses exceed photon luminosity during most of the hot white dwarf stages. As a matter of fact, except for the hot and low-gravity DO sample shown in Fig. 12, it is during this "neutrino epoch" that most DO white dwarfs are observed. Note from Fig. 14 that the imprints of neutrino emission on the cooling curve are more noticeable as the mass increases. Less massive sequences are older than more massive sequences for $\log(L/L_\odot) \gtrsim -1$. At this stage, neutrino emission arrives at its end, thus causing a change in the slope in the cooling curve around $\log(L/L_\odot) \sim -1$, and later for the less massive sequences. At lower luminosities, Coulomb interactions become more important, increasing the specific heat, until crystallization and the associated release of energy start at the center. At this point, cooling can be well understood on the basis of the simple cooling theory of Mestel, which predicts less massive white dwarfs to cool faster (see Sect.2.5.2).

5.2 Hot DQ white dwarfs

The recent discovery of a new lukewarm population of white dwarfs with carbon-rich atmospheres — known as hot DQs (Dufour et al. 2007; 2008a) — has sparked the attention of researchers since it has raised the possibility of the existence of a new evolutionary channel of formation of H-deficient white dwarfs. Dufour et al. (2008a) have reported that nine hot white dwarfs identified in the Fourth Data Release of the SDSS are characterized by atmospheres dominated by carbon. The existence of these new white dwarfs — all of them found in a narrow effective temperature strip (between $\approx$ 18,000 K and 24,000 K) — poses a challenge to the stellar evolution theory, which cannot adequately explain their origin. As proposed by Dufour et al. (2008a) the hot DQ population could be related to the very hot ($\approx 200,000$ K) and massive ($0.83\,M_\odot$) member of the PG 1159 family, the enigmatic star H1504+65, for which a post born-again origin is not discarded (Althaus et al. 2009c). Interestingly enough, H1504+65 is the only known star with no traces of either H or He until the discovery of the hot DQ white dwarfs. Dufour et al. (2008a) have outlined an evolutionary scenario in which undetected traces of He remaining in the carbon- and oxygen-rich outer layers of H1504+65 would diffuse upwards leading to a He-rich white dwarf. In this picture, a carbon-rich atmosphere should eventually emerge as the result of convective mixing at smaller effective temperatures. The first quantitative assessment of such evolutionary scenario was presented in Althaus et al. (2009b). These authors demonstrated that mixing between the outer He convection zone with the underlying convective carbon intershell gives rise to white dwarf structures with the appropriate effective temperatures and surface compositions inferred from the observation of hot DQs. With the help of detailed born-again simulations for massive remnants, the study of Althaus et al. (2009b) provides the first theoretical evidence for an evolutionary link between the H- and He-deficient PG 1159 star H1504+65 with the high-gravity DQ white dwarf SDSS J142625.70+575218.4, a connection that can be traced back to strong mass-loss episodes after the VLTP. For the intermediate-gravity DQ white dwarfs, the scenario predicts the formation of carbon-dominated envelopes for residual He contents of the order of $M_{\rm He} = 10^{-8}\,M_*$ or smaller. The existence of H-deficient white dwarfs with such small He content could be indicative of the existence of a new evolutionary scenario for the formation of white dwarfs, as suggested by Dufour et al. (2008a). Alternatively, in view of the evolutionary connection between H1504+65 and the high-gravity SDSS J142625.70+575218.4, it cannot be discarded that the hot DQ white dwarf population of intermediate-gravity could be the descendants of some PG 1159 stars with small He contents. Finally, we recall that some of the possible evolutionary paths that H-deficient white dwarfs may follow are outlined in Fig. 4.

6 Stellar pulsations and variable white dwarfs

Until about a couple of decades ago, almost all what we knew about the properties of stars was derived from observations of their surface layers. Fortunately, the handsome circumstance that many stars pulsate opened a new opportunity to probe the interior of stars. The study of stellar pulsations, also called *stellar seismology* or *asteroseismology*, is a relatively young field of stellar astrophysics that, by means of the confrontation between the observed frequencies (periods) of pulsating stars and the appropriate theoretical models, is able to infer details about their origin, internal structure and evolution. The larger the number of frequencies detected in a given star, the more powerful asteroseismology becomes. Asteroseismological inferences are not limited to global quantities, such as gravity, effective tem-

perature or stellar mass. They provide, in addition, information about the internal rotation profile, the chemical composition, the run of the local sound speed, the presence and strength of magnetic fields, the extent of convective regions, and several other interesting properties. It is important to note that the main observable of asteroseismology, the oscillation frequencies, are the quantities that most accurately one can measure for a star.

Stellar pulsations are the eigenmodes of stars, that is, standing waves characterized by specific discrete values of frequency — the eigenfrequencies of the star — and the associated time-dependent perturbations in displacement, pressure, density, gravitational field,... are called eigenfunctions. Each star has an unique spectrum of eigenfrequencies, which is fixed by the details of its structure. Pulsation modes that maintain the spherical symmetry are called radial modes. They are the simplest oscillations that a star is able to sustain, and are the type of pulsations that undergo the classical variable stars such as Cepheids and RR Lyra. When pulsations depart from spherical symmetry, the modes are called non-radial modes. Radial pulsations can be considered as a special case of non-radial modes. In recent years it has been realized that different kinds of stellar objects at different locations in the Hertzsprung-Russell diagram and evolutionary stages, undergo non-radial pulsations: solar-like, γ Doradus, δ Scuti, roAp, SPB, β Cephei, R CrB, WR/LBV, V361 Hya, V1093 Her, and, relevant for this review, variable white dwarf stars. For specific details, we refer the reader to the excellent reviews of Cox (1980), Unno et al. (1989), Brown & Gilliland (1994), and Gaustchy & Saio (1995, 1996).

In the course of their lives, white dwarfs cross several instability strips where they become non-radial pulsating variable stars. Pulsations manifest themselves as periodic bright variations in the optical and also in the FUV regions of the electromagnetic spectrum. Typical light curves show peak-to-peak amplitudes between 0.4 mmag and 0.3 mag. Pulsating white dwarfs are found at four regimes of effective temperature and gravity (see Fig. 15). The hottest known class ($80,000$ K $\leq T_{\mathrm{eff}} \leq 180,000$ K and $5.5 \leq \log g \leq 7.5$) is constituted by variable H-deficient, C-, O- and He-rich atmosphere pre-white dwarf stars, named pulsating PG 1159 stars. This family includes some objects that are still surrounded by a nebula, they are the variable planetary nebula nuclei, designed as PNNVs. Pulsating PG 1159 stars that lack a nebula are called DOVs. Both groups (DOVs and PNNVs) are frequently referred to as GW Vir variable stars after the prototype of the class, PG 1159−035 (McGraw et al. 1979). Going to substantially lower effective temperatures and higher gravities ($22,000$ K $\leq T_{\mathrm{eff}} \leq 29,000$ K and $7.6 \leq \log g \leq 8.2$), we find the pulsating DB (He-rich atmospheres) white dwarfs, also called DBVs or V777 Her variable stars, the existence of which was theoretically predicted by Winget et al. (1982b) before their discovery. The next class of degenerate pulsators are the cool ($10,500$ K $\leq T_{\mathrm{eff}} \leq 12,500$ K and $7.8 \leq \log g \leq 8.8$) pulsating DA (H-rich atmospheres) white dwarfs, also called DAVs or ZZ Ceti variable stars. It was the first class of pulsating white dwarfs to be observed (Landolt 1968). Between the DBV and the DAV instability strips, we find the recently discovered class of hot DQ variable white dwarfs, or DQVs ($19,000$ K $\leq T_{\mathrm{eff}} \leq 22,000$ K). They are white dwarfs with C- and He-rich atmospheres. The analysis of the prototype of this class (SDSS J142625.71+575218.3) carried out by Green et al. (2009) appeared to confirm the pulsating nature of this star, thus unequivocally ruling out the interacting binary hypothesis that was initially put forward by Montgomery et al. (2008a) in the discovery paper. Table 2, adapted from O'Brien (2003), presents a summary of the main characteristics of each class of pulsating white dwarf stars. The first column corresponds to the name of each class and the year of discovery of the first member of the group, the second column shows the number of members, columns 3 to 6 list the visual magnitudes, effective temperatures, periods and amplitudes, respectively, and the last column shows the driving mechanism supposed to act in each case.
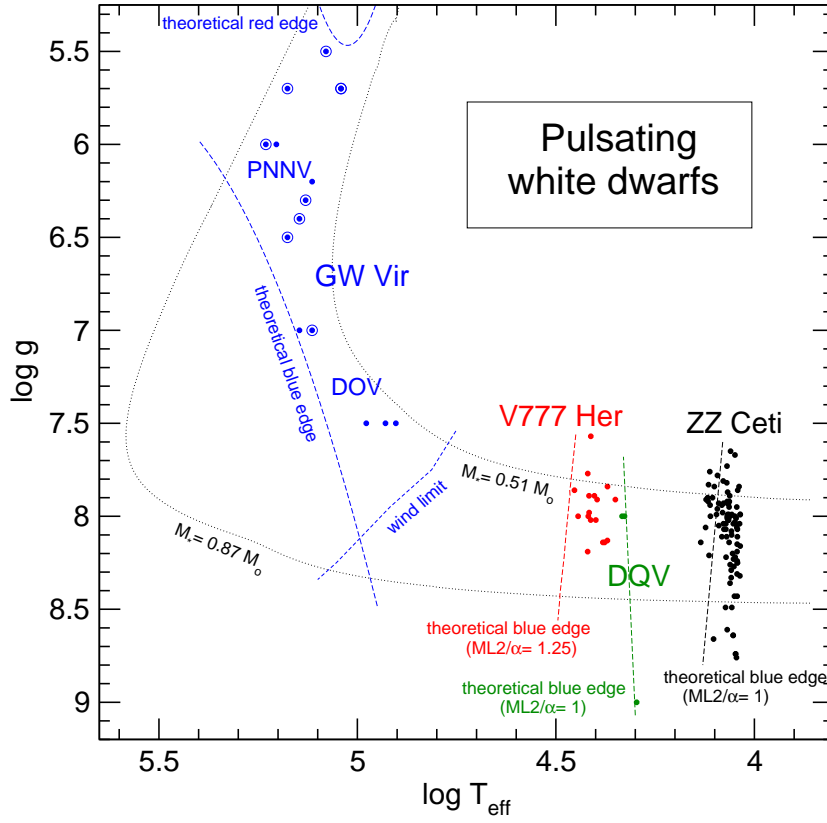
Fig. 15 The location of the several classes of pulsating white dwarf stars in the $\log T_{\rm eff} - \log g$ plane. Two post-VLTP (H-deficient) evolutionary tracks are plotted for reference. Also shown is the theoretical blue edge of the instability strip for the GW Vir stars (Córsico et al. 2006), the V777 Her stars (Córsico et al. 2009a), the DQV stars (Córsico et al. 2009d), and the ZZ Ceti stars (Fontaine & Brassard 2008).

Table 2 Properties of pulsating white dwarfs.

Class	Known pulsators	Visual magnitudes	$T_{\rm eff}$ [kK]	Periods [min]	Amplitudes [mag]	Driving mechanism
PNNV (1984)	10	$11.8 - 16.6$	$110 - 170$	$7 - 100$	$0.01 - 0.15$	$\kappa - \gamma$ (C/O)
DOV (1979)	6	$14.8 - 16.7$	$80 - 160$	$5 - 43$	$0.02 - 0.1$	$\kappa - \gamma$ (C/O)
V777 Her (1982)	20	$13.6 - 16.7$	$22.4 - 28.4$	$2 - 18$	$0.05 - 0.3$	$\kappa - \gamma$ (HeII) (convection?)
DQV (2008)	3	$17.7 - 19.6^{\dagger}$	$19 - 22$	$4 - 18$	$0.005 - 0.015$	$\kappa - \gamma$ (C) (convection?)
ZZ Ceti (1968)	145	$12.2 - 16.6$	$10.4 - 12.4$	$1.6 - 23.3$	$0.01 - 0.3$	$\kappa - \gamma$ (HI) convection

$^{\dagger}g$ magnitude of the SDSS *ugriz* system.

Among the several classes of pulsating stars, the study of pulsating white dwarfs is probably the area that has experienced the most rapid progress. According to the classical review of Winget (1988), this has been the result of several fortunate facts: (i) the relatively simple physical structure of white dwarfs, combined with the apparently slow rotation rate and weak magnetic field, which ensures simplicity also in their pulsation properties; (ii) the pulsation amplitudes are small enough as to be treated in the framework of the linear theory, but large enough still to be readily detectable; (iii) the multiperiodic nature of white dwarf pulsations, that provides many independent clues to their underlying stellar structures; and (iv) the periods are typically short enough, thus enabling observers to detect many cycles in a single run. For recent excellent reviews about pulsating white dwarf stars we refer the reader to the papers of Winget & Kepler (2008) and Fontaine & Brassard (2008).

6.1 Brief history of discovery

A full account of the history of discovery of pulsating white dwarf stars can be found in the work of Vuille (1998) and in the review articles of Winget (1988) and Winget & Kepler (2008). The notion of pulsations in white dwarfs goes back to the mid-twentieth century, when Sauvenier-Goffin (1949) and Ledoux & Sauvenier-Goffin (1950) explored for the first time the possibility that white dwarfs could undergo stellar pulsations. They found that rapid variability, associated to radial modes driven by H burning, should be exhibited by white dwarfs. The absence of high frequency variability typical of radial modes in these stars led to the conclusion that the energy source of white dwarfs could not be nuclear reactions. This, in turn, clarified the role of release of thermal energy as the main agent of white dwarf evolution, paving the way to the development of the Mestel's (1952) model of white dwarf cooling (Sect. 2.5.2).

The first variable white dwarf, HL Tau 76, was serendipitously discovered by A. Landolt (Landolt 1968), who did not even suspect that the finding would result later in a new and fascinating field of stellar research. In fact, in the abstract of his paper, Landolt just announced: "Photoelectric data which point to a $12^m.5$ variation in the brightness of a white-dwarf-like star are discussed". The luminosity variations detected in HL Tau 76, with a period of about 740 s, were too long to be attributed to radial modes, according to the theoretical studies available at that time (Faulkner & Gribbin 1968; Ostriker & Tassoul 1968). Two other variable white dwarfs were discovered in the meantime by Lasker & Hesser (1969, 1971): G 44−32 (with periods in the range 600−800 s) and R 548 (with periods in the range 200−300 s). The newly discovered variabilities in these compact objects were attributed to non-radial gravity modes, rather than purely radial modes (Warner & Robinson 1972; Chanmugam 1972), in agreement with the at that available theoretical estimations of Baglin & Schatzman (1969) and Harper & Rose (1970).

Further confirmation that the variability of white dwarfs was due to non-radial gravity modes came from the detection of rotational splitting in R 548 (Robinson et al. 1976), where rotation breaks the mode degeneracy and each frequency is split into multiplets of frequencies. McGraw (1979) carried out a very important observational work that provided a strong confirmation of the gravity-mode nature of variable white dwarfs. The multicolour Strömgen high-speed photometric data of that work suggested that the bright variations were entirely due to surface temperature variations, and not to changes in radius, in line with the fact that gravity modes are characterized by a predominantly tangential displacement (see Sect. 7). The very important work by Robinson et al. (1982) provided unequivocal theoretical support to the idea that the luminosity variations are entirely due to surface temperature

variations, and that the variations of radius are as small as $\delta R_*/R_* \sim 10^{-4}$. Note that the lineal theory of non-radial pulsations does not provide any clue about the value of the fractional change in radius, since the governing equations are homogeneous and the normalization of the eigenfunctions is arbitrary (Cox 1980).

A breakthrough in the field of white dwarf pulsations was the foundation of the Whole Earth Telescope consortium (Nather et al. 1990), most commonly known as WET, the first of several global networks for asteroseismology that enabled to obtain uninterrupted light curves spanning one to two weeks, thus avoiding the regular gaps in the data caused by the inevitable regular appearance at each site of the Sun. Details about WET and its first applications are described in Nather et al. (1990) and Winget et al. (1991, 1994).

The study of pulsating white dwarf stars through asteroseismology has in the recent years enabled astronomers to access a wealth of details about the internal structure of white dwarfs, otherwise inaccessible by means of traditional techniques. Before going on the pulsational properties of white dwarfs and the asteroseismological tools and applications, we briefly review below the theory of stellar pulsations, with emphasis in non-radial gravity-mode pulsations.

7 Overview of non-radial pulsations

In what follows, we briefly describe the basic properties of non-radial modes. This overview will be necessarily succinct, so we refer the reader to the excellent monographs by Unno et al. (1989) and Cox (1980) for further details about the theory of linear non-radial stellar pulsations. Non-radial modes are the most general kind of stellar oscillations. There exist two subclasses of non-radial pulsations, namely, *spheroidal* modes, for which $(\nabla \times \xi)_r = 0$ and $\sigma \neq 0$, and *toroidal* modes, for which $(\nabla \cdot \xi) = 0$ and $\sigma = 0$, where ξ is the displacement vector and σ the pulsation frequency. Of interest in this review are the spheroidal modes, which are further classified into g-, f- and p-modes according to the main restoring force acting on the oscillations, being gravity (buoyancy) for the g- and f-modes and pressure gradients for the p-modes.

For a spherically symmetric star, a linear non-radial pulsation mode can be represented as a three-dimensional standing wave of the form:

$$\psi'_{k\ell m}(r,\theta,\phi,t) = \psi'_{k\ell m}(r)\, Y_\ell^m(\theta,\phi)\, e^{i\sigma_{k\ell m}t}, \tag{32}$$

where the prime indicates a small Eulerian perturbation of a given quantity ψ (like the pressure, gravitational potential,...) and $Y_\ell^m(\theta,\phi)$ are the corresponding spherical harmonics. Geometrically, $\ell = 0, 1, 2, \ldots$ is the number of nodal lines in the stellar surface and $m = 0, \pm 1, \ldots, \pm\ell$ is the number of such nodal lines in longitude. Note that radial pulsations are recovered when $\ell = 0$. In absence of any physical agent able to remove spherical symmetry (like magnetic fields or rotation), the eigenfrequencies $\sigma_{k\ell m}$ are dependent upon ℓ but are $(2\ell + 1)$ times degenerate in m. Finally, $\psi'_{k\ell m}(r)$ is the radial part of the eigenfunctions, which for realistic models must be necessarily computed numerically together with $\sigma_{k\ell m}$. The eigenfunctions and eigenvalues are obtained as solution of a eigenvalue problem of fourth order in space, if we are considering the adiabatic approximation ($dS = 0$), which has analytical solution only for a unrealistic star model consisting of a homogeneous compressible sphere (Pekeris 1938). The index $k = 0, 1, \ldots$, known as the radial order of the mode, represents (in the frame of simple stellar models like those of white dwarf stars) the number of nodes in the radial component of the eigenfunction. They constitute concentric spherical

surfaces where radial displacement is null. For *g*-modes, the larger the value of k, the lower the oscillation frequency, while for *p*-modes the opposite holds.

White dwarf and pre-white dwarf stars pulsate in non-radial *g*-modes with periods between about 100 s and 1,200 s, although PNNVs are able to pulsate with much longer periods, up to about 6,000 s. Curiously, the *g*-mode periods of white dwarfs are of the order of magnitude of *p*-mode periods for non-degenerate pulsating stars. It is interesting to note that radial modes and *p*-modes with periods between 0.1 and 10 s have been found to be pulsationally unstable in a number of theoretical stability analysis (Saio et al. 1983; Kawaler 1993) but, however, these short period modes have not been ever observed in any white dwarf star, although the interest in the topic has been recently renewed (Silvotti et al. 2007). Finally, we mention that until now, only modes with $\ell = 1$ and $\ell = 2$ have been identified with high confidence in pulsating white dwarfs. Modes with higher values of ℓ are thought to be excited, but due to geometric cancellation effects (Dziembowski 1977), they should be very difficult to detect (however, see Sect. 7.5).

7.1 Classes of spheroidal modes and critical frequencies

Generally speaking, *g*-modes are characterized by low oscillation frequencies (long periods) and by displacements of the stellar fluid essentially in the horizontal direction. The structure of the *g*-mode period spectrum is governed by the Brunt-Väisälä frequency, given by:

$$N^2 = g \left(\frac{1}{\Gamma_1} \frac{d \ln p}{dr} - \frac{d \ln \rho}{dr} \right) \tag{33}$$

where g is the local gravitational acceleration. If $N^2 > 0$ then N is the (real) frequency of oscillation of a parcel of stellar fluid around its equilibrium level under gravity (Unno et al. 1989). On the other hand, *p*-modes have high frequencies (short periods) and are characterized by essentially radial displacements of the stellar fluid. The critical frequency for *p*-modes is the Lamb frequency, defined as:

$$L_\ell^2 = \ell(\ell+1) \frac{c_s^2}{r^2} \tag{34}$$

c_s being the local adiabatic sound speed, defined as $c_s^2 = \Gamma_1 p / \rho$, with $\Gamma_1 = (d \ln p / d \ln \rho)_{\text{ad}}$. A sound wave travels a distance $\approx 2\pi r / \ell$ horizontally in a time interval of $\approx 2\pi / L_\ell$ (Unno et al. 1989).

Finally, there is a single *f*-mode for a given $\ell \, (\geq 2)$ value. Usually, this mode does not have any node in the radial direction ($k = 0$) and possesses an intermediate character between *g*- and *p*-modes. In fact, its eigenfrequency lies between that of the low order *g*- and *p*-modes, and generally slowly increases when ℓ increases.

7.2 The asymptotic behavior for high radial order

When the radial order is high enough ($k \gg 1$) and for a small value of ℓ, the frequency of *p*-modes is approximately given by (Tassoul 1980):

$$\sigma_{k\ell} \approx \frac{\pi}{2} \left(2k + \ell + n + \frac{1}{2} \right) \left[\int_0^{R_*} \frac{1}{c_s(r)} dr \right]^{-1}, \tag{35}$$

Here n is the politropic index characterizing the structure of the surface layers of a stellar model. On the other hand, for completely radiative or completely convective and chemically homogeneus stellar models, the frequency of g-modes for $k \gg 1$ is given by:

$$\frac{1}{\sigma_{k\ell}} \approx \frac{\pi}{2} \left(2k + \ell + n + \frac{1}{2} \right) \frac{1}{\sqrt{\ell(\ell+1)}} \left[\int_0^{R_*} \frac{N(r)}{r} dr \right]^{-1}, \tag{36}$$

From Eq. (35) we have, for p-modes with fixed ℓ:

$$\Delta\sigma^{\mathrm{a}} = \sigma_{k+1\ell} - \sigma_{k\ell} = \pi \left[\int_0^{R_*} \frac{1}{c_{\mathrm{s}}(r)} dr \right]^{-1} = \text{constant}, \tag{37}$$

that is, the asymptotic frequency spacing of p-modes is constant (and not dependent from ℓ) in the limit of high radial order. The value of the constant depends only on the profile of the adiabatic sound speed, $c_{\mathrm{s}}(r)$, in the interior of the star. Similarly, from Eq. (36) we have, for g-modes with fixed ℓ,

$$\Delta\Pi_\ell^{\mathrm{a}} = \Pi_{k+1\ell} - \Pi_{k\ell} = \frac{2\pi^2}{\sqrt{\ell(\ell+1)}} \left[\int_0^{R_*} \frac{N(r)}{r} dr \right]^{-1} = \text{constant}, \tag{38}$$

where $\Pi_{k\ell} = 2\pi/\sigma_{k\ell}$ is the pulsation period. Thus, the asymptotic period spacing of g-modes is a constant value (which dependens on ℓ) in the limit of high radial order. This constant value is fixed by the Brunt-Väisälä frequency.

7.3 Local analysis and propagation diagrams

Important insights on the properties of non-radial pulsation modes can be derived by means of a "local analysis". If we consider modes with very short wavelengths (large wave number k_r), that is, high radial order modes ($k \gg 1$), and in the frame of the Cowling approximation — $\Phi' = 0$, Φ being the gravitational potential (Cowling 1941) — the coefficients in the pulsation equations vary slowly in comparison with the eigenfunctions, and then the solutions are proportional to $e^{ik_r r}$. The result of this local analysis is the following dispersion relation:

$$k_r^2 = \frac{1}{\sigma^2 c_s^2} \left(\sigma^2 - L_\ell^2 \right) \left(\sigma^2 - N^2 \right) \tag{39}$$

If $\sigma^2 > N^2, L_\ell^2$ or $\sigma^2 < N^2, L_\ell^2$ then $k_r^2 > 0$ and $k_r \in \mathrm{Re}$, being the solutions able to propagate radially. These inequalities define two propagation regions or "resonant cavities" in the interior of the star: the p-region (corresponding to propagating p-modes) and the g-region (associated with propagating g-modes). If, on the contrary, $N^2 > \sigma^2 > L_\ell^2$ or $L_\ell^2 > \sigma^2 > N^2$ then $k_r^2 < 0$ and $k_r \in \mathrm{Im}$ and thus the solutions are evanescent, that is, the amplitude of oscillation increases or decreases exponentially with r.

To illustrate the behavior described by the dispersion relation of Eq. (39) in the specific case of white dwarfs, we display in Fig. 16 the propagation diagrams corresponding to four selected pre-white dwarf and white dwarf stellar models. Panel (a) corresponds to a PG 1159 model at stages before the evolutionary knee (see Fig. 15), which is representative of a PNNV star; panel (b) shows the situation of a PG 1159 model located after the evolutionary knee, representative of a DOV star; panel (c) is representative of a DBV star; and finally, panel (d) corresponds to a DAV star. In each diagram, the profile of the Brunt-Väisälä frequency and the Lamb frequency (for $\ell = 1$) are plotted.
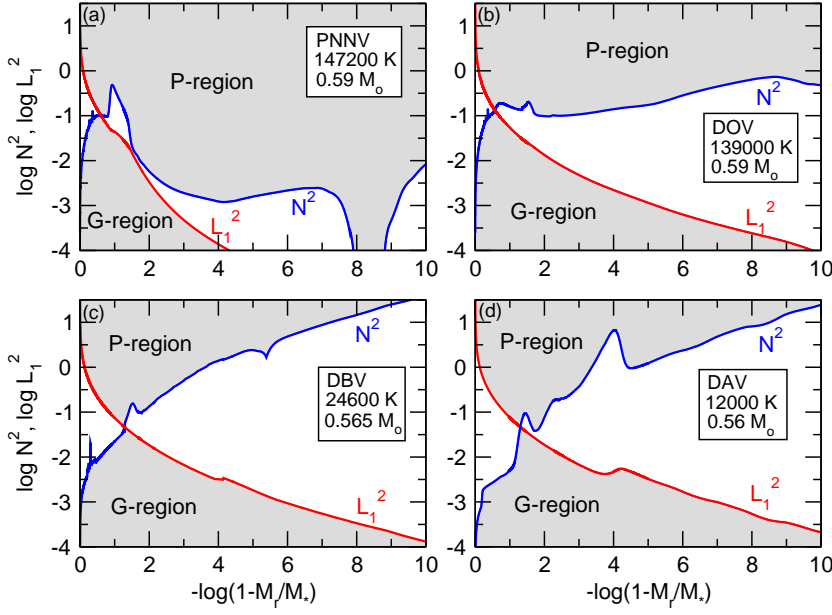
Fig. 16 Propagation diagrams ($\log N^2, L_\ell^2$ as a function of $-\log(1 - M_r/M_*)$) corresponding to selected pre-white dwarf and white dwarf stellar models. Panel (a) depicts the situation of a PNNV star, panel (b) corresponds to a DOV star, panel (c) is representative of a DBV star, and panel (d) depicts the case of a DAV star. Gray zones correspond to wave propagation regions.

Two outstanding features shown in this figure are worth to be commented. To begin with, while the Lamb frequency exhibit a similar qualitative behavior for all the four models, the Brunt-Väisälä frequency shows very important changes, basically produced by changes in the strength of electronic degeneracy at the different evolutionary stages considered. This is particularly notorious when we compare the case of the DOV model with the DBV model, and, in turn, with the DAV model. The changes in the Brunt-Väisälä frequency lead to important changes in the extension and location of the propagation cavities. For instance, in the case of the PNNV and DOV models, g-modes are allowed to propagate mainly at the deep regions of the core due to the large values of N^2 there. This is because electron degeneracy is not important at these stages. The p-modes, on the other hand, are able to propagate in more external regions. This behavior is shared by all the "normal" (non-degenerate) pulsating stars. Note that in the case of the PNNV model, there is a range of frequencies for which the modes are allowed to propagate in the p-region as well as in the g-region. They correspond to modes with a mixed (p and g) character. In the case of the DAV model, the most degenerate configuration, the Brunt-Väisälä frequency is very small at the core region, forcing g-modes to propagate mainly in the stellar envelope. On the contrary, p-modes are restricted to propagate in the inner zones of the star. In summary, while g-modes probe mainly the central regions in the case of PNNV and DOV stars, they are strongly sensitive to the outer layers in the case of DBV and DAV stars. Note, however, that some g-modes with low-order k are still able to probe the deep interior of DAVs and DBVs, thus allowing to make some inferences on the structure of the carbon-oxygen core.

The second important feature exhibited by the propagation diagrams of Fig. 16 is the presence of several bumps and peaks in the run of the Brunt-Väisälä frequency. They are

due to the presence of steep density gradients in the interior of white dwarfs models, induced by several chemical transition regions (see 4.1). If white dwarfs were chemically homogeneous, then the Brunt-Väisälä frequency should exhibit a very smooth behavior. The chemical structure of realistic white dwarf and pre-white dwarf models (with different evolutionary histories) described in Fig. 16, is shown in Fig. 17. This figure shows the fractional abundances of the main chemical species. For white dwarfs and pre-white dwarfs, the Brunt-Väisälä frequency must be numerically assessed by means of the relation (Tassoul et al. 1990; Brassard et al. 1991):

$$N^2 = \frac{g^2 \, \rho}{P} \, \frac{\chi_T}{\chi_\rho} \, \left(\nabla_{\mathrm{ad}} - \nabla + B \right), \tag{40}$$

where $\chi_T = (\partial \ln P / \partial \ln T)_\rho$ and $\chi_\rho = (\partial \ln P / \partial \ln \rho)_T$, ∇ and ∇_{ad} are the actual and adiabatic temperature gradients, respectively, and B, the Ledoux term, is given by

$$B = -\frac{1}{\chi_T} \sum_{i=1}^{n-1} \chi_{X_i} \frac{d \ln X_i}{d \ln P}. \tag{41}$$

Here X_i is the abundance by mass of species i, n is the total number of considered species and

$$\chi_{X_i} = \left(\frac{\partial \ln P}{\partial \ln X_i} \right)_{\rho, T, \{X_{j \neq i}\}}. \tag{42}$$

This formulation (the "modified Ledoux" treatment) has the advantage of avoiding the numerical problems that appear when Eq. (33) is employed to compute N in the strongly degenerate matter typical of white dwarf interiors (Brassard et al. 1991), and at the same time it explicitly accounts for the contribution to N from any change in composition in the interior of model (the zones of chemical transition) by means of the Ledoux term B of Eq. (41). The correct treatment of the Brunt-Väisälä frequency in the interfaces of chemical composition in stratified white dwarfs is very important, particularly in connection with the resonance effect of modes known as "mode trapping" (see Sect. 8.2 below).

7.4 Effects of slow rotation and weak magnetic fields

We have seen that, in absence of rotation and/or magnetic fields, each eigenfrequency is $(2\ell + 1)$-fold degenerated. This degeneracy takes place due to the absence of a preferential axis of symmetry for oscillations. In the presence of slow rotation, as it appears to be the case of most white dwarfs, we have $\Omega \ll \sigma_{k\ell m}$, where Ω is the angular frequency of rotation. In this case, the theory of perturbations can be applied to a first order, and then each frequency is split in $(2\ell + 1)$ equally-spaced components, thus completely lifting the degeneracy in frequency. Each component of the multiplet is given by:

$$\sigma_{k\ell m}(\Omega) = \sigma_{k\ell}(\Omega = 0) + \delta \sigma_{k\ell m}. \tag{43}$$

If rotation is rigid ($\Omega = $ constant), the correction to the eigenfrequencies is expressed as:

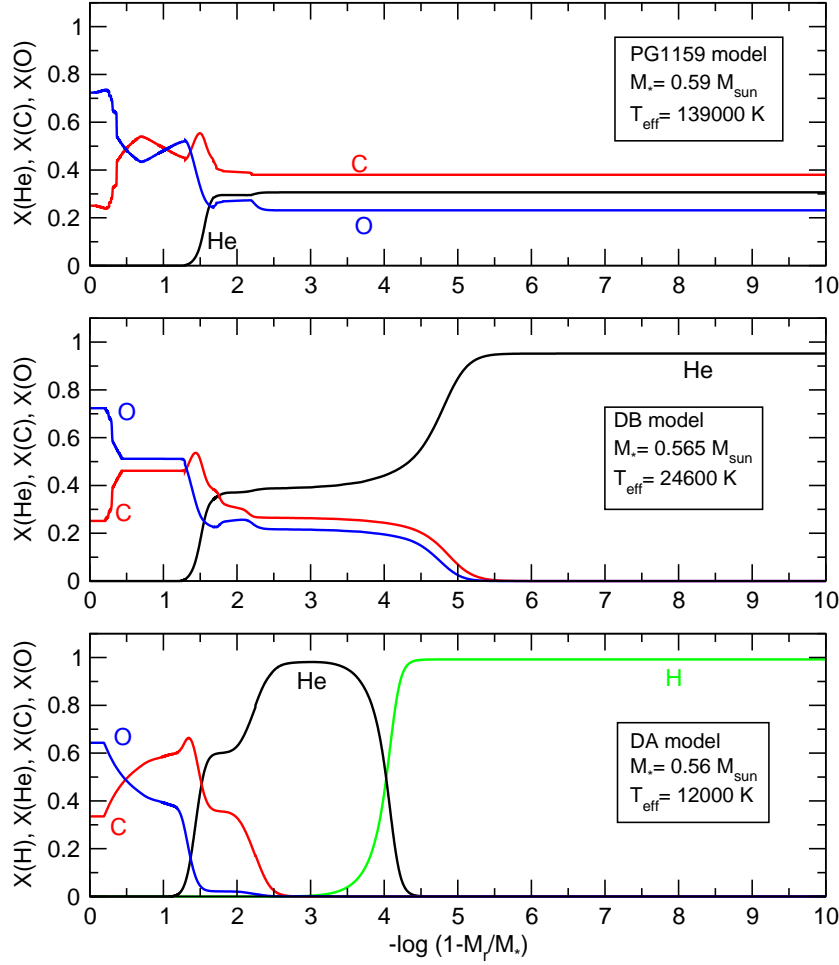$$\delta \sigma_{k\ell m} = -m \, \Omega \, (1 - C_{k\ell}), \tag{44}$$

Fig. 17 The internal chemical structure of the white dwarf and pre-white dwarf models described in Fig. 16.

with $m = 0, \pm 1, \ldots, \pm \ell$ and $C_{k\ell}$ being coefficients that depend on the details of the stellar structure and the eigenfunctions obtained in the non-rotating case. Such coefficients are given by (Cowling & Newing 1949; Ledoux 1951):

$$C_{k\ell} = \frac{\int_0^{R_*} \rho r^2 \left[2\xi_r \xi_t + \xi_t^2\right] dr}{\int_0^{R_*} \rho r^2 \left[\xi_r^2 + \ell(\ell+1)\xi_t^2\right] dr} \tag{45}$$

where ξ_r and ξ_t are the radial and the tangential eigenfunctions. We note that in the case of p-modes, if k increases then $\xi_r \gg \xi_t$ and thus $C_{k\ell} \to 0$. In the case of g-modes, on the other hand, when k is large then $\xi_r \ll \xi_t$, in such a way that $C_{k\ell} \to 1/\ell(\ell+1)$.

If the condition of rigid rotation is relaxed and we assume spherically symmetric rotation, $\Omega = \Omega(r)$, the correction to the eigenfrequencies is given by (Hansen et al. 1977):

$$\delta\sigma_{k\ell m} = -m \int_0^{R_*} \Omega(r) K_{k\ell}(r) dr, \tag{46}$$

where $K_{k\ell}(r)$ is the first-order rotation kernel computed from the rotationally unperturbed eigenfunctions according to:

$$K_{k\ell}(r) = \frac{\rho r^2 \left\{\xi_r^2 - 2\xi_r\xi_t - \xi_t^2 \left[1 - \ell(\ell+1)\right]\right\}}{\int_0^{R_*} \rho r^2 \left[\xi_r^2 + \ell(\ell+1)\xi_t^2\right] dr} \tag{47}$$

The presence of a weak magnetic field in a pulsating white dwarf also destroys the frequency degeneracy, but at variance with the case of rotation, the degeneracy is only partially lifted. In this case it can be shown that, after applying the perturbative approach and assuming a simple configuration for the magnetic field of the star, each eigenfrequency is split into $(\ell+1)$ components:

$$\sigma_{k\ell m}(B) = \sigma_{k\ell}(B=0) + \sigma'_{k\ell}(B) \tag{48}$$

where the correction $\sigma'_{k\ell}$, which involves complex mathematical expressions, depends on $B^2 = |\mathbf{B}|^2$, and also on m^2 instead m (Jones et al. 1989). We note that in the presence of a magnetic field, even the component $m = 0$ can be shifted. This is at variance with the case of rotation. Also, we mention that generally g-modes are more affected than p-modes by the presence of a magnetic field.

7.5 Mode identification

Mode identification consists in assigning the indices k, ℓ and m to a given observed pulsation mode. This is the first step in an asteroseismological analysis because it connects the models to observations. It is generally a very difficult task, in particular in the case of the radial order k, because it is not an observable quantity. Traditionally, identification of ℓ and m in white dwarfs has been performed through rotational mode splitting. Due to the presence of rotation, each frequency appears as a multiplet containing $(2\ell+1)$ components (see Sect. 7.4). Thus, a triplet of modes corresponds to dipole ($\ell = 1$) modes, a quintuplet corresponds to quadrupole ($\ell = 2$) modes, and so on. In some cases, it is possible to assign m to each component of the multiplets. Another way to obtain the value of ℓ of a series of pulsation modes is using the period spacing. The idea is to compare the observed mean period spacing between adjacent modes ($\overline{\Delta\Pi_k} = \overline{\Pi_{k+1} - \Pi_k}$) and the asymptotic period spacing ($\Delta\Pi_\ell^{\mathrm{a}}$), which, for g-modes, is dependent on ℓ — see Eq. (38) in Sect. 7.2. Thus, by matching the observed period spacing with the theoretically predicted value of $\Delta\Pi_\ell^{\mathrm{a}}$ the value of ℓ can be inferred. The observation of $\overline{\Delta\Pi_k}$ also is employed to infer the stellar mass of white dwarfs (see Sect. 8.1 below).

The two above mentioned methods have been applied successfully to the DOV stars PG 1159−035 (Winget et al. 1991) and PG 2131+066 (Kawaler et al. 1995), and to the DBV white dwarf GD 358 (Winget et al. 1994). This has been possible thanks to the long and continuous time series photometry obtained with the WET array, that allowed the rotation multiplet structure to be resolved and a large number of modes to be detected. This has allowed to derive the period spacing. However, in spite of the employment of the WET, it has not been possible to obtain the same success for any DAV star. This is due to the small number of periods detected and/or the complex and changing structure of the pulsation spectrum characterizing DAVs. Robinson et al. (1995) devised a method for mode identification that applies even in the cases in which there is a very reduced number of periods detected. The method is based on the effects of limb-darkening on the pulsation amplitudes. A non-radial g-mode in a white dwarf manifest itself as perturbations in the temperature which, in turn,

create bright and dark regions on the stellar surface. Non-radial modes of each ℓ value experience geometrical cancellation due to the presence of these regions with opposing phases. At short wavelenghts, the limb-darkening is stronger, and reduces the effects of cancellation on modes with high values of ℓ. As a result, the amplitudes of pulsations are sensitive to ℓ (and are insensitive to m), and then it is possible to derive the harmonic degree. Using this method (called "time-resolved ultra-violet spectroscopy") allowed Robinson et al. (1995) to infer that the largest amplitude mode of the DAV G 117−B15A had $\ell = 1$. Kepler et al. (2000) employed this method and found that the pulsations in the DAVs G 226-29 and G 185-32 are consistent with $\ell = 1$. Nitta et al. (1998) also used this method for the DBV white dwarf GD 358 and were only able to rule out the presence of modes with $\ell > 2$.

A variant of the above mentioned method to identify ℓ was proposed by van Kerkwijk et al. (2000) and Clemens et al. (2000) and applied to the DAV white dwarf G 29-38. The method, called "time-resolved optical spectroscopy", is based on the dependence of the amplitudes of non-radial pulsation modes within the Balmer lines at visual wavelengths only. They found that for this star several modes are consistent with $\ell = 1$, and that one mode is characterized by $\ell = 2$. Kotak et al. (2002a) studied the DAV HS 0507+0434B and Kotak et al. (2003) studied the DBV GD358. In both cases they found that $\ell = 1$ for most of the modes present in these stars. Kotak et al. (2004) also studied G 117−B15A, and by comparing the fractional wavelength dependence of the pulsation amplitudes (chromatic amplitudes) with models, they confirmed a previous report that the strongest mode, at 215 s, has $\ell = 1$. The chromatic amplitude for the 272 s mode, on the other hand, is very puzzling, showing an increase in fractional amplitude with wavelength that cannot be reproduced by the models for any ℓ at optical wavelengths. Recently, Thompson et al. (2008) revisited the case of G 29-38, and confirmed several ℓ identifications and add four new values, including an additional $\ell = 2$ and a possible $\ell = 4$.

8 Asteroseismological tools

When a rich spectrum of non-radial g-modes of a variable white dwarf is available, and the eigenmodes have been correctly identified, asteroseismology can be applied to infer the fundamental parameters of the star. Obviously, the larger the number of independent periods detected, the larger the amount of information that can be inferred. Below, we describe the asteroseismological methods currently employed to probe the interiors of pulsating white dwarfs. They can provide information about the stellar mass, the internal chemical stratification, the rate of rotation, the existence of magnetic fields, the cooling timescale and core composition, and the outer convection zone.

8.1 Period spacing: determination of the stellar mass

The stellar mass of a pulsating white dwarf can be obtained from the observed period spacing once the harmonic degree ℓ is identified. ¿From Eq. (33) or Eq. (40) it is clear that the Brunt-Väisälä frequency is directly proportional to the gravity. Thus, the period spacing is inversely proportional to the gravity through Eq. (38), and to the stellar mass. Therefore, by measuring the period spacing in a real star, the total mass can be inferred. This is particularly true for DOVs and PNNVs stars because in these cases the periods and period spacings depend almost exclusively on the stellar mass, and to a much smaller extent, on the luminosity and the thickness of the He-rich outer envelope. This was first recognized by Kawaler
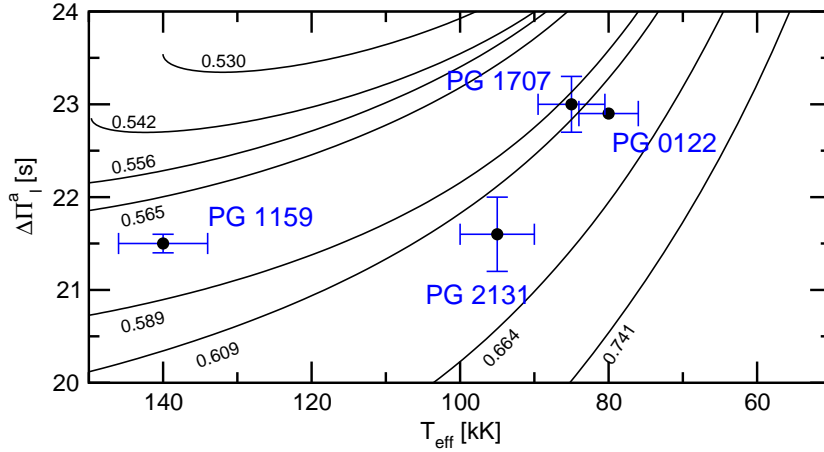
Fig. 18 The dipole ($\ell = 1$) asymptotic period spacing ($\Delta \Pi_\ell^a$) for different stellar masses in terms of the effective temperature. Numbers along each curve denote the stellar mass (in solar units) of the PG 1159 evolutionary sequences. The plot also shows the location of the high-gravity, low-luminosity GW Vir stars PG 0122+200, PG 1159−035, PG 2131+066, and PG 1707+427.

(1987). The method, however, is not directly appliable to DBVs and DAVs because for those stars the periods and period spacings are sensitive to the thickness of the He and/or H envelopes, in addition to the stellar mass. The approach consists in computing the asymptotic period spacing for white dwarf models of different effective temperatures, corresponding to evolutionary sequences of different stellar masses. By adopting the effective temperature of the target star as derived from spectroscopy, the observed period spacing can be matched to the asymptotic period spacing. We illustrate this procedure in Fig. 18 for the case of DOV stars. Specifically, in this figure we show the asymptotic period spacing ($\Delta \Pi_\ell^a$) for $\ell = 1$ corresponding to PG 1159 evolutionary sequences of different stellar masses. In addition, selected low-luminosity, high-gravity pulsating PG 1159 stars have been included by using their observed $T_{\rm eff}$ and $\Delta \Pi$ values. The value of the stellar mass for each star can be obtained by simple linear interpolation.

The method described above is computationally inexpensive and has been widely used in the past because it does not involve pulsational calculations. However, we must emphasize that the derivation of the stellar mass using the asymptotic period spacing may not be entirely reliable in pulsating white dwarfs that have modes characterized by low and intermediate radial orders. This is because Eq. (38), which describes the asymptotic behavior of the period spacing, is strictly valid only in the limit of very high radial order (long periods) and for chemically homogeneous stellar models, while white dwarf stars are expected to be chemically stratified and characterized by strong chemical gradients built up during the progenitor star life (see Sect. 4.1). Generally, this method can lead to an over-estimate of the stellar mass, except for stars that pulsate with very high radial orders, such as the PNNV stars (Althaus et al. 2008a).

A more realistic approach to infer the stellar mass of PG 1159 stars is to compare the observed period spacing with the average of the computed period spacings. The average of the computed period spacings is computed as $\overline{\Delta \Pi_\ell} = (n-1)^{-1} \sum_k^n \Delta \Pi_k$, where $\Delta \Pi_k = \Pi_{k+1} - \Pi_k$ are the calculated period spacings and n is the number of computed periods laying in the range of the observed periods. Fig. 19 illustrates this method for the case of
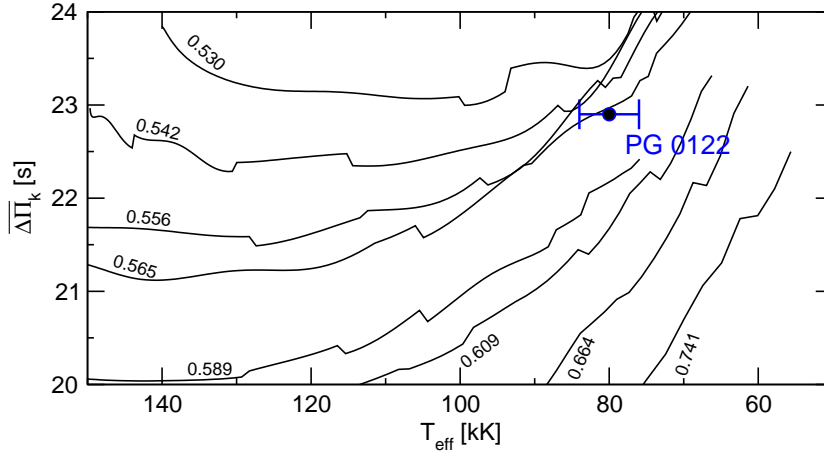
Fig. 19 Same as Fig. 18, but for the average of the computed period spacings ($\overline{\Delta\Pi_\ell}$).

PG 0122+200. In this case, the curves (notably jagged and irregular) correspond to $\overline{\Delta\Pi_\ell}$ for each PG 1159 evolutionary sequence with different stellar masses. Again, the location of the target star is given by the observed T_{eff} and $\Delta\Pi$ values, and the stellar mass of the target star can be inferred by simple interpolation. This method is more reliable for estimating the stellar mass of PG 1159 stars than that described above because, provided that the average of the computed period spacings is evaluated at the appropriate range of periods, the approach is adequate for the regimes of short, intermediate and long periods (i.e., for all k). When the average of the computed period spacings is taken over a range of periods characterized by high k values, then the predictions of the present method become closer to those of the asymptotic period spacing approach. On the other hand, the present method requires detailed period computations, at variance with the method described above. Note that in the case of PG 0122+200, the employment of the asymptotic period spacing overestimates the stellar mass, as compared with the inference from the average of the computed period spacing (0.62 vs 0.565 $M_\odot$) Finally, we note that the methods described in this section for assessing the stellar mass rely on the spectroscopic effective temperature, and the results are unavoidably affected by its associated uncertainty.

8.2 Mode trapping: hints about the chemical stratification

The period spectrum of chemically homogeneous stellar models is characterized by a constant period separation, given very accurately by Eq. (38). However, current evolutionary calculations predict that white dwarfs must have one or more composition gradients in their interiors (Sect. 4.1). The presence of one or more abrupt chemical transitions strongly modifies the character of the resonant cavity in which modes should propagate as standing waves. Specifically, chemical interfaces act like reflecting boundaries that partially trap certain modes, forcing them to oscillate with larger amplitudes in specific regions (bounded either by two interfaces or by one interface and the stellar center or surface) and with smaller amplitudes outside those regions. The requirement for a mode to be trapped is that the wavelength of its radial eigenfunction matches the spatial separation between two interfaces or between one interface and the stellar center or surface. This mechanical resonance, known
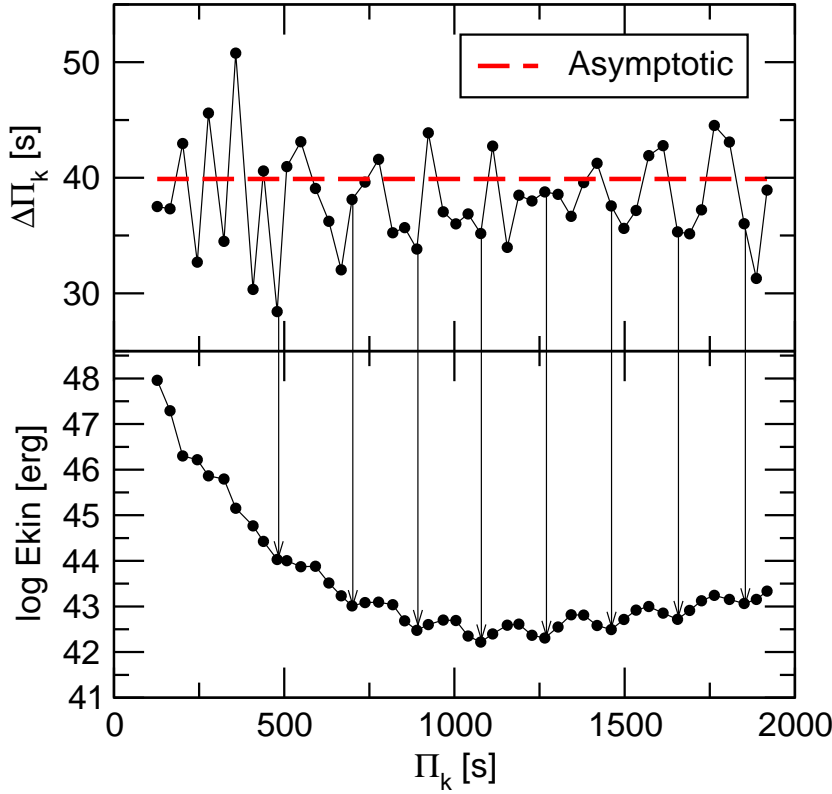
Fig. 20 The forward period spacing $\Delta\Pi_k$ (upper panel) and the pulsation kinetic energy (lower panel) in terms of the pulsation periods for a typical DB white dwarf model. Modes trapped in the outer He-rich envelope correspond to minima in E_{kin}.

as *mode trapping*, was first studied by Winget et al. (1981) and has been the subject of intense study in the context of stratified DA and DB white dwarfs — see, e.g., Brassard et al. (1992a) and Córsico et al. (2002a). In the field of PG 1159 stars, mode trapping has been extensively explored by Kawaler & Bradley (1994) and Córsico & Althaus (2006).

There are (at least) two ways to identify trapped modes in a given stellar model. First, we can consider the oscillation kinetic energy. Because the amplitude of eigenfunctions is arbitrarily normalized at the surface of the model, the values of the kinetic energy are useful only in a relative sense. The oscillation kinetic energy is proportional to the integral of the squared amplitude of eigenfunctions, weighted by the density. Thus, modes propagating in the deep interior of the white dwarf, where densities are very high, will exhibit larger values than modes which are oscillating in the low-density, external regions. When only a single chemical interface is present, modes can be classified as modes trapped in the outer layers, modes confined in the core regions, or simply "normal modes" — which oscillate everywhere in the star — characterized by low, high, and intermediate values of kinetic energy, respectively (Brassard et al. 1992a).

A second (and more important from an observational point of view) consequence of mode trapping is that the period spacing $\Delta\Pi_k$, when plotted in terms of the pulsation period Π_k, exhibits strong departures from uniformity. The period difference between an observed

mode and its adjacent modes ($\Delta k = \pm 1$) is an observational diagnostic of mode trapping, at variance with the kinetic energy, whose value is very difficult to estimate only from observation. For stellar models characterized by a single chemical interface, local minima in $\Delta \Pi_k$ usually correspond directly to modes trapped in the outer layers, whereas local maxima in $\Delta \Pi_k$ are associated to modes confined in the core region.

The diagrams $\Delta \Pi_k$ versus Π_k have valuable information about the structure of the outer layers and the thickness of the outer envelope of a white dwarf. In particular, the difference of period between successive trapped modes (successive minima), or "cycle of trapping", is inversely proportional to the thickness of the outer envelope where the modes are trapped. On the other hand, the amplitude of the variation of $\Delta \Pi_k$, or "amplitude of trapping", is a measure of the thickness of the chemical transition region. The potential use of mode trapping to measure the thicknesses of the outer envelopes in DA and DB white dwarfs led to several groups of researchers to derive a relation between the period of modes trapped in the outer envelope and the location of the transition region responsible for such a trapping, the so called "trapped mode-period" relation — see Kawaler & Weiss (1990) and Brassard et al. (1992a) for DAVs, Bradley et al. (1993) for DBVs, and Kawaler & Bradley (1994) for DOVs.

This method for estimating the thickness of the outer envelopes in white dwarfs, very appealing and extremely useful from an asteroseismological point of view, relies however on two important assumptions: (i) the existence of a *unique* relevant composition gradient in the interior of the star, that is, the most external one (He/H in the DAVs, C/He in the DBVs), thus neglecting other possible chemical interfaces located at the core regions; and (ii) the assumption of diffusive equilibrium in the trace element approximation (Tassoul et al. 1990) to model the chemical transition regions. Córsico et al. (2001a, 2002a, 2002b) published a serie of pulsation studies based on detailed evolutionary DA white dwarf models characterized by outer chemical interfaces modeled through time-dependent element diffusion, and the chemical structure at the deep regions of the core resulting from the progenitor evolution. They showed that the mode-trapping features produced by the outer chemical transition region is actually much less important than thought before, due to the fact that chemical profiles shaped by chemical diffusion are very smooth as compared with the predictions of the trace element approximation. In addition, these studies demonstrated that the chemical structure of the core regions can be a relevant source of mode trapping/confinement, in particular for modes with low radial order.

Thus, the rather simple picture of mode trapping in simplified models characterized by only one chemical interface becomes markedly complex when the stellar model is characterized by several chemical composition gradients, in particular for the regime of low order modes (short periods), where it is very difficult to disentangle which specific chemical interface is responsible for a given feature of mode trapping. In addition, Montgomery et al. (2003) have found an intrinsic degeneracy in the way that pulsation modes sample the core and the envelope of white dwarfs, which can potentially lead to an ambiguity in the asteroseismologically inferred locations of internal chemical structures. Fig. 20 shows the period spacing and the kinetic energy for a realistic evolutionary DB white dwarf model with $M_* = 0.565 M_\odot$ and $T_{\mathrm{eff}} = 28\,400$ K. In this case, the strong mode-trapping features are found even at high-order modes (long periods). Note that modes trapped in the outer He-rich envelope, which are characterized by minima of kinetic energy, do not correspond to minima in period spacing. The dashed line corresponds to the asymptotic period spacing. The chemical structure of this model is plotted in the central panel of Fig. 17. The model has three different chemical transition regions, which combined produce the complex pattern of mode trapping displayed in Fig. 20.

In summary, when realistic evolutionary models of white dwarfs are considered in pulsational studies, the potential of mode trapping to infer the location of the chemical interfaces (and the thickness of the envelope) is strongly weakened and becomes almost useless. Instead, all we can infer is that white dwarfs are in fact chemically stratified stars, thus confirming the predictions of the stellar evolution theory.

8.3 Frequency splitting: constraining the rotation rate and/or the magnetic field

We have seen in Sect. 7.4 that slow and solid-body rotation of a star produces a set of equally-spaced frequencies, with a separation between each component of the multiplet given by $\delta\sigma_{k\ell m} = m\,(1-C_{k\ell})\Omega$. This rotational splitting of frequencies is found in a large number of pulsating white dwarf stars. This fact can be exploited to estimate the rotation period of the star ($P_{\mathrm{R}} = 2\pi/\Omega$), as well as to identify the harmonic degree ℓ and the azimuthal order m of the modes. In practice, generally there are one o more components missing in the observed multiplets, and frequently the present components can show very different amplitudes. The mechanism of selection operating here is at present unknown (Winget & Kepler 2008). As an illustration of the inference of the rotation period in white dwarfs, we consider the prototypical star PG 1159−035. For this star, 20 triplets ($\ell = 1, m = -1, 0, +1$) and 8 quintuplets ($\ell = 2, m = -2, -1, 0, +1, +2$) have been identified (Winget et al. 1991). By computing the average of the frequency spacings between the components of multiplets ($\overline{\delta\sigma_{k\ell m}}$), a rotation period of $P_{\mathrm{R}} = 1.38 \pm 0.01$ days has been inferred.

Employing a more self-consistent approach, Charpinet et al. (2009) have recently revised the issue of the stellar rotation of PG 1159−035. On the basis of the asteroseismological model of Córsico et al. (2008) for that star, Charpinet et al. (2009) have carried out a detailed analysis of the individual multiplets by assuming solid-body and also differential internal rotation profiles, and have arrived at the firm conclusion that the star is rotating as a solid body with a rotation period of $P_{\mathrm{R}} = 33.61 \pm 0.59$ h, in very good agreement with the previous result by Winget et al. (1991).

Finally, pulsating white dwarfs can exhibit magnetic frequency splitting. In this case, we have seen in Sect. 7.4 that a magnetic field can lead to a mode characterized by a harmonic degree ℓ to split into $\ell + 1$ components, instead $2\ell + 1$ components due to rotational splitting. Since the frequency separation of the multiplets depends on B^2, by measuring the frequency separation, the magnitude of the magnetic field can be, in principle, estimated. Historically, the prototypical pulsating white dwarf showing magnetic splitting (doublets of frequency) is the DAV star R 548. However, solid arguments lead to the conclusion that the supposed magnetic doublets of this star can be actually rotational triplets with the central component $m = 0$ having very small amplitudes (Fontaine & Brassard 2008).

8.4 The rate of period changes: clues to the core chemical composition

The rates of period change of pulsation g-modes in white dwarfs are a very important observable quantity that can yield information about the core chemical composition. As a variable white dwarf evolves, its oscillation periods vary in response to evolutionary changes in the mechanical structure of the star. Specifically, as the temperature in the core of a white dwarf decreases, the plasma increases its degree of degeneracy so the Brunt-Väisälä frequency — the most important physical quantity in g-mode pulsations — decreases, and the pulsational spectrum of the star shifts to longer periods. On the other hand, residual gravitational

contraction (if present) acts in the opposite direction, thus shortening the pulsation periods. Competition between the increasing degeneracy and gravitational contraction gives rise to a detectable temporal rate of change of periods ($\dot{\Pi} \equiv d\Pi/dt$). Roughly, the rate of change of the pulsation period is related to the rates of change of the temperature at the region of the period formation, $\dot{T}$, and of the stellar radius, $\dot{R}_*$ (Winget et al. 1983):

$$\frac{\dot{\Pi}}{\Pi} \approx -a\frac{\dot{T}}{T} + b\frac{\dot{R}_*}{R_*}, \tag{49}$$

where a and b are constants whose values depend on the details of the white dwarf modeling (however, both a and $b \approx 1$). The first term in Eq. (49) corresponds to the rate of change in period induced by the cooling of the white dwarf and it is a positive contribution, while the second term represents the rate of change due to gravitational contraction and it is a negative contribution. In principle, the rate of change of the period can be measured by observing a pulsating white dwarf over a large time interval when one or more very stable pulsation periods are present in their light curves. In the case of pulsating DA white dwarfs, cooling dominates over gravitational contraction, in such a way that the second term in Eq. (49) is negligible, and only positive values of the rate of change of period are expected. For the high effective temperatures characterizing the DOV/PNNV instability strip, gravitational contraction is still significant, to such a degree that its influence on $\dot{\Pi}$ can overcome the effects of cooling. In this case the second term in Eq. (49) is not negligible anymore and, consequently, either positive or negative values of $\dot{\Pi}$ are possible. For these hot pre-white dwarfs, what determines that $\dot{\Pi}$ is positive or negative is the character of the mode: if the pulsation period corresponds to a mode confined to the deep regions of the star, then a positive value of $\dot{\Pi}$ is expected, while if the mode is a mode trapped mostly in the outer layers, we would expect a negative value of $\dot{\Pi}$ (Kawaler & Bradley 1994). As for the DBV stars, in which the influence of the gravitational contraction on $\dot{\Pi}$ is negligible, it is found from theoretical evolutionary calculations that the expected rate of period change should be positive.

As an illustrative example of the temporal drift of periods in a white dwarf, we show in Fig. 21 the evolution of periods with the effective temperature corresponding to a PG 1159 model before (left panel) and after (right panel) the model reaches the turning point in the Hertzsprung-Russell diagram — see Fig. 15. Pulsation periods decrease in stages in which the model is still approaching its maximum effective temperature ($T_{\mathrm{eff}} \approx 176\,600$ K). When the model has already settled into the cooling phase, the periods increase. Note in the left panel of Fig. 21 that when $T_{\mathrm{eff}} < 176\,600$ K, the low-order periods ($\Pi_k \lesssim 200$ s) exhibit a behavior reminiscent of the well-known "avoided crossing". When a pair of modes experiences avoided crossing, the modes exchange their intrinsic properties (Aizenman et al. 1977). These are modes with a mixed character, that is, modes that behave as g-modes in certain zones of the star and as p-modes in other regions. Finally, we have included in Fig. 21 two thin dashed vertical lines that define three different regimes for the theoretical rate of period change: models exhibit negative (positive) rates of period change for effective temperatures to the left (right) of that of the red (blue) line, and positive and negative rates between both lines (Córsico et al. 2008). Thus, we expect a pulsating PG 1159 star located in the region of the evolutionary knee to exhibit a mix of positive and negative values of $\dot{\Pi}$. A very recent study (Costa & Kepler 2008) suggests that the prototype star PG 1159−035 could be located precisely at the evolutionary knee in the Hertzsprung-Russell diagram, making it an excellent target to test the evolutionary models of pulsating white dwarfs.

What can be learned from the rate of period change? Observational measurements of $\dot{\Pi}$ can provide a sensitive probe of the structure and evolution of white dwarf stars. As shown
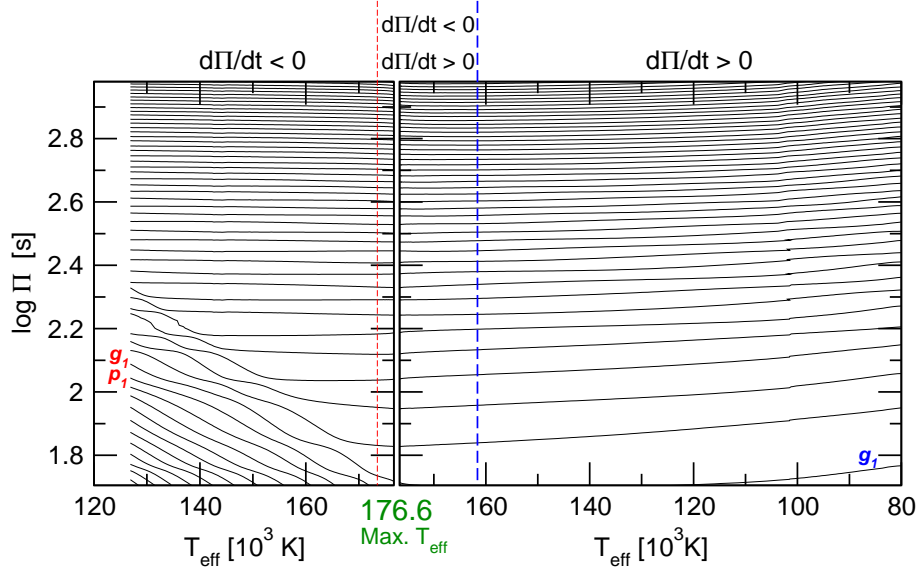
Fig. 21 The evolution of the $\ell = 1$ pulsation periods Π in terms of the effective temperature, corresponding to the sequence of PG 1159 models with $M_* = 0.5895 M_\odot$. The left panel depicts the situation before the models reach the maximum value of effective temperature, and right panel shows the situation when the models have already passed through this stage. Note that the orientation of the T_{eff} axis in the left panel is opposite that of right panel.

by Winget et al. (1983), a measurement of the rate of period change of a pulsating white dwarf constitutes, particularly for DAV and DBV white dwarfs (which evolve at almost constant radius), a direct measurement of the cooling rate of the star. This, in turn, provides valuable information about the core chemical composition. For a given mass and internal temperature distribution, the rate of period change increases if the mean atomic weight of the core is increased. The mean atomic weight of the core of a white dwarf can be inferred, in principle, comparing the observed value of $\dot{\Pi}$ with theoretical values from evolutionary sequences of white dwarfs with cores made of C and O (or heavier species such as Ne, Mg,...) with different mass fractions. A simple relation can be obtained by using the Mestel cooling law (see Sect. 2.5.2). The result is $\dot{\Pi} = (3-4) \times 10^{-15}(A/14)$ [s/s] (Kepler et al. 2005).

The measured $\dot{\Pi}$ can also be used to detect the presence of planets orbiting around pulsating white dwarfs. If a planet is orbiting around a star, its distance to the Sun will change periodically as the star orbits around the center of mass of the system. If the star is a stable pulsator, then the orbital motion will change the pulse arrival times as seen from Earth, as compared with a constant period. The variation of the pulse arrival times is given by:

$$\tau = \frac{a_{\rm p} m_{\rm p} \sin i}{M_* c} \tag{50}$$

where $a_{\rm p}$ and $m_{\rm p}$ are the orbital semi-axis and the mass of the planet, M_* is the total mass of the host star, c is the speed light, and i is the inclination of the orbit to the line of sight. Recently, Mullally et al. (2008) have studied 15 DAVs. For the star GD 66 ($T_{eff} = 11\,980$ K, $\log g = 8.05$) they found evidence ($d\Pi/dt = 1.35 \times 10^{-12}$ s/s) of the presence of a planet
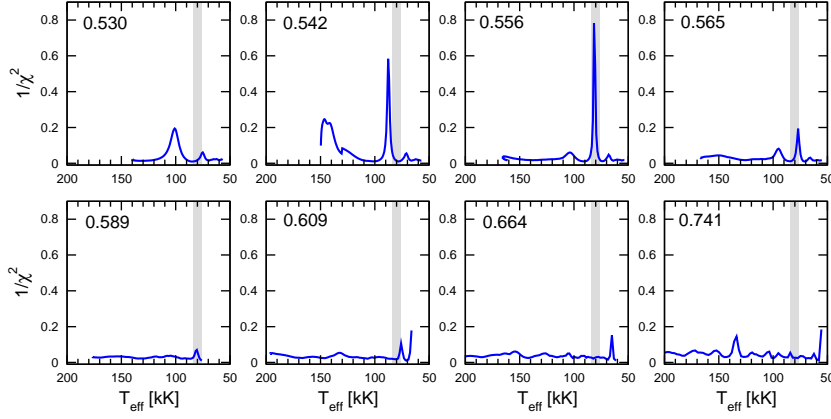
Fig. 22 The inverse of the quality function of the period fit in terms of the effective temperature. Each panel corresponds to a given value of the stellar mass. The vertical grey strip indicates the spectroscopic value of T_{eff} and its uncertainties. Note the strong maximum of the inverse of the quality function for the case $M_* = 0.556 M_\odot$ and $T_{eff} = 81\,500$ K, corresponding to the best-fit model for the pulsating PG 1159 star PG 0122+200. From Córsico et al (2007b).

with a mass of $m_p = 2M_J$, an orbital semi-axis of $a_p = 2.35$ AU, and an orbital period of 4.5 yr. In comparison, the rate of period change by cooling ($d\Pi/dt \sim 1 \times 10^{-15}$ s/s) and by proper motion ($d\Pi/dt \sim 1 \times 10^{-16}$ s/s) are much smaller. If the existence of a planet orbiting around GD 66 is confirmed it would indicate that a planet can survive the expansion in the giant phase of its host star.

In addition, the measurement of $\dot\Pi$ in variable white dwarfs can be employed to set constraints on particle physics. McGraw et al. (1979) were the first to suggest that hot pulsating white dwarfs could be employed to determine the effect of neutrino cooling as a star becomes a white dwarf — see also Winget et al. (1983). The influence of neutrino energy loss on $\dot\Pi$ was discussed in detail by Kawaler et al. (1986) for the case of DBV and DOV white dwarfs, see also Winget et al (2004). In addition, Isern et al. (1992), Córsico et al. (2001b) and Bischoff-Kim et al. (2008b) have explored the effect on the rate of period change of DAV stars of a hypothetical axion emissivity. Finally, O'Brien & Kawaler (2000) have discussed the possibility of inferring limits on the theoretically determined plasmon neutrino emission rates by employing DOV white dwarfs.

8.5 Period-to-period fits: the asteroseismological models

In this approach we seek pulsation models that best match the individual pulsation periods of the target pulsating white dwarf. To measure the goodness of the match between the theoretical pulsation periods (Π_k^T) and the observed individual periods (Π_i^O), a "quality function" is used:

$$\chi^2(M_*, T_{eff}) = \frac{1}{n} \sum_{i=1}^{n} \min \left[(\Pi_i^O - \Pi_k^T)^2 \right] \tag{51}$$

where n is the number of observed periods. For each star of interest, the model that shows the lowest value of χ^2 is adopted as the "best-fit model".

We illustrate this procedure in Fig. 22, where the quantity $(\chi^2)^{-1}$ in terms of the effective temperature for different stellar masses is displayed for the pulsating PG 1159 star PG 0122+200, together with the corresponding spectroscopic effective temperature. The quantity $(\chi^2)^{-1}$ is preferred instead of χ^2 because it emphasizes those models that provide good a agreement between the observed and the theoretical periods. Obviously, the lower the value of χ^2, the better the period match. Note the strong maximum of the inverse of the quality function in Fig. 22 for the case $M_* = 0.556 M_\odot$ and $T_{\rm eff} = 81\,500$ K. The associated PG 1159 model is adopted as the best-fit model for PG 0122+200. The quality of the period fit can be quantitatively measured by the average of the absolute period differences, $\overline{\delta \Pi_i} = (\sum_{i=1}^{n} |\delta \Pi_i|)/n$, where $\delta \Pi_i = \Pi_i^{\rm O} - \Pi_k$, and by the root-mean-square residual, $\sigma_{\delta \Pi_i} = \sqrt{(\sum |\delta \Pi_i|^2)/n}$. In the example considered here for PG 0122+200, $\overline{\delta \Pi_i} = 0.88$ s and $\sigma_{\delta \Pi_i} = 1.27$ s was obtained (Córsico et al. 2007b). It is worth mentioning that in some cases it is possible to get a stellar model (the best-fit model) that nicely reproduces the period spectrum observed in pulsating stars without artificially tuning the value of structural parameters which, instead, are kept fixed at the values predicted by the evolutionary calculations. This is the case of the asteroseismological studies on PG 1159 stars carried out by Córsico et al. (2007ab, 2008, 2009b).

We close this section by noting that the period-fit approach described here yields an asteroseismological model from which one can infer, in addition to M_*, the luminosity, radius, gravity, and distance of the target star. In addition, the period-fit approach does not require — in principle — external constraints such as the spectroscopic value of $T_{\rm eff}$, i.e., the method works "by letting the pulsation modes speak for themselves" — see Metcalfe (2005) for an interesting discussion about this issue.

8.6 Non-linear light-curve fits: constraining convection?

Light curves of pulsating white dwarfs exhibit a variety of shapes, in some cases being very simple and nearly sinusoidal, and in other cases exhibiting complex, strongly non-linear features that frequently are variable with time — see Figs. 17 to 19 of Fontaine & Brassard (2008). In the last case, the Fourier transform contains many frequencies that are not genuine eigenfrequencies (that is, they cannot be labelled with numbers ℓ, m, k), but instead they are just linear combinations and harmonics of real eigenfrequencies. As such, they do not carry information about the interior of the star. However, they can be exploited to extract information of the surface layers. As such, the study of non-linearities in the light curve of a pulsating white dwarf can be considered as other asteroseismological (but non-conventional) tool.

Assuming that non-linearities in the light curves appear as a result of the non-linear response of the convection zone, Montgomery (2005) proposed a new technique for fitting observed non-sinusoidal light curves to study convection in white dwarfs, allowing to infer the depth of the outer convection zone, and how the thickness of the convection zone changes as a function of effective temperature. Also, this technique allows to place constraints on mode identifications for the pulsation modes. Montgomery (2005) has been able to reproduce the pulse shape of a large-amplitude mode in the DAV G 29−38 and in the DBV star PG 1351+489. More recently, Montgomery (2008b) has improved and extended his technique and has applied it to the multiperiodic DBV star GD 358 and has also reexamined the case of PG 1351+489. His results indicate that GD 358 must have a thicker convection zone than PG 1351+489.

We stress that the technique of Montgomery (2005) assumes that the non-linearities in the light curves of pulsating white dwarfs are due exclusively to the non-linear response of the convection zone to the sinusoidal temperature perturbation entering at its basis. Adopting a different point of view, Brassard et al. (1995) have assumed that the non-linearities in the light curve are due to the non-linear response of the emergent radiative flux to a perturbation of the temperature. Brassard et al. (1993) and Fontaine & Brassard (1994) have been able to explain the presence of eight non-linear peaks (harmonic and cross-frequencies of the three eigenmodes) in the light curve of the DAV star G 117−B15A, without the necessity of the existence of a convection zone, a fact that is not crucial in the theory developed by Brassard et al. (1995). This does not mean in any way that convection does not affect the non-linearities in the light curve of a star, but instead, that there must be non-linear effects due exclusively to the non-linear response of the emergent radiative flux, irrespective of the presence or not of a outer convective region.

9 The various families of white dwarf pulsators

Below, we review our knowledge of asteroseismology of the different classes of pulsating white dwarfs, and we summarize the most recent results.

9.1 ZZ Ceti stars

Pulsating white dwarfs with H-rich atmospheres, the ZZ Ceti stars or simply DAVs, are the most numerous among the degenerate pulsators. ZZ Ceti stars are found within a very narrow interval of effective temperatures ($10,500 \text{ K} \lesssim T_{\text{eff}} \lesssim 12,500 \text{ K}$). Their brightness variations, which reach up to 0.30 mag, are interpreted as being caused by spheroidal, non-radial g-modes of low degree ($\ell \leq 2$) and low and intermediate overtones k, with periods between 100 and 1,200 s. Radial modes ($\ell = 0$) and non-radial p-modes, although found overstables in a number of theoretical studies of pulsating DA white dwarfs — see, e.g., Vauclair (1971) and Saio et al. (1983) — have been discarded as the cause of variability in such stars, because the periods involved are shorter than 10 s. Observationally, these high-frequency signatures have not been detected thus far (Silvotti et al. 2007). With regard to the mechanism that drives pulsations, the $\kappa - \gamma$ mechanism is the traditionally accepted one (Dolez & Vauclair 1981; Dziembowski & Koester 1981; Winget et al. 1982a). Nonetheless, Brickhill (1991) proposed the "convective driving" mechanism as being responsible for the overstability of g-modes in DAVs — see also Goldreich & Wu (1999). Although both mechanisms predict roughly the observed blue edge of the instability strip, none of them is capable to explain the observed red edge, where pulsations of DA white dwarfs seemingly cease (Kanaan 1996; Kotak et al. 2002b; Mukadam et al. 2006).

9.1.1 Observations of DAVs: the purity of the instability strip

A fundamental observational problem related to the DAVs is the quest for purity of the ZZ Ceti instability strip. That is, the question is if all DAs located within the instability strip are variable, or there exist stars in this region which do not exhibit flux variations. This problem is of particular relevance because if the instability strip is pure all DA white dwarfs must experience a phase of pulsation instability. This implies that any information about the internal structure of DAVs inferred using asteroseismology is also valid for all the DAs in

general. The study of the purity of the DAV instability strip is sensitive to two factors: (i) the accuracy and sensitivity of the photometric observations, and (ii) the accuracy of the determination of $T_{\rm eff}$ and $\log g$. As for the first point, in searching for photometric variations, a given star can be pulsating with amplitudes below the detection limit of the telescopes employed. This can render a pulsating star as non-variable. Concerning the second point, if a non-pulsating star has its values of $\log g$ and $T_{\rm eff}$ poorly determined, it may appear within the instability strip very close to the genuine variables. Employing high signal-to-noise spectra, Bergeron et al. (1995, 2004), and Gianninas et al. (2005, 2006) have found a pure instability strip for the brightest DAVs. On the other hand, there are about 20 DA stars located within the instability strip, for which pulsations are not detected (Mukadam et al. 2004). These stars suffer from a poor determination of their surface parameters. On the other hand, Castanheira et al. (2007) have found low amplitude variability for two stars previously reported as non-variables. At present, there is solid evidence suggesting that the DAV instability strip is pure (Winget & Kepler 2008).

It is worth noting as well that a large number of DAVs are known, a fact that makes them as a very attractive subject of study to the eyes of asteroseismology. Indeed, to date (late 2009) there are about 143 DAVs known, of which 83 were discovered in the SDSS since 2004 (Winget & Kepler 2008). This number is adequate to attempt a detailed study of the group properties of ZZ Ceti stars (Mukadam et al. 2006). The first steps in this direction have been done by Clemens (1993). The instability strip is populated by two categories of objects. The first group is composed by hot ZZ Ceti stars (or hDAVs) that are close to the blue edge. These stars are characterized by a very reduced number of periods, low amplitude of pulsations, and light curves which are almost sinusoidal and very stable in time. The second group is made of cool ZZ Ceti stars (or cDAVs) which are close to the red edge, exhibit many periods, large amplitudes of pulsation, non-sinusoidal light curves which are very unstable on short timescales, and populated by many linear combinations and harmonics of genuine eigenfrequencies. Mukadam et al. (2006) suggest introducing a third class of ZZ Ceti stars, to be called the intermediate DAVs (iDAVs). It would be the evolutionary subclass adjoining the hDAVs and the cDAVs, showing a large range of pulsation periods. Generally, there is a clear correlation between effective temperature and period: the cooler (hotter) the star, the longer (shorter) the periods (Mukadam et al. 2006). In addition, there is a (weaker) correlation between pulsation period and gravity (Fontaine & Brassard 2008).

9.1.2 DA white dwarf models and asteroseismological studies of DAVs

The first published complete set of DA and DB white dwarf models suitable for asteroseismology was that presented by Tassoul et al. (1990). A large parameter space was explored in such a monumental study, and for a long time (since the early eighties) this set of models represented the state-of-the-art in the area. The pulsation properties of these models were thoroughly explored in a series of important papers by Brassard et al. (1991, 1992a, 1992b). As important as these models were at that time, they suffer from a number of shortcomings: the core of the models is made of pure C, in opposition to the results of standard evolutionary calculations, that indicate that the cores of typical white dwarfs are made of a mixture of C and O; the C/He and He/H chemical interfaces are modeled on the basis of the assumption of the diffusive equilibrium in the trace element approximation, an approach that involves a quasi-discontinuity in the chemical profiles at the chemical interfaces which, in turn, leads to peaked features in the Brunt-Väisälä frequency that produces excessive mode-trapping

effects (Córsico et al. 2002a; 2002b). These models were employed for asteroseismological inferences of the DAVs G 226−29 (Fontaine et al. 1992) and GD 154 (Pfeiffer et al. 1996).

The models presented by Bradley (1996) constituted a substantial improvement in the field. These models have carbon-oxygen cores in varying proportions, and the CO/He and He/H chemical interfaces are more realistic. Maybe the most severe shortcoming of these models is the (unrealistic) ramp-like shape of the core carbon-oxygen chemical profiles. These DA models were the basis of the very important asteroseismological studies on the DAVs G 29−38 (Bradley & Kleinman 1997), G 117−B15A and R 548 (Bradley 1998), GD 165 and L 19−2 (Bradley 2001), and G 185−32 (Bradley 2006).

The next step in improving the modeling of DAVs was given by Córsico et al. (2002b) and Benvenuto et al. (2002), who employed evolutionary models characterized by He/H chemical interfaces resulting from a time-dependent element diffusion treatment (Althaus & Benvenuto 2000), and the core chemical structure extracted from the evolutionary calculations of Salaris et al. (1997). The employment of very smooth chemical interfaces, as shaped by chemical diffusion, revealed that the use of the trace element approximation is inappropriate in pulsational studies. This grid of models was employed in an asteroseismological study of G 117−B15A (Benvenuto et al. 2002). It is worth noting that the starting configurations for these sequences were obtained through an artificial procedure, and not as a result of evolutionary calculations of the progenitor stars.

Recently, Castanheira & Kepler (2008, 2009) have carried out an extensive asteroseismological study of DAVs employing DA white dwarf models similar to those of Bradley (1996), but with a simplified treatment of the core chemical structure. Specificallym, they fixed the central abundances to 50 % of O and 50 % of C. The He/H chemical interfaces adopted for these models are a parametrization of chemical profiles resulting from time-dependent element diffusion (Althaus et al. 2003). This study includes the "classical" DAVs and also the recently discovered SDSS DAVs. In total, 83 ZZ Ceti stars were analyzed. A very relevant result of these studies is that the thickness of the H envelopes inferred from asteroseismology is in the range $10^{-4} \gtrsim M_{\mathrm{H}}/M_* \gtrsim 10^{-10}$, with a mean value of $M_{\mathrm{H}}/M_* = 5 \times 10^{-7}$. This important result suggests that DA white dwarfs with envelopes substantially thinner than predicted by the standard theory of stellar evolution could exist. However, these results do not include the possible effects of realistic carbon-oxygen profiles on the fits. Almost simultaneously to the study of Castanheira & Kepler (2008, 2009), Bischoff-Kim et al. (2008a) have performed a new asteroseismological study on G 117−B15A and R 548 employing DA white dwarf models similar to those used by Castanheira & Kepler (2008, 2009), but with core chemical profiles similar to those of Salaris et al. (1997). The results of this work are in agreement with previuos studies of these ZZ Ceti stars. Recently, the models and the asteroseismological approach of Bischoff-Kim et al. (2008a) have been employed to infer the internal structure and seismological distance of the ZZ Ceti star KUV 02464+3239 (Bognár et al. 2009). Finally, Bischoff-Kim (2009) has presented the results of an asteroseismological analysis of two rich DAVs, G38−29 and R 808.

A summary of the asteroseismological inferences on individual ZZ Ceti stars performed so far is presented in Table 7 of Fontaine & Brassard (2008). As evident from what we said in the preceding paragraphs, there is no asteroseismological study of DAVs to date based on fully evolutionary models (generated from the ZAMS) that considers physically sound treatments to model the chemical interfaces at the core *and* the envelope of white dwarfs. This would be an important point for future asteroseismological studies of ZZ Ceti stars. Realistic stellar models are crucial to correctly assess the adiabatic period spectrum and

mode-trapping properties of the DAs, a very relevant aspect of white dwarf asteroseismology (Brassard et al. 1991; Brassard et al. 1992a,b; Bradley 1996; Córsico et al. 2002).

9.1.3 The paradigmatic ZZ Ceti star G 117−B15A

Now, we briefly revise some outstanding results in the field of DA white dwarf asteroseismology. In particular, we focus here on a very well studied ZZ Ceti star: G 117−B15A. This star is an otherwise typical DA white dwarf, the variability of which was discovered by McGraw & Robinson (1976) and, since then, it has been monitored continuously. The mass and the effective temperature of this star have been the subject of numerous spectroscopic re-determinations. In particular, values of $0.59 M_\odot$ and $11,620$ K, respectively, have been derived by Bergeron et al. (1995). Koester & Allard (2000) have reported a somewhat lower value for the mass, $M_* = 0.53 M_\odot$ and a higher effective temperature, $T_{eff} = 11,900 \pm 140$ K. G 117−B15A has oscillation periods of 215.2, 271 and 304.4 s (Kepler et al. 1982). As mentioned, this star has been one of the DAVs analyzed by Bradley (1998). This author obtains two different structures according the k-identification of the modes exhibited by the star. If the periods at 215, 271, and 304 s are associated with $k = 1$, $k = 2$, and $k = 3$, this author obtains an asteroseismological model with $T_{eff} = 12,160$ K, $M_* = 0.55 M_\odot$, $M_H/M_* = 3 \times 10^{-7}$, and $M_{He}/M_* = 10^{-2}$. If, instead, the periods have $k = 2$, $k = 3$, and $k = 4$, the asteroseismological model is characterized by $T_{eff} = 12,530$ K, $M_* = 0.55 M_\odot$, $M_H/M_* = 1.5 \times 10^{-4}$, and $M_{He}/M_* = 10^{-2}$. Note that there are three orders of magnitude of difference in the mass of the H envelope between the two possible (and equally valid) asteroseismological solutions. This degeneracy of seismological solutions for G 117−B15A has also been found by Benvenuto et al. (2002) on the basis of independent stellar and pulsation modeling. Finally, Bischoff-Kim et al. (2008a) also find two classes of solutions, one characterized by "thin" H envelopes and other associated with "thick" H envelopes, although their "thick" envelope solutions ($M_H/M_* = 6 \times 10^{-7}$) are considerably thinner than those of the previous works.

G 117−B15A has a very remarkable property: its 215 s period is extremely stable, a fact that has enabled to detect its rate of period change, after more than 30 years of observations. In particular, Kepler et al. (2005) have reported a value of $\dot{\Pi} = 3.57 \pm 0.82 \times 10^{-15}$ s/s. This implies a variation of 1 s in $\sim 9 \times 10^6$ yr, making this star the most stable known optical clock. Theoretical models indicate that this mode is varying its 215 s period by virtue of cooling of the core. The inferred value of $\dot{\Pi}$ is compatible with a core made of carbon and oxygen in (yet) unknown proportions. It is expected that the value of $\dot{\Pi}$ will be refined in the next years so that we will be able to obtain the fractions of carbon and oxygen in the core and, thus, to place constraints on the cross section of the reaction $^{12}C(\alpha, \gamma)^{16}O$. The most recent value for $\dot{\Pi}$ (215 s) reported by Kepler (2009) is somewhat larger, of $4.77 \pm 0.59 \times 10^{-15}$ s/s.

As a further application of the measurement of $\dot{\Pi}$ for G 117−B15A, we briefly describe the attempts to put constraints on the mass of axion, a weakly interacting particle whose existence (still not demonstrated) has been postulated to solve the CP symmetry problem in the standard model. Axions are very interesting particles because they are plausible candidates for dark matter. The theory of axions does not provide any clue about the value of the axion mass, although it is known that the more massive the axion, the stronger their interaction with matter, and in turn, the larger the emissivity. Isern et al. (1992) devised the following ingenious method to infer the mass of the axion. They considered the evolution of white dwarfs with and without axion emissivity, and compared the theoretical values of $\dot{\Pi}$ for increasing masses of the axion with the observed rate of period change of G 117−B15A.

Table 3 Stellar parameters and pulsation properties of the three known DQV stars.

Star	Mag. (g)	T_{eff} [K]	$\log g$ [cgs]	M_* [$M_\odot$]	Π [s]	Magnetic?	Ref.
SDSS J142625.70+575218.4	19.16	19 800	9	~ 1.2	$320 - 418$	yes	1
SDSS J220029.08−074121.5	17.70	21 240	8	~ 0.6	$255 - 578$	yes	2
SDSS J234843.30−094245.3	19.00	21 550	8	~ 0.6	$417 - 1044$	no	2

References: [1]Montgomery et al. (2008a) and Green et al. (2009), [2]Barlow et al. (2008) and Dufour et al. (2009a).

Isern et al. (1992) obtained a value of 8.7 meV (assuming $\cos^2 \beta = 1$) on the basis of a semi-analytical treatment. Later, Córsico et al. (2001b) found an axion mass of 4 meV using a detailed asteroseismological model for G 117−B15A. Recently, Bischoff-Kim et al. (2008b) have obtained a upper limit of $13.5 - 26.5$ meV using an improved asteroseismological model for the star and a better treatment of the error bars on the calculated $\dot{\Pi}$ values. Since both the value of the measured $\dot{\Pi}$, as well as the modeling of DA white dwarfs, have been changing over the years, it is expected that these estimates for the axion mass could change in the near future (Isern et al. 2010).

9.2 DQVs

Hot DQ white dwarfs characterized by carbon-dominated atmospheres were recently discovered at effective temperatures of between $\sim 18,000$ K and $\sim 24,000$ K by Dufour et al. (2007). This finding could be indicative of the existence a new evolutionary channel of white-dwarf formation (see Sect. 5.2). Shortly after the discovery of hot DQs, Montgomery et al. (2008a) reported the finding of the first variable hot DQ star, SDSS J142625.70+575218.4 (with $\log g \sim 9$ and $T_{\text{eff}} \sim 19,800$ K), with a confirmed period $\Pi \approx 418$ s. Shortly later, Barlow et al. (2008) reported the discovery of two additional variable hot DQ stars, SDSS J220029.08−074121.5 ($\log g \sim 8$, $T_{\text{eff}} \sim 21,240$ K) and SDSS J234843.30−094245.3 ($\log g \sim 8$, $T_{\text{eff}} \sim 21,550$ K), with periods $\Pi \approx 656$ s and $\Pi \approx 1052$ s, respectively. The measured periodicities were interpreted as non-radial g-mode pulsations, similar to the well-studied pulsations of the GW Vir, V777 Her, and ZZ Ceti classes of white-dwarf variables. The pulsation hypothesis, however, was defied by the possibility that these stars could be AM CVn systems, because of the similarity exhibited in the pulse shape of the light curves (Montgomery et al. 2008a). On the other hand, a compelling argument against the interacting binary hypothesis is that it does not explain why all hot DQ white dwarfs are grouped within the same range of temperatures, and none at higher or lower effective temperatures (Dufour et al. 2009a). Recently, the pulsating nature of the variable hot DQ white dwarfs has been conclusively confirmed at least for one of them (SDSS J142625.70+575218.4) by Green et al. (2009), who have discovered an additional period $\Pi \sim 319.7$ s (apart from the already known at 418 s). On the other hand, Dufour et al. (2009b) have carried out additional observations of SDSS J220029.08−074121.5 and SDSS J234843.30−094245.3. They have found evidence of two new periods at 254.7 s and 577.6 s for the former star, and also a probable period at 417 s for the latter star. These authors also found evidence that SDSS J220029.08−074121.5 could have a magnetic field, as is the case of SDSS J142625.70+575218.4 (Dufour et al. 2008b), but SDSS J234843.30−094245.3 not. Table 9.2 summarizes the properties of the known DQVs. The fifth column gives the spectroscopic mass derived from the evolutionary tracks of Althaus et al. (2009a).
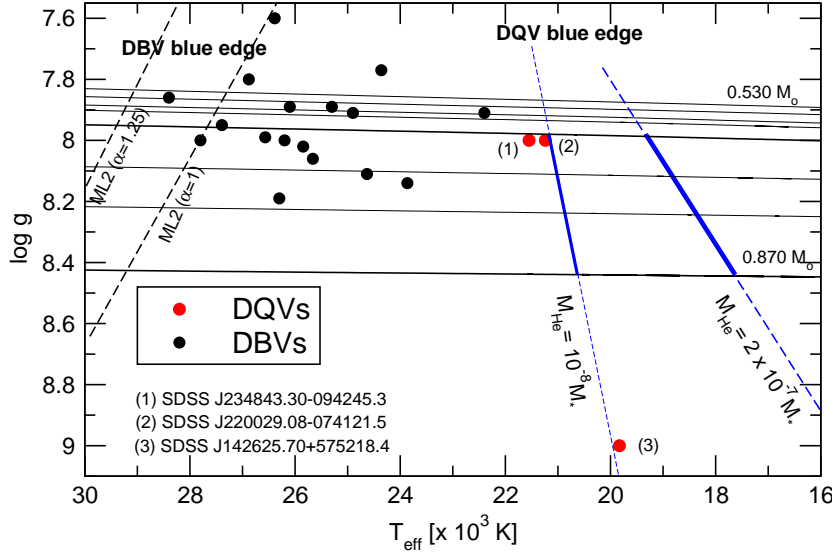
Fig. 23 A $\log g - T_{\text{eff}}$ diagram showing the location of the three known variable hot DQs (the DQVs) with red circles, and the known seventeen DBVs (black circles). Evolutionary tracks corresponding to DB white dwarf models with stellar masses of 0.530, 0.542, 0.556, 0.565, 0.589, 0.664, 0.742, and $0.87 M_\odot$ (from top to bottom) are shown using solid curves. The blue edge of the theoretical DBV instability strip (taken from Córsico et al. 2009a), is displayed with black dashed lines. The blue edge of the DQV instability domain is drawn with thick blue solid segments for two values of M_{He}. For illustrative purposes, these lines are extended to high and low gravities (blue dashed lines).

The origin of variability in hot DQ stars was first addressed theoretically by Fontaine et al. (2008), following the hypothesis that the variability could be caused by pulsations. They found that g-modes can be excited in the range of temperature where real DQs are found (below $\sim 21,500$ K), but only if the models are characterized by substantial amounts of He ($X_{\text{He}} \gtrsim 0.25$) in their carbon-rich envelopes. Dufour et al. (2008a) estimated the T_{eff}, $\log g$, and C/He ratio of the nine known hot DQ stars and constructed a dedicated stellar model for each object using the same modeling as in Fontaine et al. (2008). Using a non-adiabatic approach, Dufour et al. (2008a) predicted that only SDSS J1426+5752 should exhibit pulsations, and failed to predict variability in SDSS J220029.08−074121.5 and SDSS J234843.30−094245.3. However, it appears that the pulsation models of Fontaine et al. (2008) and Dufour et al. (2008a) are not entirely consistent with their proposed evolutionary picture for the formation of hot DQs. Indeed, the background models they assumed for their stability calculations are characterized by a He content several orders of magnitude higher than the content of He required by their evolutionary scenario to work (Dufour et al. 2008a). In fact, the bottom of the He-dominated envelope in their stellar models is located at a fractional mass depth of $\log q_{\text{env}} \equiv \log(1 - M_r/M_*) = -3$ (Fontaine et al. 2008).

Recently, Córsico et al. (2009d) have presented a new pulsation stability analysis of carbon-rich hot DQ white dwarf stars with the aim to test the convective-mixing picture for the origin of hot DQs (Dufour et al. 2007; Althaus et al. 2009b). This is done studying their pulsational properties. Córsico et al. (2009d) have employed the full evolutionary models of hot DQ white dwarfs developed by Althaus et al. (2009b), which consistently cover the entire evolution from the born-again stage to the DQ white dwarf stage. According to this study, overstable g-modes in hot DQ white dwarf models are primarily driven by the κ-

mechanism caused by the strong destabilizing effect of the opacity bump due to the partial ionization of C, the role of the partial ionization of HeII being much less relevant. Also, the theoretical blue edge of DQVs is hotter for less massive models than for more massive ones (see Fig. 23), which is at odds with the results of Fontaine et al. (2008) and Montgomery et al. (2008a). In addition, the blue edge for DQV stars is hotter for smaller amounts of He in the envelopes. In summary, the calculations of Córsico et al. (2009d) support the diffusive/convective mixing picture for the formation of hot DQs, and in particular, demonstrate that the diffusive/convective mixing scenario is not only able to explain the origin of hot DQ white dwarfs, but also accounts for the variability of these stars. We stress that the conclusions reached in Córsico et al. (2009d), and also the results of Fontaine et al. (2008) and Dufour et al. (2008a), especially those concerning the location of the blue edge of the DQV instability strip, could be altered substantially if a fully consistent treatment of the interaction between convection and pulsation were included in the stability analysis.

9.3 V777 Her stars

V777 Her (or DBV) stars are g-mode variable white dwarfs with He-rich atmospheres (DB) and intermediate effective temperatures ($T_{\mathrm{eff}} \sim 25,000$ K), that pulsate with periods between 100 and 1,100 s. The pulsating nature of DBVs was predicted almost three decades ago on theoretical grounds by Winget et al. (1982a) and shortly after confirmed observationally by Winget et al. (1982b). Since then, considerable effort has been devoted to study these stars. In particular, the multiperiodic star GD 358, the most extensively studied member of the DBV class, has been the subject of numerous investigations devoted to disentangle its internal structure and evolution, initially by means of "hands on" asteroseismological procedures (Bradley and Winget 1994b) and later employing objective fitting techniques — see, e.g., Metcalfe et al. (2000, 2001, 2002). In particular, Metcalfe et al. (2001) have applied genetic algorithm-based procedures to place constraints on the $^{12}\mathrm{C}(\alpha, \gamma)^{16}\mathrm{O}$ reaction rate from inferences for the abundance of central oxygen in GD 358.

9.3.1 Observations of DBVs and the presence of H

There are currently 20 known DBVs, 9 of which have been discovered by Nitta et al. (2009) in the SDSS and 2 have recently reported by Kilkenny et al. (2009). In Table 4 we list the main properties of all known DBVs. Although the number of DBVs has been considerably enlarged, it still is not sufficient as to assess the group characteristics.

The issue of the purity of the instability strip also matters for DBVs, as in the case of DAVs. However, in addition to the sensitivity of the photometric observations and the accuracy of the determination of T_{eff} and $\log g$, for the DBVs the picture is complicated further by the possible presence of small quantities of H in the He-rich atmospheres of DBs. The presence of H is attributed mainly to accretion from the interstellar medium. It is expected that a modest accretion rate of about $10^{-19} - 10^{-21} \, M_{\odot}/\mathrm{yr}$ could be enough to explain the presence of H in the DBs. The effective temperatures of DB stars derived from model atmospheres that contain H are considerably lower than those obtained in the case in which H is neglected (Beauchamp et al. 1999; Castanheira et al. 2006; Voss et al. 2007). Thus, the presence of (unknown) quantities of H in the He-rich atmospheres of DB stars has strong impact on the determination of the effective temperature and gravity. Concerning the purity of the DBV instability strip, before arriving at a final conclusion it is crucial to address first the three above mentioned factors.

Table 4 Stellar parameters and pulsation properties of all known V777 Her (or DBV) stars.

Star	Mag.	T_{eff} [K]	$\log g$ [cgs]	Π [s]	Ref.
KUV 0513+2605	16.70 (V)	26300	8.19	$350 - 900$	1
CBS 114	17.2 (B)	26200	8.00	$230 - 670$	1
PG 1115+158	16.1 (B)	25300	7.89	$831 - 1072$	1
PG 1351+489	16.4 (B)	26100	7.89	$333 - 490$	1
PG 1456+103	15.9 (B)	22400	7.91	$423 - 854$	1
GD 358	13.65 (V)	24900	7.91	$423 - 810$	1
PG 1654+160	16.2 (B)	27800	8.00	$149 - 851$	1
PG 2246+120	16.73 (V)	27200	7.89	$256 - 329$	1
EC 20058$-$5234	15.0 (B)	28400	7.86	$195 - 540$	1
SDSS J034153.03$-$054905.8	18.25 (g)	25087	8.02	942	2
SDSS J085202.44+213036.5	18.50 (g)	25846	8.02	951	2
SDSS J094749.40+015501.8	19.95 (g)	23453	8.13	255	2
SDSS J104318.45+415412.5	18.95 (g)	26291	7.77	420	2
SDSS J122314.25+435009.1	18.98 (g)	23442	7.84	$544 - 687$	2
SDSS J125759.03$-$021313.3	19.16 (g)	25820	7.57	$532 - 729$	2
SDSS J130516.51+405640.8	17.46 (g)	24080	8.14	$658 - 912$	2
SDSS J130742.43+622956.8	18.83 (g)	23841	8.14	890	2
SDSS J140814.63+003838.9	19.19 (g)	26073	7.98	$258 - 335$	2
EC 04207$-$4748	15.3 (V)	27300	7.8	$223 - 448$	3
EC 05221$-$4725	16.6 (V)	$-$	$-$	$704 - 976$	3

References: [1]Beauchamp et al. (1999) and Fontaine & Brassard (2008), [2]Nitta et al. (2009), [3]Kilkenny et al. (2009).

9.3.2 The theoretical blue edge

The pulsations in DBV stars are thought to be triggered by the $\kappa - \gamma$ mechanism acting on the partial ionization of He at the base of the outer convection zone. The observed instability strip of the DBV stars is located between $T_{\text{eff}} \approx 28\,400$ K and $T_{\text{eff}} \approx 22\,500$ K (Winget & Kepler 2008). All published stability analysis of DB models — see, for instance, Bradley & Winget (1994a) and Beauchamp et al. (1999) — clearly indicate a strong dependence of location of the theoretical blue (hot) edge of the DBV instability strip with the convective efficiency adopted in the envelope of the stellar models. At present, there is no general consensus between different authors about what is the right convective efficiency in DB models in order to fit the observed blue edge. Córsico et al. (2009a) have recently explored the impact of different convective efficiencies and also the presence of small amounts of H in the atmospheres of DB stars on the precise location of the theoretical blue edge of the DBV instability strip. They employed a new set of fully evolutionary DB white dwarf models that descend from the post-born again PG 1159 models (Miller Bertolami & Althaus 2006) recently presented in Althaus et al. (2009a). Details of these DB models are available in that paper. Córsico et al. (2009a) employ the following prescriptions of the MLT, in order of increasing efficiency: $\text{ML1}/\alpha = 1$, $\text{ML2}/\alpha = 0.60$, $\text{ML2}/\alpha = 1$, $\text{ML2}/\alpha = 1.25$, and $\text{ML3}/\alpha = 2$, α being the characteristic mixing length (Tassoul et al. 1990). The resulting theoretical blue edges of the DBV instability strip are shown in Fig. 24, where the case of atmospheres devoided of H is considered. Fig. 24 also shows the complete set of DB evolutionary sequences (solid lines) on the $T_{\text{eff}} - \log g$ diagram, along with the location of the known DBV stars. Note that there is a clear dependence of the blue edge with the stellar mass. It is apparent that only the $\text{ML2}/\alpha = 1.25$ prescription is able to account for the location of all known DBVs. We warn that the non-adiabatic computations of Córsico et al. (2009a) assume the "frozen convection" approximation. Thus, the results for the DBV
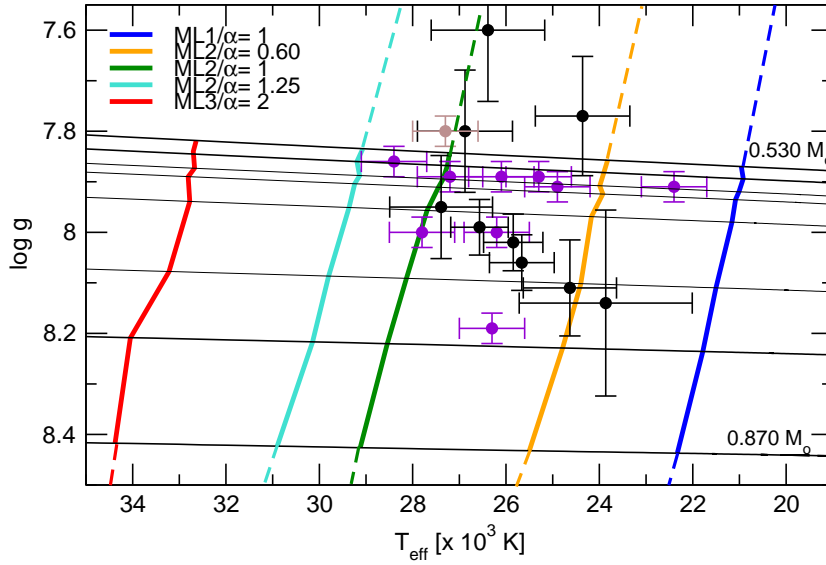
Fig. 24 The blue edge of the DBV instability strip for different prescriptions of the MLT. The location of most known DBV stars is included — black dots: Beauchamp et al. (1999), violet dots: Nitta et al. (2009), brown dot: Kilkenny et al. (2009). Only the ML2/$\alpha = 1.25$ prescription proposed by Beauchamp et al. (1999) is able to account for the location of all known DBVs.

theoretical blue edge could somewhat change if the perturbation to the convective flux were taken into account in the stability analysis.

The shift of the effective temperature of DBVs towards lower values when some impurities of H are considered in the model atmospheres has a counterpart in the location of the theoretical blue edge of the V777 Her instability strip. Córsico et al. (2009a) have performed fully non-adiabatic pulsation computations in DB models characterized by some presence of H in the almost He-pure envelopes. They have restricted themselves to the cases in which $M_* = 0.530 M_\odot$ and $M_* = 0.741 M_\odot$. For these two values of the stellar mass, they have explored the cases in which $X_H = 0.0001, 0.001$ and 0.01, corresponding to $\log(n_H/n_{He}) = \log(4X_H/X_{He}) = -3.4, -2.4$ and -1.44, respectively. The results are depicted in Fig. 25. When $X_H = 0.0001$ there is no appreciable effect on the location of the blue edge of instability. But if $X_H = 0.001$ the blue edge is shifted to lower effective temperatures by ~ 800 K (for ML3/$\alpha = 2$) and ~ 300 K (for ML1/$\alpha = 1$). Finally, for $X_H = 0.01$ the shift is of ~ 3000 K (for ML3/$\alpha = 2$) and ~ 1200 K (for ML1/$\alpha = 1$).

9.4 GW Vir stars

Pulsating PG 1159 stars or GW Vir variable stars (after the prototype of the spectral class and the variable type, PG 1159−035 or GW Vir) are very hot H-deficient post-AGB stars with surface layers rich in He ($\sim 30 - 85\%$), carbon ($\sim 15 - 60\%$) and oxygen ($\sim 2 - 20\%$) (Werner & Herwig 2006) that exhibit multiperiodic, low degree ($\ell \leq 2$), high radial order ($k \gtrsim 18$) g-mode luminosity variations with periods in the range from about 300 to 3000 seconds. As mentioned earlier, some GW Vir stars are still embedded in a planetary nebula and they are commonly called PNNVs. GW Vir stars without nebulae are usually called
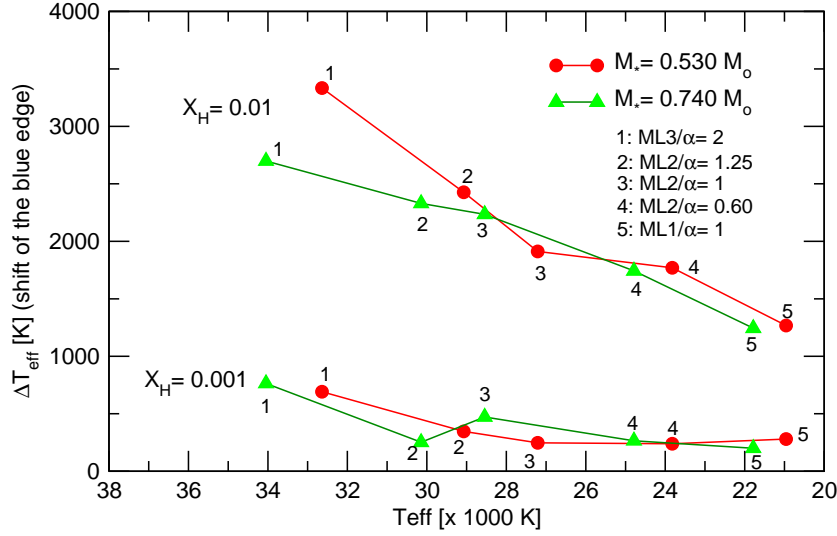
Fig. 25 The shift (in T_{eff}) of the blue edge as a result of the presence of H in the He-rich atmospheres of DBVs. A fractional abundance of H of 0.01 (0.001) is able to shift the blue edge towards lower T_{eff}s in about 3000 (800) K for the case of ML3. The shifts are substantially smaller (but non-negligible) for less efficient convection.

DOV stars. PNNV stars are characterized by much higher luminosity than DOV stars. GW Vir stars are particularly important to infer fundamental properties about pre-white dwarfs in general, such as the stellar mass and the surface compositional stratification (Kawaler & Bradley 1994; Córsico & Althaus 2006). In addition, pulsating PG 1159 stars have been shown by Córsico & Althaus (2005) to be valuable tools to constrain the occurrence of extra mixing episodes in their progenitor stars. PG 1159 stars are believed to be the evolutionary connection between post-AGB stars and most H-deficient white dwarfs. For details about the origin and evolution of PG 1159 stars, see Sect. 5.

9.4.1 Observations

There exist numerous studies in the literature focused on observational aspects of PG 1159 stars. In particular, we draw the attention of the reader to the excellent review article by Werner & Herwig (2006), which summarizes numerous spectroscopic studies and also theoretical aspects about the formation of these stars. In Table 5 we show the main properties of GW Vir stars. There are 16 members of the class known up to now, of which 10 are PPNVs and 6 are DOVs. The table also includes stars that share the pulsation properties of GW Vir stars but do not formally belong to the PG 1159 spectroscopic class. They are 5 Wolf-Rayet Central Stars of Planetary Nebula ([WCE]) type. Note that NGC 2371−2 is a transition object. We have included PG 1159 stars and [WCE] stars in the same table because the physics of mode excitation in both spectroscopic classes is the same. At least 5 GW Vir stars (RX J2117.1+3412, PG 1159−035, PG 1707+427, PG 2131+066, and PG 0122+200) have been intensively observed by the WET global instrument, and so they are particularly interesting for asteroseismology (see Sect. 9.4.4).

Table 5 Stellar parameters and pulsation properties of all known pulsating PG 1159 stars and pulsating [WC] stars.

Star	$T_{\mathrm{eff}}^{\mathrm{a}}$ [kK]	$\log g^{\mathrm{a}}$ [cgs]	M_*^{b} [$M_\odot$]	Class	PN?	Π [s]	$\Delta\Pi$ [s]
Longmore 4	120	5.5	0.63	PG 1159	yes	$831 - 2325$ [c]	—
Abell 43	110	5.7	0.53	PG 1159, H	yes	$2380 - 6075$ [d]	—
NGC 7094	110	5.7	0.53	PG 1159, H	yes	$2000 - 5000$ [e]	—
NGC 246	150	5.7	0.75	PG 1159	yes	$1460 - 4348$ [f]	—
NGC 5189	135	6.0	–	[WCE]	yes	690 [f]	—
Sk 3	140	6.0	–	[WCE]	yes	$929 - 2183$ [g]	—
NGC 2867	141	6.0	–	[WCE]	yes	769 [f]	—
NGC 6905	141	6.0	–	[WCE]	yes	$710 - 912$ [f]	—
NGC 1501	134	6.0	–	[WCE]	yes	$1154 - 5235$ [h]	22.3 ± 0.3 [h]
HE 1429-1209	160	6.0	0.66	PG 1159	no	919 [i]	—
RX J2117.1+3412	170	6.0	0.72	PG 1159	yes	$694 - 1530$ [j]	21.48 ± 0.04 [j]
HS 2324+3944	130	6.2	0.53	PG 1159, H	no	$2005 - 2569$ [k]	—
NGC 2371-2	135	6.3	–	[WC]-PG 1159	yes	$923 - 1825$ [f]	—
K 1-16	140	6.4	0.54	PG 1159	yes	$1500 - 1700$ [l]	—
Jn 1	150	6.5	0.55	PG 1159	yes	454 [m]	—
VV 47	130	7.0	0.53	PG 1159	yes	$261 - 4310$ [m]	24.21 [r]
NGC 6852	–	–	–	PG 1159	yes	$1096 - 5128$ [m]	—
PG 1159−035	140	7.0	0.54	PG 1159	no	$339 - 982$ [n]	21.5 ± 0.1 [n]
PG 2131+066	95	7.5	0.55	PG 1159	no	$339 - 598$ [o]	21.6 ± 0.4 [s]
PG 1707+427	85	7.5	0.53	PG 1159	no	$335 - 909$ [p]	23.0 ± 0.3 [p]
PG 0122+200	80	7.5	0.53	PG 1159	no	$336 - 612$ [q]	22.9 ± 0.0 [q]

References: [a]Werner & Herwig (2006), [b]Miller Bertolami & Althaus (2006), [c]Bond & Meakes (1990), [d]Vauclair et al. (2005), [e]Solheim et al. (2007), [f]Ciardullo & Bond (1996), [g]Bond & Ciardullo (1993), [h]Bond et al. (1996), [i]Nagel & Werner (2004), [j]Vauclair et al. (2002), [k]Silvotti et al. (1999), [l]Grauer et al. (1987), [m]González Pérez et al. (2006), [n]Costa et al. (2008), [o]Kawaler et al. (1995), [p]Kawaler et al. (2004), [q]Fu et al. (2007), [r]Córsico et al. (2009c), [s]Reed et al. (2000).

9.4.2 Evolutionary models for PG 1159 stars

A large variety of H-deficient models have been employed in the past for pulsation studies of PG 1159 stars. We can roughly classify these pulsation models into three main categories: static envelope models (Starrfield et al. 1983, 1984, 1985; Bradley & Dziembowski 1996; Cox 2003; Quirion et al. 2004, 2007), simplified evolutionary models (Kawaler et al. 1986; Kawaler 1988; Stanghellini et al. 1991; Kawaler & Bradley 1994; Saio 1996; Gautschy 1997), and full evolutionary models (Gautschy et al. 2005; Córsico et al. 2006). Here, we restrict ourselves to briefly describe the set of models employed in the study of Córsico et al. (2006) — see Sect. 5 for details. These models have been generated by Althaus et al. (2005a) and Miller Bertolami & Althaus (2006) by taking into account the complete evolutionary history of the progenitor stars. This is the unique set of full evolutionary sequences that covers a wide range of stellar masses, rendering such models very suitable for asteroseismology. Althaus et al. (2005a) and Miller Bertolami & Althaus (2006) computed the complete evolution of model sequences with a stellar mass in the ZAMS within 1 and $3.75\,M_\odot$. All the sequences were computed employing the LPCODE evolutionary code — see Althaus et al. (2005a) for details — and were followed from the ZAMS through the thermally pulsing and mass-loss phases on the AGB. After experiencing several thermal pulses, the progenitors departed from the AGB and evolved towards high effective temperatures. Mass loss during the departure from the AGB was arbitrarily fixed to obtain a final He shell flash during the early white dwarf cooling phase. After the born-again episode, the H-deficient, quiescent He-burning remnants evolved at constant luminosity to the domain of PG 1159 stars with a

surface chemical composition rich in He, carbon and oxygen. The masses of the remnants span the range $0.530 - 0.741 M_\odot$. A very important result of the work of Miller Bertolami & Althaus (2006) is a new determination of the spectroscopic mass of PG 1159 stars. The mean mass obtained by these authors is $0.573 M_\odot$, $0.044 M_\odot$ lower than the previously accepted value.

9.4.3 Excitation of pulsations

A longstanding problem associated with GW Vir stars is related to the excitation mechanism, although at present, this problem appears to be solved. The early work by Starrfield et al. (1983) was successful in finding the correct destabilizing agent, namely the κ-mechanism associated with the partial ionization of the K-shell electrons of carbon and/or oxygen in the envelope of models. However, their models required a driving region very poor in He in order to be capable to excite pulsations; even very low amounts of He could weaken or completely extinguish the destabilizing effect of carbon and oxygen (the so called "He poisoning" effect). The latter requirement led to the conjecture that a composition gradient would exist to make compatible the He-devoid driving regions and the He-rich photospheric composition. Even modern detailed calculations still point out the necessity of a compositional gradient in the envelopes of models (Bradley & Dziembowski 1996; Cox 2003). The presence of a chemical composition gradient is difficult to explain in view of the fact that PG 1159 stars are still experiencing mass loss — for instance for PG 1159−035 the mass-loss rate is $\dot{M} \sim 10^{-8.1} M_\odot$ yr^{-1} (Koesterke et al. 1998) — a fact that prevents the action of gravitational settling of carbon and oxygen, and instead, tends to homogenize the envelope of hot white dwarfs (Unglaub & Bues 2000).

   Clearly at odds with the hypothesis of a composition gradient in the PG 1159 envelopes, calculations by Saio (1996), Gautschy (1997), and Quirion et al. (2004, 2007) — based on modern opacity OPAL data — demonstrated that g-mode pulsations in the correct ranges of effective temperatures and periods could be easily excited in PG 1159 models having an uniform envelope composition. In particular, Quirion et al. (2004) found that the presence of non-variable PG 1159 stars among GW Vir stars could be readily explained by the presence of an excessively large abundance of He. Hence, in contrast with the case of DAVs and DBVs, the GW Vir instability strip appears to be intrinsically impure.

   As important as they are, the vast majority of the studies of pulsation driving in PG 1159 stars performed in the past rely on simplified stellar models. Indeed, the earliest works employed static envelope models and old opacity data. Even more modern works, although based on updated opacity data (OPAL), still use a series of static envelope models that do not represent a real evolutionary sequence, or evolutionary calculations based on simplified descriptions of the evolution of their progenitors. The only exception is the very important work of Gautschy et al. (2005), which employs equilibrium PG 1159 models that evolved through the AGB and born-again stages, beginning from a $2.7 M_\odot$ zero age main sequence model star. Gautschy et al. (2005) analyzed four model sequences, with $0.530, 0.55, 0.589$ and $0.64 M_\odot$, being the $0.589 M_\odot$ sequence derived directly from the evolutionary computations of Althaus et al. (2005a). However, the remainder sequences were created from the $0.589 M_\odot$ one by artificially changing the stellar mass shortly after the end of the born-again episode.

   The work of Córsico et al. (2006) constitutes one of the most complete and detailed studies on pulsation stability of PG 1159 stars performed so far. Specifically, Córsico et al. (2006) have carried out detailed non-adiabatic pulsation computations on full PG 1159 evolutionary models with stellar masses in the range $0.530 - 0.741 M_\odot$ resulting from the complete

evolutionary calculations of Althaus et al. (2005a) and Miller Bertolami & Althaus (2006). Numerous detailed investigations about pulsating PG 1159 stars have been performed on the basis of artificial stellar models. In spite of the fact that significant pulsation damping and driving occur in PG 1159 envelope stars, the employment of such simplified stellar configurations appear not well justified in the case of these stars. This is in contrast to the situation of their more evolved counterparts, white dwarf stars, for which their thermo-mechanical structure has relaxed to the correct one by the time the domains of pulsational instability are reached. One of the main goals of the work of Córsico et al. (2006) has been to assess to what degree the conclusions arrived at in previous studies on PG 1159 stars change when realistic stellar configurations are adopted. The study of Córsico et al. (2006) confirms many results already known from previous studies, namely: (i) g-modes in PG 1159 models are excited by the κ-mechanism due to partial ionization of carbon and oxygen, and no abundance gradients between the driving region and the stellar surface are necessary to drive g-mode pulsations at the correct effective temperatures and period ranges; (ii) there exists a well-defined instability domain with a blue edge which is strongly dependent on the stellar mass (see Figs. 26 and 28); (iii) different surface He abundances lead to sizeable differences in the precise location of the theoretical blue edge of the instability domain; (iv) the instability domain splits into two separated regions, one of them at high luminosities characterized by long periods, and the other at low luminosities, corresponding to shorter periods (Fig. 26); (v) all pulsating PG 1159 stars lay into the predicted instability domain in the $\log(T_{\text{eff}}) - \log g$ plane (see Fig. 28); (vi) there is a very good agreement between the full period spectrum observed in GW Vir stars and the theoretical ranges of unstable periods; and (vii) the pulsation periods of excited modes decrease with decreasing luminosity (increasing surface gravity), in line with the observational trend (Fig. 26). As for the new results, Córsico et al. (2006) found that there exists a red edge of the instability domain at the high-luminosity (low-gravity) regime. This red edge is mass-dependent. The border of the instability domains in the $\log T_{\text{eff}} - \log \Pi$ plane at the high-luminosity, long-period regime is well delineated (Fig. 26). Finally, Córsico et al. (2006) found that some non-variables occupying the instability strip have standard He abundances and the presence of them between pulsators can not be explained through the argument of Quirion et al. (2004).

The more recent stability study on GW Vir star is that of Quirion et al. (2007). These authors have carried out a impressive non-adiabatic survey of pulsating PG 1159 stars and confirmed their previous result that the extent of the instability domain in the $\log g - T_{\text{eff}}$ diagram is a strong function of the C and O content in the envelopes of these stars. Because the chemical composition of the envelope of PG 1159 stars varies from star to star, the blue edge of the GW Vir instability strip must necessarily be the superposition of several blue edges, i.e., a fuzzy edge. In the study of Quirion et al. (2007), the effects of varying the total mass, of adding H, and of changing the metallicity are investigated, and the expected ranges of excited periods under various conditions are provided.

9.4.4 Asteroseismological inferences on GW Vir stars

In recent years, considerable observational effort has been invested to study pulsating PG 1159 stars. Particularly noteworthy are the works of Vauclair et al. (2002) on RX J2117.1+3412, Fu et al. (2007) on PG 0122+200, and Costa et al. (2008) and Costa & Kepler (2008) on PG 1159−035. These stars have been monitored through long-term observations carried out with the WET. On the theoretical front, recent important progress in the numerical modeling of PG 1159 stars (Althaus et al. 2005a; Miller Bertolami & Althaus 2006) has paved the way for unprecedented asteroseismological inferences for the mentioned stars (Córsico et al.
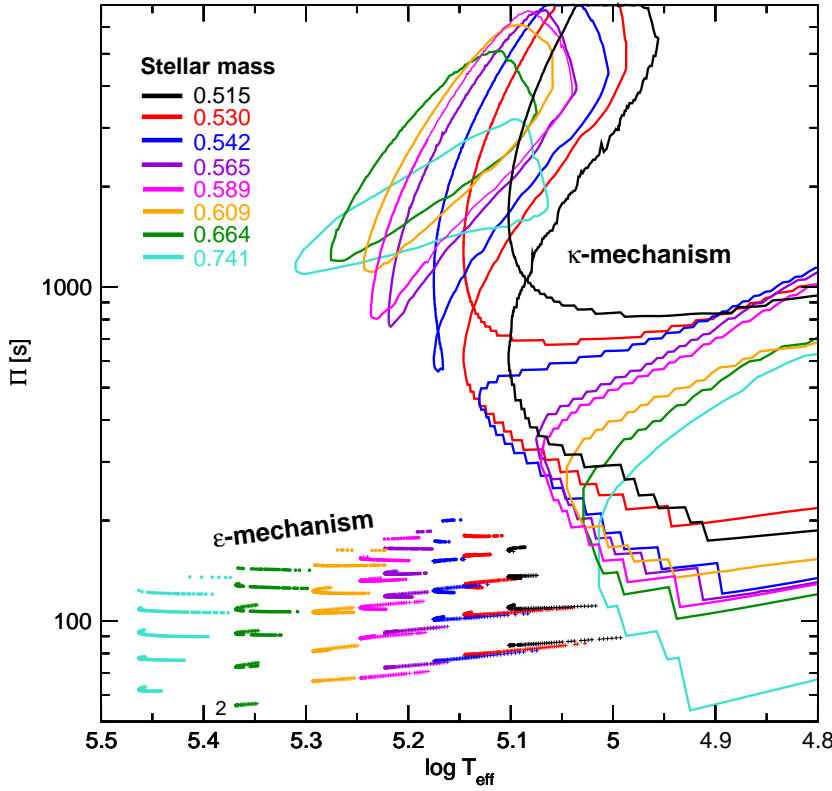
Fig. 26 The dipole ($\ell = 1$) instability domains for overstable κ-destabilized g-modes, bounded with lines of different colours for the various stellar masses, according to Córsico et al. (2006). Short-period dipole unstable ε-destabilized g-modes (see Sect. 9.4.6) are depicted with dot (plus) symbols for stages before (after) the evolutionary knee.

2007a, 2007b, 2008, 2009b). In these studies, three different methods have been employed to infer the stellar mass of GW Vir stars (see Sect. 8.1 and 8.5). With the first method, the stellar mass is obtained by comparing the observed period spacing with the asymptotic period spacing of the models. The second method consists in a comparison of the observed period spacing with the average of the computed period spacings. Finally, with the third method, models that best reproduce the individual observed periods of each star are sought, and, if possible, an unique asteroseismological model is found. The period-to-period fits (third method) performed in these studies are of unprecedented quality, and no artificial tuning of the value of structural parameters such as the thickness of the outer envelope, the surface chemical abundances, or the shape of the core chemical profile is made. Instead, they are kept fixed at the values predicted by the evolutionary calculations. Also, for the first time, in this series of studies the same evolutionary tracks are used for both the asteroseismological and the spectroscopic derivations of the stellar mass. This remarkable refinement (as compared with previous works) leads to a better agreement between asteroseismological and spectroscopic masses of GW Vir stars.

Table 6 summarizes the asteroseismological masses obtained for each star, along with the associated values of the spectroscopic mass. A graphical representation of these results

Table 6 Stellar masses for all of the intensively studied pulsating PG 1159 stars, including also one pulsating [WCE] star. All masses are in solar units.

Star	$\Delta\Pi_\ell^a$	$\overline{\Delta\Pi_\ell}$	Approximate formula	Period fit	Pulsations (other works)	Spectroscopy
NGC 1501	0.571[a]	0.576[a]	0.530[a]	—	0.55[j] ($\Delta\Pi_\ell^a$)	0.56
RX J2117.1+3412	0.568[b]	0.560[b]	0.525[a]	0.565[b]	0.56[h] ($\Delta\Pi_\ell^a$)	0.72
PG 1159−035	0.577–0.585[d]	0.561[d]	0.570[a]	0.565[d]	0.59[i] ($\Delta\Pi_\ell^a$)	0.54
PG 2131+066	0.627[a]	0.578[a]	0.609[a]	0.589[a]	0.61[e] (period fit)	0.55
PG 1707+427	0.597[a]	0.566[a]	0.587[a]	0.542[a]	0.57[g] ($\Delta\Pi_\ell^a$)	0.53
PG 0122+200	0.625[c]	0.567[c]	0.593[a]	0.556[c]	0.69[f] ($\Delta\Pi_\ell^a$)	0.53

References: [a]Córsico et al. (2009b), [b]Córsico et al. (2007a), [c]Córsico et al. (2007b), [d]Córsico et al. (2008), [e]Reed et al. (2000), [f]Fu et al. (2007), [g]Kawaler et al. (2004), [h]Vauclair et al. (2002), [i]Costa et al. (2008), [j]Bond et al. (1996).

is presented in Fig. 27. The internal (formal) errors (not plotted) of the asteroseismological mass determinations are $\lesssim 0.01 M_\odot$. Note that there is a good agreement between the asteroseismological and spectroscopic masses, except for the case of RX J2117.1+3412, where the spectroscopic mass is too large ($\sim 0.72 M_\odot$) to be compatible with all the three asteroseismological mass determinations ($\sim 0.56 - 0.57 M_\odot$). This discrepancy could be due to large errors in the spectroscopic T_{eff} and/or g values. We also note that the asymptotic period spacing overestimates the stellar mass of the studied PG 1159 stars, as expected on the grounds that these stars (except RX J2117.1+3412) are not in the asymptotic limit of g-mode pulsations, and then the asymptotic theory is not completely valid in such cases.

The main conclusion of the series of studies by Córsico et al. (2007b, 2008, 2009b) is that for most well-observed pulsating PG 1159 stars (PG 0122+200, PG 1159−035, PG 2131+066, and PG 1707+427) it is possible to find a stellar model (the asteroseismological model) with M_* near the spectroscopic determinations to a high internal accuracy. The next step is an assessment of the question if the asteroseismological models can provide more accurate masses for these objects. At first glance, the scatter in the masses derived from the different asteroseismological methods (see Table 6) suggests that it could not be the case. In fact, when all asteroseismological methods are considered, the uncertainty in the seismological determination of the mass amounts to $\sim 0.05 M_\odot$, comparable to the spectroscopic one — which is $\sim 0.05 - 0.1 M_\odot$ (Werner et al. 2008). However, it is worth noting that, when results based on the asymptotic period spacing — an approach that is not entirely correct for the high-gravity regime of PG 1159 stars, see Althaus et al. (2008b) — are not taken into account, the scattering in the derived masses is of only $\sim 0.02 M_\odot$. It can be concluded that asteroseismology of PG 1159 stars is a precise and powerful technique which can determine the masses of GW Vir stars even more accurately than spectroscopy.

9.4.5 The rate of period change of PG 1159−035

Recently, Costa & Kepler (2008) have measured the rate of period change for a large number of modes present in the star PG 1159−035. This study demonstrates that some $\dot{\Pi}$ values are positive (periods increase with time), and other $\dot{\Pi}$ values are negative (periods decrease with time). This is at odds with the asteroseismological model for PG 1159−035 derived by Córsico et al. (2008). Also, the rates of period changes measured by Costa & Kepler (2008) are 10 times larger than those predicted by the asteroseismological model. We stress that the PG 1159 evolutionary models employed in the series of asteroseismological studies of Córsico et al. (2007a, 2007b, 2008, 2009b) are characterized by thick He-rich outer
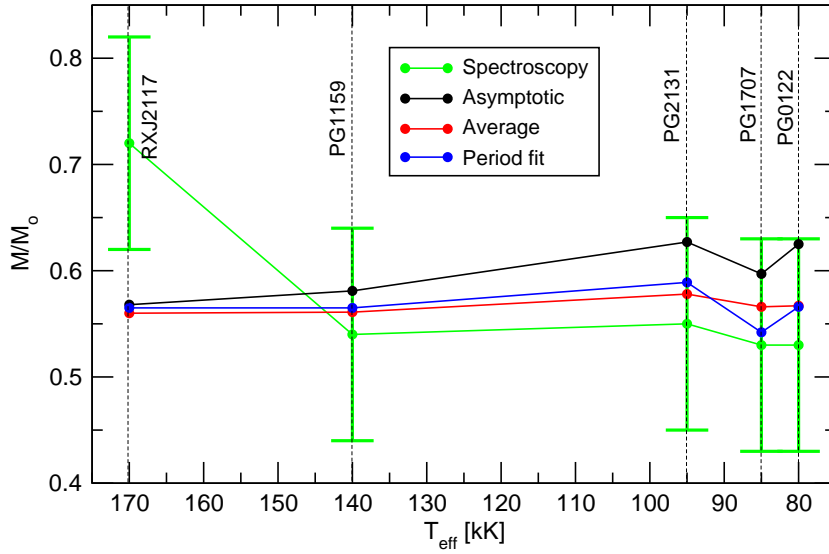
Fig. 27 A comparison between the stellar mass of GW Vir stars inferred from different approaches.

envelopes, as they are predicted by the standard theory for the formation of PG 1159 stars. However, Althaus et al. (2008b) have demonstrated that thinner He-rich envelopes ($2-3$ times thinner) solve the severe discrepancy between the measured rates of period change in PG 1159$-$035 and the theoretical values. In view of this important result, and to place it on a solid basis, it would be useful to recompute the asteroseismological models for all the pulsating PG 1159 stars (and, in particular, for PG 1159$-$035) analyzed in Córsico et al. (2007a, 2007b, 2008, 2009b) with non-canonical models characterized by thinner He-rich envelopes.

9.4.6 Short period g-modes driven by the ε-mechanism?

A recent stability study on PG 1159 star models carried out by Córsico et al. (2009c) has revealed the presence of unstable short-period g-modes destabilized by the He-burning shell through the ε-mechanism. This work, which covers a broad range of stellar masses and effective temperatures, confirms and extends the pioneering studies of Kawaler et al. (1986), Saio (1996) and Gautschy (1997) on this topic. The main results of this study can be summarized as follows: there exists a separate, well-defined theoretical PG 1159 instability strip in the $\log T_{\mathrm{eff}} - \log g$ diagram characterized by short-period g-modes excited by the ε-mechanism due to the presence of active He-burning shells. Notably, this instability strip partially overlaps the already known GW Vir instability strip due to the κ-mechanism acting on the partial ionization of carbon and/or oxygen in the envelope of the PG 1159 stars, as can be seen in Fig. 28. At variance with the classical κ-mechanism, responsible for the intermediate/long-period GW Vir pulsations, the ε-mechanism should be efficient even in PG 1159 stars with low carbon and oxygen content in their envelopes. The ε-driven g-modes probably have time enough to reach observable amplitudes before the star leaves the instability strip. VV 47 is the only PG 1159 star for which observational evidence of the presence of short-period g-modes exists (González Pérez et al. 2006). The stability analysis of Córsico et al. (2009c) provides very strong support to the idea that the physical origin of the
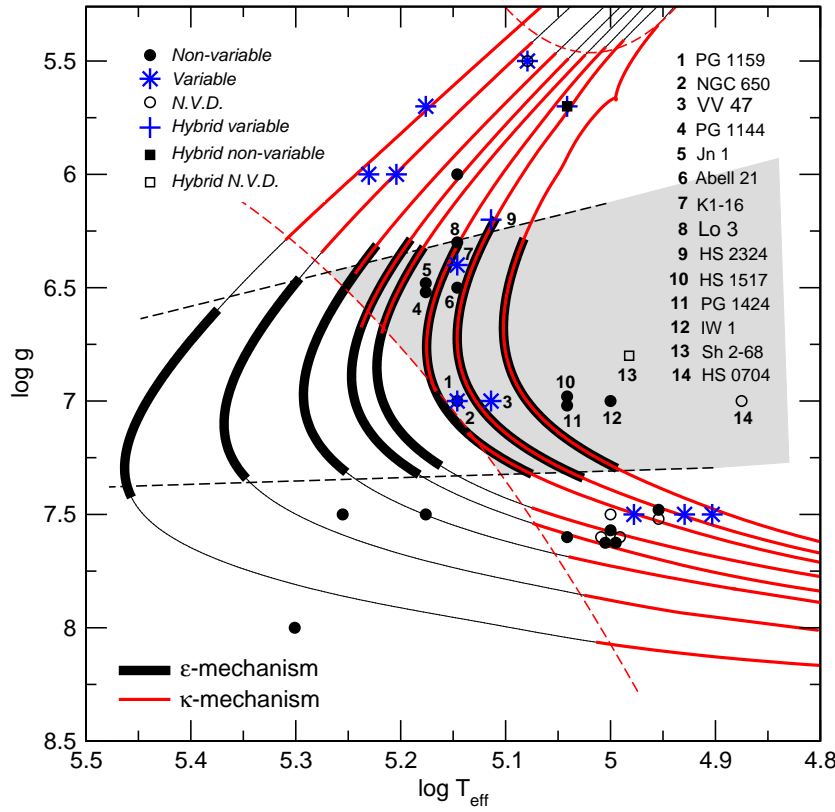
Fig. 28 The PG 1159 evolutionary tracks (thin solid lines) of Althaus et al. (2005a), Miller Berto-lami & Althaus (2006) and Córsico et al. (2006), with stellar masses of (from right to left): $M_* = 0.515, 0.530, 0.542, 0.565, 0.589, 0.609, 0.664, 0.742 M_\odot$. The location of models having $\ell = 1$ (dipole) κ-destabilized modes according to Córsico et al. (2006) is displayed with solid red curves along the tracks, and models harboring short-period ε-destabilized modes according to Córsico et al. (2009c) are shown with thick solid curves. The superposition of both types of curves corresponds to stellar models with both ε- and κ-destabilized modes (shaded area). The location and designation of relevant PG 1159 stars is also shown.

short periodicities of VV 47 could be the ε-mechanism powered by the active He-burning shell, whereas the long-period branch of the period spectrum of this star should be due to the κ-mechanism acting on the region of partial ionization of carbon and oxygen. If true, this could be indicating that VV 47 should have a thick He-rich envelope able to support stable He-shell burning. However, the real existence of the short periods of VV 47 must be confirmed by follow-up observations. If this were done, this star could be the first known pulsating PG 1159 star undergoing non-radial g-modes destabilized by the ε-mechanism. Even more, VV 47 could be the first known pulsating star in which both the κ-mechanism and the ε-mechanism of mode driving are operating simultaneously.

10 Conclusion

There are several reasons that make white dwarfs reliable cosmic clocks and laboratories to study different kind of problems. Indeed, they constitute the final evolutionary stage for the

vast majority of stars. They are a homogeneous class of stars with a narrow mass distribution and well known structure with slow rotation rates and low magnetic fields. And most importantly, their evolution, as we have shown, is relatively simple and can be described in terms of a cooling problem. Additionally, their pulsational properties can be well described, and the excellent observational data gathered over the years provide strong constraints to the theory, allowing to refine the theoretical models. However, there are still some open questions regarding the evolutionary history of white dwarf progenitors, the physics of white dwarf cooling and their pulsational properties that still need to be addressed. Once this is done, white dwarfs will constitute the best studied class of stars and will allow the astronomical community to use them as tracers of the evolution of the Galaxy.

References

1. Abrikosov AA (1960) Soviet Phys JETP 12: 1254
2. Adams WS (1915) Publ Astron Soc Pacific 27: 236-237
3. Adams WS (1925) Proc Nat Acad Sci 11: 382-387
4. Aizenman M, Smeyers P, Weigert A (1977) Astron Astrophys 54: 41-46
5. Alcock C, Allsman RA, Alves D et al. (2000) Astrophys J 541: 270-297
6. Alcock C, Allsman RA, Alves D et al. (1997) Astrophys J 486: 697-726
7. Alcock C, Allsman RA, Alves D et al. (1995) Astrophys J Lett 454: L125-L128
8. Althaus LG, Córsico AH, Bischoff-Kim A., Romero AD, Renedo I, García-Berro E, Miller Bertolami MM (2010a) Astrophys J, to be published
9. Althaus LG, García-Berro E, Renedo I, Isern J, Córsico AH, Rohrmann RD (2010b) Astrophys J, submitted
10. Althaus LG, Panei JA, Miller Bertolami MM et al. (2009a) Astrophys J 704: 1605-1615
11. Althaus LG, García-Berro E, Córsico AH, Miller Bertolami MM, Romero AD (2009b) Astrophys J Lett 693: L23-L26
12. Althaus LG, Córsico AH, Torres S, García-Berro E (2009c) Astron Astrophys 494: 1021-1024
13. Althaus LG, Córsico AH, Kepler SO, Miller Bertolami MM (2008a) Astron Astrophys 478: 175-180
14. Althaus LG, Córsico AH, Miller Bertolami MM, García-Berro E, Kepler SO (2008b) Astrophys J Lett 677: L35-L38
15. Althaus LG, Serenelli AM, Panei JA, Córsico AH, García-Berro E, Scóccola CG (2005a) Astron Astrophys 435: 631-648
16. Althaus LG, Miller Bertolami MM, Córsico AH, García-Berro, Gil-Pons P (2005b) Astron Astrophys 440: L1-L4
17. Althaus LG, Serenelli AM, Córsico AH, Montgomery MH (2003) Astron Astrophys 404: 593-609
18. Althaus LG, Serenelli AM, Benvenuto OG (2001) Mon Not R Astron Soc 323: 471-483
19. Althaus LG, Benvenuto OG (2000) Mon Not R Astron Soc 317: 952-964
20. Anderson W (1929) Z Phys 54:433-444
21. Baglin A, Schatzman E (1969) Low-Luminosity Stars. Gordon and Breach Science Publishers, New York 385
22. Barlow BN, Dunlap BH, Rosen R, Clemens JC (2008) Astrophys J 688: L95
23. Barstow MA (2006) The Ultraviolet Universe. Stars from Birth to Death. IAU Joint Discussion 4 XXVI IAU General Assembly, Prague, 39
24. Beauchamp A, Wesemael F, Bergeron P, Fontaine G, Saffer RA, Liebert J, Brassard P (1999) Astrophys J 516: 887-891
25. Becker AC, Rest A, Stubbs C et al (2005) IAU Symp 225: 357-362
26. Bedin LR, King IR, Anderson J, Piotto G, Salaris M, Cassisi S, Serenelli AM (2008) Astrophys J 678: 1279- 1291
27. Benvenuto OG, De Vito MA (2005) Mon Not R Astron Soc 362: 891-905
28. Benvenuto OG, Córsico AH, Althaus LG, Serenelli AM (2002) Mon Not R Astron Soc 332: 399-408

29. Bergeron P, Fontaine G, Billères M, Boudreault S, Green EM (2004) Astrophys J 600: 404-408
30. Bergeron P, Leggett SK, Ruiz M-T (2001) Astrophys J Suppl 133: 413-449
31. Bergeron P, Wesemael F, Lamontagne R, Fontaine G, Saffer RA, Allard NF (1995) Astrophys J 449: 258-279
32. Bergeron P, Wesemael F, Fontaine G (1991) Astrophys J 367: 253-269
33. Bischoff-Kim A (2009) American Institute of Physics. Conference Series 1170: 621
34. Bischoff-Kim A, Montgomery MH, Winget DE (2008a) Astrophys J 675: 1505-1511
35. Bischoff-Kim A, Montgomery MH, Winget DE (2008b) Astrophys J 675: 1512-1517
36. Bognár Zs, Paparó, M Bradley PA, Bischoff-Kim A (2009) Mont Not R Astron Soc 399: 1954-1963
37. Bond HE, Kawaler SD, Ciardullo R et al (1996) Astron J 112: 2699-2711
38. Bond HE, Ciardullo R (1993) NATO ASI Series. Kluwer, Dordrecht 403: 491
39. Bond HE, Meakes MG (1990) Astron J 100: 788-792
40. Bradley PA (2006) Mem Soc Astron Italiana 77: 437-438
41. Bradley PA (2001) Astrophys J 552: 326-339
42. Bradley PA (1998) Astrophys J Suppl 116: 307-319
43. Bradley PA, Kleinman S J (1997) White dwarfs. Kluwer, Dordrecht 214: 445
44. Bradley PA (1996) Astrophys J 468: 350-368
45. Bradley PA, Dziembowski W A Astrophys J (1996) 462: 376-385
46. Bradley PA, Winget DE (1994a) Astrophys J 421: 236-244
47. Bradley PA, Winget DE (1994b) Astrophys J 430: 850-857
48. Bradley PA, Winget DE, Wood MA (1993) Astrophys J 406: 661-673
49. Branch D, Livio M, Yungelson L, Boffi F, Baron E (1995) Pub Astron Soc Pac 107: 1019-1029
50. Brassard P, Fontaine G, Wesemael F (1995) Astrophys J Suppl 96: 545-580
51. Brassard P, Fontaine G, Wesemael F, Talon A (1993) White Dwarfs: Advances in Observation and Theory. Kluwer, Dordrecht 403: 485
52. Brassard P, Fontaine G, Wesemael F, Hansen C J (1992a) Astrophys J Suppl 80 369-401
53. Brassard P, Pelletier C, Fontaine G, Wesemael F (1992b) Astrophys J Suppl 80: 725-752
54. Brassard P, Fontaine G, Wesemael F, Kawaler SD, Tassoul M (1991) Astrophys J 367: 601-611
55. Brickhill AJ (1991) Mon Not R Astron Soc 251: 673-680
56. Brown TM, Gilliland RL (1994) Annu Rev Astron Astrophys 32: 37-82
57. Camacho J, Torres S, Isern J, Althaus LG, García–Berro E (2007) Astron Astrophys 471: 151-158
58. Casewell SL, Dobbie PD, Napiwotzki R, Burleigh MR, Barstow MA, Jameson RF (2009) Mon Not R Astron Soc 395: 1795-1804
59. Castanheira BG, Kepler SO (2009) Mon Not R Astron Soc 396: 1709-1731
60. Castanheira BG, Kepler SO (2008) Mon Not R Astron Soc 385: 430-444
61. Castanheira BG, Kepler SO, Costa AFM et al (2007) Astron Astrophys 462: 989-993
62. Castanheira BG, Kepler SO, Handler G, Koester D (2006) Astron Astrophys 450: 331-337
63. Catalán S, Isern J, García-Berro E, Ribas I (2008) Mon Not R Astron Soc 387: 1693-1706
64. Chandrasekhar S (1931) Astrophys J 74: 81-82
65. Chandrasekhar S (1939) An introduction to the study of stellar structure. University of Cambridge, Cambridge
66. Chanmugam G (1972) Nature 236: 83-86
67. Charpinet S, Fontaine G, Brassard P (2009) Nature 461: 501-503
68. Ciardullo R, Bond HE (1996) Astron J 111: 2332-2348
69. Clemens JC, van Kerkwijk MH, Wu Y (2000) Mon Not R Astron Soc 314: 220-228
70. Clemens JC (1993) Balt A 2: 407
71. Córsico AH, Althaus LG, Miller Bertolami MM, García-Berro E (2009a) Journal of Physics. Conference Series 172: 12075-12079
72. Córsico AH, Althaus LG, Miller Bertolami MM, García-Berro E (2009b) Astron Astrophys 499: 257-266
73. Córsico AH, Althaus LG, Miller Bertolami MM, González Pérez JM, Kepler SO (2009c) Astrophys J 701: 1008-1014
74. Córsico AH, Romero AD, Althaus LG, García-Berro E (2009d) Astron Astrophys 506: 835-843
75. Córsico AH, Althaus LG, Kepler SO, Costa JES, Miller Bertolami MM (2008) Astron Astrophys 478: 869-881
76. Córsico AH, Althaus LG, Miller Bertolami MM, Werner K (2007a) Astron Astrophys 461: 1095-1102
77. Córsico AH, Miller Bertolami MM, Althaus LG, Vauclair G, Werner K (2007b) Astron Astrophys 475: 619-627
78. Córsico AH, Althaus LG, Miller Bertolami M M (2006) Astron Astrophys 458: 259-267
79. Córsico AH, Althaus LG (2006) Astron Astrophys 458: 863-881
80. Córsico AH, Althaus LG (2005) Astron Astrophys 439: L31-L34
81. Córsico AH, Althaus LG, Benvenuto OG, Serenelli AM (2002a) Astron Astrophys 387: 531-549

82. Córsico AH, Benvenuto OG, Althaus LG, Serenelli AM (2002b) Mon Not R Astron Soc 332: 392-398
83. Córsico AH, Althaus LG, Benvenuto OG, Serenelli AM (2001a) Astron Astrophys 380: L17-L20
84. Córsico AH, Benvenuto OG, Althaus LG, Isern J, García-Berro E (2001b) New Astron 6: 197-213
85. Costa JES, Kepler SO, Winget DE et al (2008) Astron Astrophys 477: 627-640
86. Costa JES, Kepler SO (2008) Astron Astrophys 489: 1225-1232
87. Cowling TG (1941) Mon Not R Astron Soc 101: 367-375
88. Cowling TG, Newing RA (1949) Astrophys J 109: 149-158
89. Cox AN (2003) Astrophys J 585: 975-982
90. Cox JP (1980) Theory of stellar pulsation. Princeton University Press, Princeton
91. D'Antona F, Mazzitelli I (1990) Annu Rev Astron Astrophys 28: 139-181
92. D'Antona F, Mazzitelli I (1989) Astrophys J 347: 934-949
93. DeGennaro S, von Hippel T, Winget DE, Kepler SO, Nitta A, Koester D, Althaus LG (2008) Astron J 135: 1-9
94. Deloye CJ, Bildsten L (2002) Astrophys J 580: 1077-1090
95. Díaz–Pinto A, García–Berro E, Hernanz M, Isern J, Mochkovitch, R. (1994) Astron Astrophys 282: 86-92
96. Dolez N, Vauclair G (1981) Astron Astrophys 102: 375-385
97. Domínguez I, Straniero O, Tornambe A, Isern J (1996) Astrophys J 472: 783-788
98. Dreizler S, Heber U (1998) Astron Astrophys 334: 618-632
99. Dreizler S, Werner K (1996) Astron Astrophys 314: 217-232
100. Dreizler S, Werner K, Heber U, Reid N, Hagen H (1997) The Third Conference on Faint Blue Stars. L Davis Press, New York, 303
101. Driebe T, Schönberner D, Blöcker T, Herwig F (1998) Astron Astrophys 339: 123-133
102. Dufour P et al (2009a) Journal of Physics. Conference Series 172: 12012
103. Dufour P, Green EM, Fontaine G, Brassard P, Francoeur M, Latour M (2009b) Astrophys J 703: 240-251
104. Dufour P, Fontaine G, Liebert J, Schmidt GD, Behara N (2008a) Astrophys J 683: 978-989
105. Dufour P, Fontaine G, Liebert J, Williams, K, Lai DK (2008b) Astrophys J Lett 683: L167-L170
106. Dufour P, Liebert J, Fontaine G, Behara N (2007) Nature 450: 522-524
107. Dziembowski W, Koester D (1981) Astron Astrophys 97: 16-26
108. Dziembowski W (1977) Acta Astron 27: 203-211
109. Eisenstein DJ, Liebert J, Harris HC et al (2006) Astrophys J Supp 167: 40-58
110. Faulkner J, Gribbin JR (1968) Nature 218: 734-736
111. Fontaine G, Brassard P, Dufour P (2008) Astron Astrophys 483: L1-L4
112. Fontaine G, Brassard P (2008) Pub Astron Soc Pac 120: 1043-1096
113. Fontaine G, Brassard P, Bergeron P (2001) Pub Astron Soc Pac 113: 409-435
114. Fontaine G, Brassard P (1994) Astron Soc Pac Conf Ser, San Francisco 57: 195-208
115. Fontaine G, Brassard P, Bergeron P, Wesemael F (1992) Astrophys J 399: L91-L94
116. Fowler RH (1926) Mon Not R Astron Soc 87: 114-122
117. Fu J-N, Vauclair G, Solheim J-E et al (2007) Astron Astrophys 467: 237-248
118. Fujimoto M Y (1977) Pub Astron Soc Pac 29: 331-350
119. García-Berro E, Torres S, Althaus LG, Renedo I, Lorén-Aguilar P, Córsico AH, Rohrmann R, Salaris M, Isern J (2010) Nature 465: 194-196
120. García-Berro E, Althaus LG, Córsico AH, Isern J (2008) Astrophys J 677: 473-482
121. García–Berro E, Torres S, Isern J, Burkert A (2004) Astron Astrophys 418: 53-65
122. García–Berro E, Torres S, Isern J, Burkert A (1999) Mon Not R Astron Soc 302: 173-188
123. García-Berro E, Hernanz M, Isern J, Mochkovitch R (1995) Mon Not R Astron Soc 277: 801-810
124. García-Berro E, Hernanz M, Mochkovitch R, Isern J (1988a) Astron Astrophys 193: 141-147
125. García-Berro E, Hernanz M, Isern J, Mochkovitch R (1988b) Nature 333: 642-644
126. Gautschy A, Althaus LG, Saio H (2005) Astron Astrophys 438: 1013-1020
127. Gautschy A (1997) Astron Astrophys 320: 811-822
128. Gautschy A, Saio H (1996) Annu Rev Astron Astrophys 34: 551-606
129. Gautschy A, Saio H (1995) Annu Rev Astron Astrophys 33: 75-114
130. Gianninas A, Bergeron P, Fontaine G (2006) Astron J 132: 831-835
131. Gianninas A, Bergeron P, Fontaine G (2005) Astrophys J 631: 1100-1112
132. Goldman B, Afonso C, Alard Ch (2002) Astron Astrophys 389: L69-L73
133. Goldreich P, Wu Y (1999) Astrophys J 511: 904-915
134. González Pérez JM, Solheim J-E, Kamben R (2006) Astron Astrophys 454: 527-536
135. Grauer AD, Bond HE, Liebert J, Fleming TA, Green RF (1987) Astrophys J 323: 271-279
136. Green EM, Dufour P, Fontaine G, Brassard P (2009) Astrophys J 702: 1593-1603
137. Guerrero J, García-Berro E, Isern J (2004) Astron Astrophys 413: 257-272

138. Hansen BMS, Anderson J, Brewer J et al (2007) Astrophys J 671: 380-401
139. Hansen BMS, Liebert J (2003) Annu Rev Astron Astrophys 41: 465-515
140. Hansen BMS, Brewer J, Fahlman GG et al (2002) Astrophys J Lett 574: L155-158
141. Hansen BMS (1998) Nature 394: 860-862
142. Hansen BMS, Phinney ES (1998) Mon Not R Astron Soc 294: 569-581
143. Hansen CJ, Cox JP, van Horn HM (1977) Astrophys J 217: 151-159
144. Harper RVR, Rose WK (1970) Astrophys J 162: 963-969
145. Harris HC, Munn JA, Kilic M. et al (2006) Astron J 131: 571-581
146. Hernanz M, García-Berro E, Isern J, Mochkovitch R, Segretain L, Chabrier G (1994) Astrophys J 434: 652-661
147. Herwig F, Blöcker T, Langer N, Driebe T (1999) Astron Astrophys 349: L5-L8
148. Hügelmeyer SD, Dreizler S, Homeier D, Krzesiński J, Werner K, Nitta A, Kleinman SJ (2006) Astron Astrophys 454: 617-624
149. Ibata R, Richer HB, Gilliland RL, Scott D (1999) Astrophys J Lett 524: L95-L97
150. Iben I Jr, MacDonald J (1986) Astrophys J 301: 164-176
151. Iben I Jr, MacDonald J (1985) Astrophys J 296: 540-553
152. Iben I, Jr Kaler JB, Truran JW, Renzini A (1983) Astrophys J 264: 605-612
153. Isern J, García-Berro E, Althaus LG, Córsico AH (2010) Astron Astrophys (RN) 512: A86-A89
154. Isern J, García-Berro E, Torres S, Catalán S (2008) Astrophys J Lett 682: L109-L112
155. Isern J, García–Berro E, Hernanz M, Chabrier G (2000) Astrophys J, 528: 397-400
156. Isern J, García-Berro E, Hernanz M, Mochkovitch R, Torres S (1998) Astrophys J 503: 239-246
157. Isern J, Mochkovitch R, García-Berro E, Hernanz M (1997) Astrophys J 485: 308-312
158. Isern J, Hernanz M, García-Berro E (1992) Astrophys J Lett 392: L23-L25
159. Isern J, Hernanz M, Mochkovitch R, García-Berro E (1991) Astron Astrophys 241: L29-L32
160. Itoh N, Hayashi H, Nishikawa A, Kohyama Y (1996) Astrophys J Suppl 102: 411-424
161. Jones PW, Hansen CJ, Pesnell WD, Kawaler SD (1989) Astrophys J 336: 403-408
162. Kanaan AN (1996) PhD Thesis. Univ Texas, Austin
163. Kawaler SD, Potter EM, Vuĉković M et al (2004) Astron Astrophys 428: 969-981
164. Kawaler SD, O'Brien MS, Clemens JC et al (1995) Astrophys J 450: 350-363
165. Kawaler SD, Bradley PA (1994) Astrophys J 427: 415-428
166. Kawaler SD (1993) Astrophys J 404: 294-304
167. Kawaler SD, Weiss P (1990) Lect Not Phys. Springer-Verlag 367: 431
168. Kawaler SD (1988) Astrophys J 334: 220-228
169. Kawaler SD (1987) The Second Conference on Faint Blue Stars. IAU Colloquium 95. Schenectady: Davis, 297-307
170. Kawaler SD, Winget DE, Iben I Jr, Hansen CJ (1986) Astrophys J 302: 530-535
171. Kawaler SD, Winget DE, Hansen CJ, Iben I Jr (1986) Astrophys J 306: L41-L44
172. Kawka A, Vennes S (2009) Astron Astrophys 506: L25-L28
173. Kepler SO (2009) New Advances in Helio- and Asteroseismology. IAU Joint Discussion 11 XXVII IAU General Assembly, Rio de Janeiro
174. Kepler SO, Kleinman SJ, Nitta A, Koester D, Castanheira BG, Giovannini O, Costa AFM, Althaus LG (2007) Mon Not R Astron Soc 375: 1315-1324
175. Kepler SO, Costa JES, Castanheira BG et al (2005) Astrophys J 634: 1311-1318
176. Kepler SO, Robinson EL, Koester D, Clemens JC, Nather RE, Jiang XJ (2000) Astrophys J 539: 379-391
177. Kepler SO, Nather RE McGraw JT, Robinson EL (1982) Astrophys J 254: 676-682
178. Kilic M, Mendez RA, von Hippel T, Winget DE (2005) Astrophys J 633: 1126-1141
179. Kilkenny D, O'Donoghue D, Crause LA, Hambly N, MacGillivray H (2009) Mon Not R Astron Soc 397: 453-457
180. Kippenhahn R, Weigert A (1990) Stellar structure and evolution, Springer-Verlag
181. Kirshnitz DA, (1960) Soviet Phys JETP 11: 365
182. Kleinman SJ, Harris HC, Eisenstein DJ et al (2004) Astrophys J 607: 426-444
183. Koester D, Voss B, Napiwotzki R et al (2009) Astron Astrophys 505: 441-462
184. Koester D (2002) Astron Astrophys Rev 11: 33-66
185. Koester D, Allard NF (2000) Balt Astron 9: 119-124
186. Koester D, Chanmugam G (1990) Rep Prog Phys 53: 837-915
187. Koester D (1978) Astron Astrophys 64: 289-294
188. Koester D (1972) Astron Astrophys 16: 459-470
189. Koesterke L, Dreizler S, Rauch T (1998) Astron Astrophys 330: 1041-1046
190. Kotak R (2008) Astron Soc Pac Conf Ser 401, 150
191. Kotak R, van Kerkwijk MH, Clemens JC (2004) Astron Astrophys 413: 301-308

192. Kotak R, van Kerkwijk MH, Clemens JC, Koester D (2003) Astron Astrophys 397: 1043-1055
193. Kotak R, van Kerkwijk MH, Clemens JC (2002a) Astron Astrophys 388: 219-234
194. Kotak R, van Kerkwijk MH, Clemens JC, Bida TA (2002b) Astron Astrophys 391: 1005-1012
195. Lamb DQ, Van Horn HM (1975) Astrophys J 200: 306-323
196. Landolt AU (1968) Astrophys J 153: 151-164
197. Lasker BM, Hesser JE (1971) Astrophys J Lett 163: L89-L93
198. Lasker BM, Hesser JE (1969) Astrophys J Lett 158: L171-L173
199. Lasserre T, Afonso C, Albert JN et al (2000) Astron Astrophys 355: L39-L42
200. Ledoux PJ (1951) Astrophys J 114: 373-384
201. Ledoux PJ, Sauvenier-Goffin E (1950) Astrophys J 111: 611-624
202. Liebert J, Bergeron P, Holberg J (2005) Astrophys J Supp 156 47-68
203. Lorén-Aguilar P, Isern J, García-Berro E (2009) Astron Astrophys 500: 1193-1205
204. Luyten WM (1922) Pub Astron Soc Pac 34: 156-160
205. Madej J, Nalezyty M, Althaus LG (2004) Astron Astrophys 419: L5-L8
206. Marsh TR, Dhillon VS, Duck SR (1995) Mon Not R Astron Soc 275: 828-840
207. McGraw JT, Liebert J, Starrfield SG, Green R (1979) White dwarfs and variable degenerate stars. University of Rochester, Rochester NY 377-381
208. McGraw JT (1979) Astrophys J 229: 203-211
209. McGraw JT, Robinson EL (1976) Astrophys J Lett 205: L155-L158
210. Méndez RA, Ruiz MT (2001) Astrophys J 547: 252-262
211. Méndez RA, Minniti D (2000) Astrophys J 529: 911-916
212. Mestel L (1952) Mon Not R Astron Soc 112: 583-597
213. Metcalfe TS (2005) Astrophys J 26: 273-281
214. Metcalfe TS, Salaris ME, Winget DE (2002) Astrophys J 573: 803-811
215. Metcalfe TS, Winget DE, Charbonneau P (2001) Astrophys J 557: 1021-1027
216. Metcalfe TS, Nather RE, Winget DE (2000) Astrophys J 545: 974-981
217. Miller Bertolami MM, Althaus LG (2006) Astron Astrophys 454: 845-854
218. Miller Bertolami MM, Althaus LG, Serenelli AM, Panei JA (2006) Astron Astrophys 449: 313-326
219. Miller Bertolami MM, Althaus LG, Córsico AH (2005) Bol Asoc Arg Astron 48: 185-191
220. Mochkovitch R (1983) Astron Astrophys 122: 212-218
221. Montgomery MH, Williams KA, Winget DE, Dufour P, DeGennaro S, Liebert J (2008a) Astrophys J Lett 678: L51-L54
222. Montgomery MH (2008b) Comm in Asteroseismology 154: 38-48
223. Montgomery MH (2005) Astrophys J 633: 1142-1149
224. Montgomery MH, Metcalfe TS, Winget DE (2003) Mon Not R Astron Soc 344: 657-664
225. Mukadam AS, Montgomery MH, Winget DE, Kepler SO, Clemens JC (2006) Astrophys J 640: 956-965
226. Mukadam AS, Mullally F, Nather RE et al (2004) Astrophys J 607: 982-998
227. Mullally F, Winget DE, DeGennaro S, Jeffery E, Thompson SE, Chandler D, Kepler SO (2009) Astrophys J 676: 573-583
228. Muraki Y, Sumi T, Abe F et al (1999) Prog Theor Phys Suppl 133: 233-246
229. Nagel T, Werner K (2004) Astron Astrophys 426: L45-L48
230. Nather RE, Winget DE, Clemens JC, Hansen CJ, Hine BP (1990) Astrophys J 361 309-317
231. Nitta A, Kleinman SJ, Krzesinski J et al (2009) Astrophys J 690: 560-565
232. Nitta A, Kepler SO, Winget DE et al (1998) Balt Astron 7: 203-209
233. O'Brien MS (2003) Astrophys Space Sci 284: 45-52
234. O'Brien MS, Kawaler SD (2000) Astrophys J 539: 372-378
235. Ostriker JP, Tassoul J-L (1968) Nature 219: 577-579
236. Pekeris CL (1938) Astrophys J 88: 189-199
237. Pfeiffer B, Vauclair G, Dolez N et al (1996) Astron Astrophys 314: 182-190
238. Prada Moroni PG, Straniero O (2009) Astron Astrophys 507: 1575-1583
239. Quirion P-O, Fontaine G, Brassard P (2007) Astrophys J Suppl 171: 219-248
240. Quirion P-O, Fontaine G, Brassard P (2004) Astrophys J 610: 436-441
241. Raffelt GG (1996) Stars as laboratories for fundamental physics: the astrophysics of neutrinos, axions, and other weakly interacting particles. University of Chicago Press, Chicago
242. Rauch T, Reiff E, Werner K, Herwig F, Koesterke L, Kruk JW (2006) Astron Soc Pac Conf Ser, San Francisco 348: 194-196
243. Reed MD, Kawaler SD, O'Brien MS (2000) Astrophys J 545: 429-434
244. Renedo I, Althaus LG, Miller Bertolami MM, Romero AD, Córsico AH, Rohrmann RD, García-Berro E (2010) Astrophys J, to be published
245. Richer HB, Anderson J, Brewer J, Davis S, Fahlman GG (2006) Science 313: 936-940
246. Richer HB, Fahlman GG, Ibata RA et al (1997) Astrophys J 484: 741-760

247. Ritossa C, García-Berro E, Iben I Jr (1996) Astrophys J 460: 489-505
248. Ritossa C, García-Berro E, Iben I Jr (1999) Astrophys J 515: 381-397
249. Robinson EL, Mailloux TM, Zhang E, Koester D, Stiening RF et al (1995) Astrophys J 438: 908-916
250. Robinson EL, Kepler SO, Nather RE (1982) Astrophys J 259: 219-231
251. Robinson EL, Nather RE, McGraw JT (1976) Astrophys J 210: 211-219
252. Rohrmann RD, Serenelli AM, Althaus LG, Benvenuto OG (2002) Mon Not R Astron Soc 335: 499-511
253. Rohrmann RD (2001) Mon Not R Astron Soc 323: 699-712
254. Russell HN (1914) Pop Astron 22: 275-294
255. Saio H, Jeffery CS (2000) Mon Not R Astron Soc 313: 671-677
256. Saio H (1996) Astron Soc Pac Conf Ser, San Francisco 96: 361-373
257. Saio H, Winget DE, Robinson EL (1983) Astrophys J 265: 982-995
258. Salaris M, Serenelli AM, Weiss A, Miller Bertolami MM (2009) Astrophys J 692: 1013-1032
259. Salaris M, Domínguez I, García-Berro E, Hernanz M, Isern J, Mochkovitch R (1997) Astrophys J 486: 413-419
260. Salpeter EE (1961) Astrophys J 134: 669-682
261. Sarna MJ, Antipova J, Ergma E (1999) Astron Soc Pac Conf Ser, San Franciso 169: 400-407
262. Saumon D, Bergeron P, Lunine JI, Hubbard WB, Burrows A (1994) Astrophys J 424: 333-344
263. Saumon D, Jacoboson SB (1999) Astrophys J 511: L107-L110
264. Sauvenier-Goffin E (1949) Annales d'Astrophysique 12: 39-51
265. Schmidt M (1959) Astrophys J 129: 243-258
266. Schönberner D (1979) Astrons Astrophys 79: 108-114
267. Segretain L, Chabrier G, Hernanz M, García-Berro E, Isern J, Mochkovitch R (1994) Astrophys J 434: 641-651
268. Shaviv G, Kovetz A (1976) Astron Astrophys 51: 383-391
269. Siess L (2007) Astron Astrophys 476: 893-909
270. Silvotti R, Fontaine G, Pavlov M, Marsh TR, Dhillon VS, Littlefair SP (2007) Astron Soc Pac Conf Ser, San Francisco 372: 593
271. Silvotti R, Dreizler S, Handler G, Jiang X J (1999) Astron Astrophys 342: 745-755
272. Solheim J-E, Vauclair G, Mukadam AS, Janulis R, Dobrovolskas V (2007) Astron Astrophys 468: 1057-1061
273. Stanghellini L, Cox AN, Starrfield S (1991) Astrophys J 383: 766-778
274. Starrfield S, Cox AN, Kidman RB, Pesnell WD (1985) Astrophys J Lett 293: L23-L27
275. Starrfield S, Cox AN, Kidman RB, Pesnell WD (1984) Astrophys J 281: 800-810
276. Starrfield S, Cox AN, Hodson SW, Pesnell WD (1983) Astrophys J Lett 268: L27-L32
277. Stevenson DJ (1980) J Phys Colloq 41: C2/61-64
278. Stoner EC (1930) Philos Mag 9: 944-963
279. Straniero O, Domínguez I, Imbriani G, Piersanti L (2003) Astrophys J 583: 878-884
280. Tassoul M, Fontaine G, Winget DE (1990) Astrophys J Suppl 72: 335-386
281. Tassoul M (1980) Astrophys J Suppl 43: 469-490
282. Thompson SE, van Kerkwijk MH, Clemens JC (2008) Mon Not R Astron Soc 389: 93-101
283. Tisserand P, Le Guillou L, Afonso C et al (2007) Astron Astrophys 469: 387-404
284. Torres S, García–Berro E, Isern, J (1998) Astrophys J Lett 508: L71-L74
285. Torres S, García–Berro E, Burkert A, Isern J (2001) Mon Not R Astron Soc, 328: 492-500
286. Torres S, García–Berro E, Burkert A, Isern J (2002) Mon Not R Astron Soc 336: 971-978
287. Torres S, Camacho J, Isern J, García–Berro E (2008) Astron Astrophys, 486: 427-435
288. Udalski A, Szymanski M, Kaluzny J, Kubiak M (1994) Acta Astron 44: 1-20
289. Unglaub K, Bues I (2000) Astron Astrophys 359: 1042-1058
290. Unno W, Osaki Y, Ando H, Saio H, Shibahashi H (1989) Non-radial oscillations of stars. University of Tokyo Press, Tokyo
291. van Horn HM (1968) Astrophy J 151: 227-238
292. van Kerkwijk MH et al (2005) Astron Soc Pac Conf Ser, San Franciso 328: 357-370
293. van Kerkwijk MH, Clemens JC, Wu Y (2000) Mon Not R Astron Soc 314: 209-219
294. Vauclair G, Solheim J-E, Østensen RH (2005) Astron Astrophys 433: 1097-1100
295. Vauclair G, Moskalik P, Pfeiffer B et al (2002) Astron Astrophys 381: 122-150
296. Vauclair G (1971) Astrophys Lett 9: 161-164
297. Von Hippel T, Gilmore G (2000) Astron J 120: 1384-1395
298. Von Hippel T, Jefferys WH, Scott J et al (2006) Astrophys J 645: 1436-1447
299. Voss B, Koester D, Napiwotzki R, Christlieb N, Reimers D (2007) Astron Astrophys 470: 1079-1088
300. Vuille F (1998) PhD Thesis, Univ Capetown
301. Warner B, Robinson E L (1972) Nature 239: 2-7
302. Weidemann V (2000) Astron Astrophys 363: 647-656

303. Werner K, Rauch T, Kruk JW (2008a) Astron Soc Pac Conf Ser, San Franciso 391: 239-240
304. Werner K, Rauch T, Kruk JW (2008b) Astron Astrophys 492: L43-L47
305. Werner K, Herwig F (2006) Pub Astron Soc Pac 118: 183-204
306. Werner K (2001) Astrophy and Space Sci 275: 27-39
307. Winget DE, Kepler SO, Campos F, Montgomery MH, Girardi L, Bergeron P, Williams K (2009) Astrophys J Lett 693: L6-L10
308. Winget DE, Kepler SO (2008) Annu Rev Astron Astrophys 46: 157-199
309. Winget DE, Sullivan DJ, Metcalfe TS, Kawaler SD, Montgomery MH (2004) Astrophys J Lett 602: L109-L112
310. Winget DE, Nather RE, Clemens JC et al. (1994) Astrophys J 430: 839-849
311. Winget DE, Nather RE, Clemens JC et al. (1991) Astrophys J 378: 326-346
312. Winget DE (1988) Advances in Helio- and Asteroseismology. IAU Symp 123: 305-324
313. Winget DE, Hansen CJ, Liebert J, Van Horn HM, Fontaine G, Nather RE, Kepler SO, Lamb DQ (1987) Astrophys J Lett 315: L77-L81
314. Winget DE, Hansen CJ, van Horn HM (1983) Nature 303: 781-782
315. Winget DE, van Horn, HM, Tassoul M, Fontaine G, Hansen, CJ, Carroll BW (1982a) Astrophys J Lett 252: L65-L68
316. Winget DE, Robinson EL, Nather RD, Fontaine, G. (1982b) Astrophys J Lett 262: L11-L15
317. Winget DE, van Horn H M, Hansen C J (1981) Astrophys J Lett 245: L33-L36
318. Xu ZW, Van Horn HM (1992) Astrophys J 387: 662-672
319. Yoo J, Chanamé J, Gould A (2004) Astrophys J 601: 311-318
320. York DG, Adelman J, Anderson JE Jr et al (2000) Astron J 120: 1579-1587